# SOLID STATE SUPERCAPACITORS

BASED ON METAL/YTTRIA-STABILISED
ZIRCONIA COMPOSITES

**PROEFSCHRIFT**

ter verkrijging van
de graad van doctor aan de Universiteit Twente,
op gezag van de rector magnificus,
prof. dr. F.A. van Vught,
volgens besluit van het College voor Promoties
in het openbaar te verdedigen
op vrijdag 5 oktober 2001 te 13:15 uur

door

**Mark Gerard Hendrik Maria Hendriks**

geboren op 4 maart 1973
te Haps

Dit proefschrift is goedgekeurd door de promotor

prof. dr. ir. H. Verweij

en de assistent promotor

dr. ir. J.E. ten Elshof

Hendriks, Mark Gerard Hendrik Maria
Solid state supercapacitors based on metal/yttria-stabilised zirconia composites
Thesis University of Twente. With Summary in Dutch.

ISBN 90 365 1630 7

© M.G.H.M. Hendriks, Enschede, The Netherlands, 2001.

Al rights reserved.

Printed by PrintPartners Ipskamp B.V., Enschede, The Netherlands.
Cover by Kim van der Ven.

# Contents

# Chapter 1
# Introduction

## Conventional capacitors

Conventional capacitors consist of two electrodes separated by a thin layer of dielectric material. Due to electronic and ionic polarisation of the dielectric medium upon application of an electric field, electrical charge can be stored at the electrodes. The capacitance ($C$) can be calculated with

$$C = \frac{\Delta q}{\Delta V}, \tag{1}$$

where $\Delta q$ is the electrical charge stored at the electrodes and $\Delta V$ the applied potential difference between the electrodes. In an ideal capacitor the capacitance does not change upon variation in the potential difference. The capacitance can be increased by making use of a dielectric medium with a large dielectric constant, increasing the electrode surface area or decreasing the distance between the electrodes, since

$$C = \frac{\varepsilon_r \varepsilon_0 A}{d}, \tag{2}$$

where $\varepsilon_r$ (also referred to as $k$') is the relative dielectric constant of the dielectric medium, $\varepsilon_0$ the permittivity of vacuum, $A$ the geometric electrode surface area and $d$ the distance between the electrodes. By decreasing the distance between the electrodes, the electric field strength is increased. If the electric field strength exceeds a certain threshold value called the dielectric strength, the material will lose its insulating property [1].

Several polarisation effects contribute to the value of the dielectric constant. The type of contribution is frequency dependent as shown in Fig. 1 [2]. The electronic and ionic polarisation occur at high frequencies in a dielectric medium. The space-charge polarisation occurs at low frequencies in materials that are not perfect dielectrics, but in which long-range charge transport may occur, especially in electrolytes. As expected from the frequency dependence of the polarisation, a fast charge release is obtained in conventional capacitors, while the space charge effects are slower.

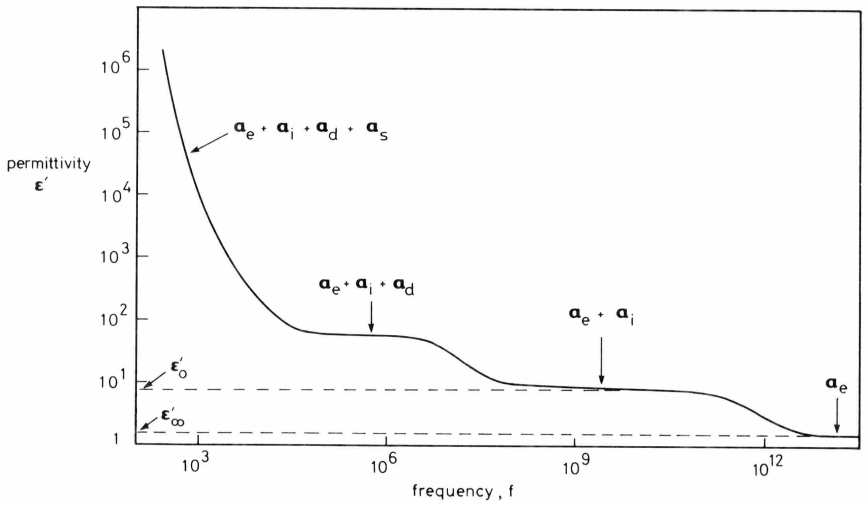


***Fig. 1:*** *Polarisation effects in a dielectric. $\alpha_e$ electronic polarisability, $\alpha_i$ ionic polarisability, $\alpha_d$ dipole polarisability and $\alpha_s$ space charge polarisation [2].*

Barium titanate-based and other perovskite-related materials are commonly used as the dielectric medium in capacitors. The main reason is related to the very high value of the relative dielectric constant of these materials in the vicinity of the phase transition temperatures. In $BaTiO_3$- type materials, several phase transitions occur. The largest dielectric constant is obtained at the so-called Curie point, where the transition from a tetragonal to a cubic structure takes place. According to the Curie-Weiss law the dielectric constant becomes very large near this particular phase

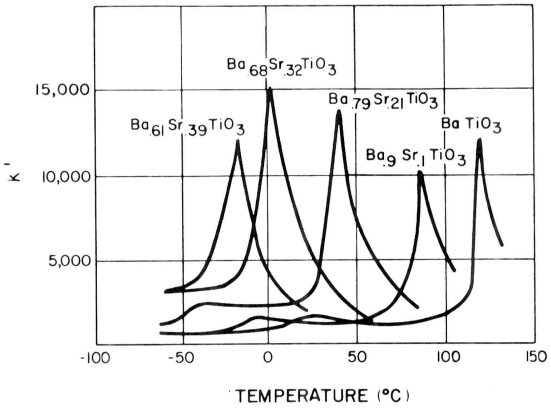


***Fig. 2:*** *Effect of a solid solution of $BaTiO_3$ doped with strontium on the Curie temperature [4].*

transition. For pure $BaTiO_3$ the Curie point lies at 130ºC [3]. However, by doping the perovskite with Sr, for instance, this Curie point can be decreased as shown in Fig. 2 [4]. In this manner the high values for the dielectric constant can be reached at lower temperatures [5].

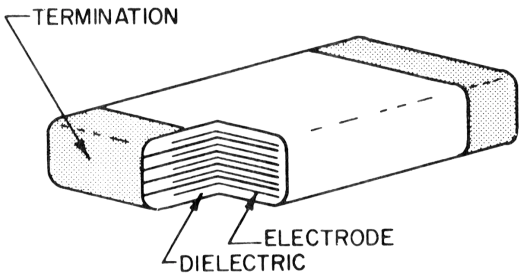


***Fig. 3:*** *Schematic drawing of a multi-layered ceramic capacitor [4].*

As mentioned above, the capacitance can be enlarged by increasing the electrode surface area and decreasing the distance between the electrodes. This can be achieved by forming multilayered structures of the dielectric phase and electrode materials as shown in Fig. 3 [6]. Upon decreasing the layer thickness by a factor of 2, while the volume of the capacitor is kept constant, the total capacitance can be increased by a factor of 4. This effect is due to a combination of the decreased distance between the electrodes and the doubling of the electrode surface area [7].

*Cermet capacitors*

An alternative way to prepare capacitors with an increased electrode surface area and a decreased distance between electrodes is the use of metal/dielectric composites with a random distribution of the metal phase. At the percolation threshold of the metal phase (the volume fraction at which the metal phase starts to form an electrically conducting network inside the composite), $p_c$, the composite undergoes a transition from an isolating to a conducting material. Efros and Shklovskii [8], McLachlan [9] and Dubrov *et al.* [10] described the behaviour of such a composite near its percolation threshold. The dielectric constant of the composite increases with the volume fraction of metal and diverges in the immediate vicinity of the percolation threshold. The increase in the dielectric constant of metal/dielectric composites near the insulating-to-conducting transition appears to be comparable to the increase obtained during a phase transition in the dielectric phase near

the Curie temperature. It should be noted that in a conventional capacitor only the component of the electrode surface area perpendicular to the electric field strength contributes in the polarisation of the dielectric medium. The main increase in the capacitance for random composites will result from an effective decrease in the distance between the electrodes.

## Supercapacitors

In contrast to conventional capacitors, supercapacitors make use of electrolytes instead of a dielectric medium and therefore have the ability to store electrochemical energy at the interface between electrodes and the electrolyte. Both liquid and solid electrolytes can be used in supercapacitors. However, taking charging times into account, fast ion conductivity is a requirement. In the electrolyte, mobile charge carriers with a positive charge can accumulate near a negatively charged electrode, while the concentration of negative charge carriers becomes depleted (see Fig. 4). In this way a space-charge region is developed in the electrolyte near the interface with the electrode and a large electrochemical capacitance is obtained. In these electrochemical capacitors the double-layer capacitance can reach values up to ~100 $\mu F/cm^2$, depending on the nature of the electrolyte [11]. In general, the thickness of the space-charge layer is negligible compared with the distance between the electrodes. Moreover, the entire interface between the electrodes and electrolyte contributes to the formation of this double layer. Therefore, supercapacitors normally consist of electrodes possessing a very large electrode surface area in the order of $10^3$ $m^2/g$ [12]. A combination of both the double-layer capacitance and the large interfacial area between electrode and electrolyte results in supercapacitors with typical capacitances of 1-10 F compared to $10^{-10}$–$10^{-3}$ F for conventional capacitors [13]. As mentioned before, polarisation due to the build up of a space charge layer consumes more time than electronic and ionic polarisation. Therefore in contrast with conventional capacitors, which are used in ac applications, supercapacitors are more suitable for dc applications.

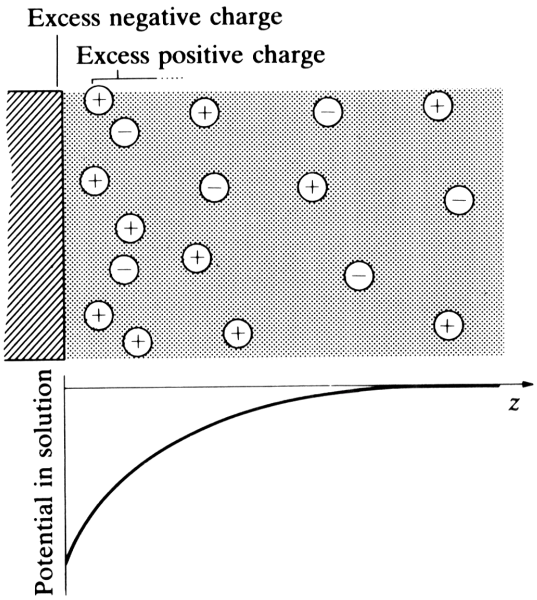


***Fig. 4:*** *The space charge region at a negatively charged electrode in an electrolyte consisting of mobile anions and cations, following the Gouy-Chapman model.*

For each supercapacitor the space-charge layer of the mobile ions is built up differently, depending on the thermodynamic and chemical behaviour of the electrolyte [11, 14]. In Fig. 4 an example of a diffuse double-layer according to the Gouy-Chapman model is shown [15]. This example describes a system with an electrolyte consisting of mobile anions and cations. By charging the electrode negatively, the cations are attracted towards this electrode and accumulate at the interface, while the anions are depleted.

Depending on the nature of the electrolyte and the electrodes ions can adsorb on the electrode surface and form an immobile monolayer, due to electrostatic forces between the ions and the electrode interface. This monolayer is known as the Helmholtz layer and is a part of the total double layer. Next to this rigid Helmholtz layer a diffuse Gouy-Chapman layer as described above is formed. The total capacitance of the electrode can be calculated with [16]:

$$\frac{1}{C} = \frac{1}{C_{\mathrm{H}}} + \frac{1}{C_{\mathrm{GC}}} \tag{3}$$

where $C_{\mathrm{H}}$ is the contribution to the capacitance due to the formation of the Helmholtz layer and $C_{\mathrm{GC}}$ the contribution to the capacitance due to the diffuse double-layer. In liquid electrolytes a combination of both layers is often

obtained. However, in solid electrolytes the Helmholtz layer has not been experimentally observed.

Together with the formation of a double-layer, another type of electrochemical capacitance can also be obtained. This type of supercapacitor is also known as a pseudo-capacitor [11, 17]. In contrast with the two former supercapacitors, in this type of supercapacitor charge is stored due to fast faradaic redox reactions occurring at the electrode surfaces. During charging and discharging, ions are transferred from one electrode to the other across the electrolyte. This is different from the processes in the other types of supercapacitors, where zero net ion exchange between the electrode and the electrolyte occurs.

Due to the faradaic transfer, this pseudocapacitor behaviour looks very similar to that of batteries. However, in batteries the bulk of the electrode also participates in the faradaic reactions and insertion of the mobile species into the bulk of the electrode takes place [18]. This effect does not occur in the pseudocapacitors. Moreover, in batteries, the anode and cathode are made from different materials, resulting in net ion exchange during charging and discharging.

## Applications for supercapacitors

A so-called Ragone plot is shown in Fig. 5 and it demonstrates the provided available energy of an energy storage device for a constant active power request [19]. Ragone plots are usually presented in a log-log diagram and are standard in the battery community. First, the plots provide the limit of the available power of a battery or a capacitor. Second, they provide the optimum work region, which is given by the part of the curve in the inset in Fig. 5 where both energy and power are high. The boundaries of the areas are determined by internal losses and/or leakages of the various energy storage devices.

From the plot it can be seen that the energy and power densities of supercapacitors and electrolytic capacitors lie between those of batteries and thin film capacitors. The properties of the supercapacitors therefore vary from battery (dc) behaviour to capacitor (ac/dc) behaviour and since the properties

can be varied (through different material choices), special applications can be imagined and practically realised.

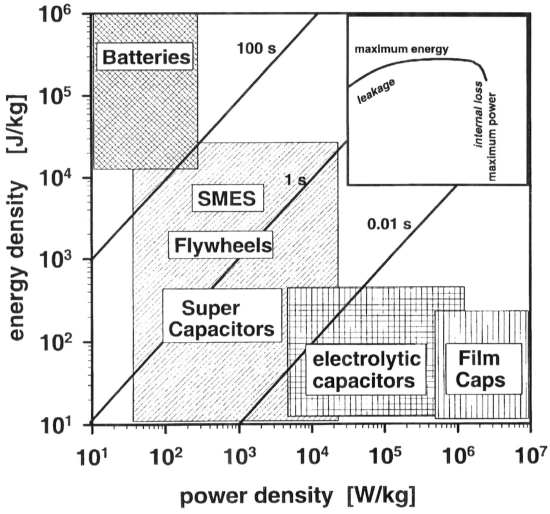


***Fig. 5:*** *Ragone plot: the available energy of an energy storage device at fixed power for different devices. Each energy storage device is represented by the curve shown in the inset. The characteristic operating times of the energy storage devices correspond with the diagonal lines [19].*

Due to their high energy density, supercapacitors are suitable for application as a buffer between the production and consumption of electricity. Among the different kinds of energy storage systems, supercapacitors remain the best solution for applications such as microelectronics. For that reason double-layer capacitors based on polymer electrolytes have been used as memory backup systems in computers [20].

The constant improvement in the development of supercapacitors has led to other applications that may involve power supply optimisation in electric vehicles, which could help to reduce pollution in future. The specific characteristics expected for these supercapacitors (see Fig. 5) are based on their very high reversibility and the high power density associated with a low internal leakage current of only a few milli-amperes. Furthermore, they should give less technological problems than lithium-based batteries, regarding the self-discharge due to internal current leakage. One application could be in electric vehicles for interfacial energy storage between battery and motor where it may be possible to recover the braking energy and to deliver it back for acceleration [21].

Another possibility for supercapacitors is the replacement of emergency generators. If connected in series, several supercapacitors can accomodate

higher voltages. By switching between different capacitor banks using specific circuit designs, controlled charge/discharge systems, including ac energy storage systems can be envisioned [22]. When power is disrupted during peak hour, supercapacitors can supply the desired amount of electrical energy for several hours [23].

## State of the art materials for supercapacitors

Several materials for both electrodes and electrolytes have been investigated and developed for supercapacitor technology. In the next sections the most commonly used materials are summarised.

*Electrodes*

Different reasons to choose particular materials suitable for production of supercapacitor electrodes can be considered, provided that these materials are electronically conducting and blocking mobile ions in the electrolyte. Further requirements for the materials are low cost and more importantly a large electrode surface area [24].

Amongst others, carbon black is a suitable material since it possesses a large specific surface area if the grains are small [25, 26]. For that reason $RuO_2$ is also a commonly used material. Moreover, with $RuO_2$ a redox reaction can take place at the interface, which results in a very large pseudo-capacitance. The electrochemical reactions for (hydrated) $RuO_2$ electrodes can be expressed as

$$HRuO_2 \underset{\text{discharge}}{\overset{\text{charge}}{\leftrightharpoons}} H_{1-\delta}RuO_2 + \delta H^+ + \delta e^-$$

for the positive electrode and

$$HRuO_2 + \delta H^+ + \delta e^- \underset{\text{discharge}}{\overset{\text{charge}}{\leftrightharpoons}} H_{1+\delta}RuO_2$$

for the negative electrode, which makes the overall reaction

$$HRuO_2 + HRuO_2 \underset{\text{discharge}}{\overset{\text{charge}}{\leftrightharpoons}} H_{1-\delta}RuO_2 + H_{1+\delta}RuO_2 ,$$

where $0<\delta<1$.

Due to these electrode reactions an additional advantage compared with carbon black is obtained in this manner [11, 12, 27, 28]. However, the high cost

of $RuO_2$ makes it economically less attractive to use and cheaper electronically conducting polymers [25, 29, 30] have been used as an alternative. An advantage of polymers is the ease of processing, but a disadvantage is that they can not tolerate high temperatures. Another possibility is the utilisation of noble metals, since these materials are easy to process [31], but similar to $RuO_2$, noble metals are expensive.

*Electrolytes*

The electrolyte should not conduct electrons but needs to have a high ionic conductivity, because this will reduce the charging and discharging times. Furthermore a low current leakage is desirable [32]. Commonly used materials for electrolytes are, amongst others, ion-conducting polymers, also known as ionomers [33]. However, the ion conduction is often poor, which can be solved by using aqueous solutions of KOH or $H_2SO_4$ [20, 24] at the risk of obtaining leakage in these liquid electrolytes. This can be overcome by adding soluable polymers to the aqueous solution so that gels are obtained [30, 34]. Another possibility to prevent leakage is using a ceramic electrolyte, but one main disadvantage of these materials is that the ionic conductivity necessary for the double-layer formation is typically insufficient at room temperature [32].

## Scope of this thesis

Supercapacitors normally consist of an electrolyte and electrodes with very large surface area. The aim of the research described in this thesis was to prepare a solid state supercapacitor based on unstructured composites of a solid oxygen-conducting electrolyte and a dispersed metal phase. Yttrium-stabilised zirconia (YSZ) was utilised as electrolyte. At elevated temperatures (>400ºC) YSZ conducts oxygen ions by hopping to neighbouring vacant lattice sites in the oxygen sub-lattice. The behaviour of a solid electrolyte such as YSZ is quite different from that of a liquid electrolyte, since YSZ contains only one mobile charge carrier, namely the oxygen ions, while liquid electrolytes posses two or more oppositely charged mobile charge carriers. Moreover, in YSZ site exclusion effects of oxygen ions must be considered, due to the high concentrations in the double layer, while in liquid electrolytes the electrostatic interactions between the mobile charge carriers

play an important role. These effects result in different electrochemical properties.

The contents of this thesis is divided into two parts. A thermodynamic model of the formation of the double-layer capacitance in YSZ in thermodynamic equilibrium as function of temperature and oxygen vacancy concentration is first developed in Chapter 2. This model is generally applicable for oxygen conducting electrolytes with only one mobile charge carrier.
Based on differential capacitance measurements the near surface defect structure in YSZ is investigated in Chapter 3. Using this defect model a detailed equation for the double-layer capacitance of YSZ is developed.

In the second part of this thesis, attempts for creating large electrode surface areas are made by preparing unstructured metal/YSZ composites. Additionally, the capacitive behaviour of these composites is studied and compared with models known from literature. In Chapter 4 the influence of the microstructure of platinum/YSZ composites on the room temperature capacitance behaviour is studied. Three different conventional processing methods are applied for the preparation of composites with a randomly distributed Pt phase.
In Chapter 5 palladium/YSZ composites with a randomly distributed Pd phase are produced via conventional processing. The capacitance behaviour of these composites is investigated. In addition, the influence of the amount of Pd on the homogeneity of these composites is studied and a correlation with the capacitance behaviour is made.
To create 3D metal networks, which are connected to the electrodes, porous zirconia is impregnated with a Pt-salt solution and subsequently reduced in Chapter 6. The capacitance behaviour of these composites is investigated with impedance spectroscopy both at room temperature and elevated temperature.
In chapter 7 layered structures of YSZ sandwiched between two layers of Pt/YSZ composites are prepared via conventional processing. The capacitance behaviour of these structures is investigated at 550ºC with impedance spectroscopy.
The work described in Chapters 2 to 7 is summarised and evaluated in Chapter 8 and some recommendations for future research are given.

## References


1. A.F. Kip, Fundamentals of electricity and magnetism, Tosho Printing Co., Tokyo, Japan, 1969.
2. A.R. West, in Solid state chemistry and its applications, John Wiley & Sons Ltd., New York, USA, 1984, p. 525.
3. A. Morell and J.-C. Niepce, **13**, 173-232, 1991.
4. G. Goodman and T.G. Reynolds in Ceramic materials for electronics: processing, properties and applications. Edited by R.C. Buchanan, Marcel Dekker, Inc., New York, USA, 1991, p. 69.
5. S. van der Gijp, Preparation of homogeneously-doped barium titanate, *PhD Thesis*, University of Twente, Enschede, 1998.
6. W. S. Young and S.H. Knickerbocker, in Ceramic materials for electronics: Processing, properties and applications. Edited by R.C. Buchanan, Marcel Dekker, Inc., New York, USA, 1991, p. 489.
7. R. Höppener and A. Daemen, in CARTS-EUROPE '94, Electron. Components Inst. Int., 1995. Proc. 8th Eur. Pass. Comp. Symp., Crowborough, UK, October 17-20 (1994) p. 47.
8. A.L. Efros and B.I. Shklovskii, *Phys. Stat. Sol.*, **B** [76] 475-85, 1976.
9. D.S. McLachlan, *Mat. Res. Symp. Proc.*, **411**, 309-20, 1996.
10. V.E. Dubrov, M.E. Levinshtein and M.S. Shur, *Zh. Eksper. Teor. Fiz.*, **70**, 2014-24, 1976.
11. S. Trassatti and P. Kurzweil, *Platinum Metals Rev.*, **38** [2], 46-56, 1994.
12. J.P. Zheng and T.R. Jow, *J. Electrochem. Soc.*, **142** [1], L6-7, 1995.
13. M. Wixom, L. Owens, J. Parker, J. Lee, I. Song and L. Thompson, *Proc. Electrochem. Soc.*, **96** [25], 63-74, 1997.
14. R.A. Huggins, *Solid State Ionics*, **134**, 179-95, 2000.
15. P.W. Atkins, Physical chemistry, 4th edition, Oxford University Press, Oxford, 1990, p. 907.
16. R.D. Armstrong and M. Todd, in Solid state electrochemistry. Edited by P.G. Bruce, 1st edition, Cambridge University Press, Cambridge, 1997, p. 269.
17. J.P. Zheng, J. Huang and T.R. Jow, "The limitations of energy density for electrochemical capacitors", *J. Electrochem. Soc.*, **144** [6], 2026-31, 1997.
18. O. Yamamoto, in Solid state electrochemistry. Edited by P.G. Bruce, 1st edition, Cambridge University Press, Cambridge, 1997, p. 292.
19. T. Christen and M.W. Carlen, *J. Power Sources*, **91**, 210-16, 2000.
20. S. Sarangapani, B.V. Tilak and C.-P. Chen, *J. Electrochem. Soc.*, **143** [11], 3791-99, 1996.
21. P. Baudry and A. Marquet, "Applications of solid state electrolyte generators for electric utilities", *Electrochimica Acta*, **37** [9], 1627-9, 1992.
22. S. Sugimoto, I. Kouda and Y. Murai, *Elec. Eng. Japan*, **133** [3], 83-92, 2000.

23. L.P. Jarvis, T.B. Atwater and P.J. Cygan, *J. Power Sources*, **79**, 60-3, 1999.
24. A. Burke, *J. Power Sources*, **91**, 37-50, 2000.
25. C. Arbizzani, M. Mastragostino, L. Meneghello and R. Paraventi, *Adv. Mater.* **8** [4], 331-4, 1996.
26. M. Pham-Thi, G. Velasco and Ph. Colomban, *J. Mater. Sci. Lett.*, **5**, 415-7, 1986.
27. J.P. Zheng and T.R. Jow, *J. Electrochem. Soc.* **142** [1], L6-7, 1995.
28. H.J. Bang, W. Lu, F. Cao and J. Prakash, *Electrochem. Comm.*, **2**, 653-7, 2000.
29. C. Arbizzani, M. Catellani, M. Mastragostino and C. Mingazzini, *Electrochimica Acta*, **40** [12], 1871-6, 1995.
30. S. Panero, A. Clemente and E. Spila, *Solid State Ionics*, **86-88**, 1285-9, 1996.
31. K. Rajeshwar, C. Wei, W. Wampler, C.S.C. Bose, S. Basak, S. German, D. Evans and V. Krishna, *Polym. Prep.*, **35** [1], 234-5, 1994.
32. B.C.H. Steele, *Current Opinion Solid Sta.*, **1** 684-91, 1996.
33. S. Sarangapani, P.M. Lessner and A.B. LaConti, *U.S. Patent* 5 136 474, 1992.
34. S. Panero, E. Spila and B. Scrosati, *J. Electroan. Chem.*, **396**, 385-9, 1995.

# Chapter 2
# The electrochemical double-layer capacitance of yttria-stabilised zirconia

*The capacitance of the double layer at the interface between irreversible (current-blocking) gold electrodes and yttria-stabilised zirconia (YSZ) has been measured by impedance spectroscopy as a function of the applied electrode potential and yttria content (2-8 mol%). At moderate temperatures, 300-660 K, the dielectric constant of zirconia stabilised with 8 mol% yttria is thermally activated with an apparent activation energy of 12.6±2.1 kJ/mol. Above 700 K, where the oxygen vacancies in YSZ are rendered mobile, contributions arise from space charge polarisation at the blocking electrolyte/electrode interface. A simple thermodynamic model is presented for the formed double layer, based upon Gouy-Chapman theory, which takes into account the effect of site exclusion of the doubly ionised oxygen vacancies. Fair agreement is obtained with the experimental capacitance characteristics, showing a maximum around -125 mV at 822 K. The apparent activation energy of the dielectric constant of YSZ with 8 mol% yttria in the temperature range 700-900 K is found to be 116±34 kJ/mol.*

## Introduction

Stabilised zirconia is widely employed as the electrolyte in oxygen sensors, water electrolysers and solid oxide fuel cells, because of its high oxygen ion conductivity at elevated temperatures [1]. Surprisingly, despite its great technological interest only little attention has been paid to the nature of the double layer at the metal electrode-solid oxide electrolyte interface and the magnitude of its capacitance. Determination of the latter is usually based on studies of electrode kinetics at porous metal electrodes using ac impedance spectroscopy. Corresponding results are evaluated by modelling the electrode response to an equivalent circuit consisting of linear circuit elements. Robertson and Michaels [2] have listed various equivalent circuits used in the interpretation of experimental data by different investigators, who obtained widely different values for the interface capacitance. Besides the uncertainty in the true contact area between the porous metal electrode and the solid oxide electrolyte, it is recognised that time dependent faradaic processes may obscure the charging of the double layer. This last effect is liable to be very important in the case of porous electrodes and makes quantitative measurement of the interface capacitance very difficult.

In this work, the capacitance at the interface between irreversible (current-blocking) gold electrodes and yttria-stabilised zirconia (YSZ) has been measured by low-frequency impedance spectroscopy, as a function of electrode potential and yttria content. The experimental data are compared with theoretical predictions of the Gouy-Chapman theory [3]. In this model, the double layer is produced by the distribution of mobile oxygen vacancies in the electrolyte in the vicinity of the interface. Details of this distribution depend only on the interface potential and the defect structure. The model takes into account the effect of site exclusion, which is necessary in view of the high concentration of oxygen vacancies in stabilised zirconia. In addition, to enable quantitative comparison of the model to the experimental data the dielectric properties of YSZ at low temperatures (<500 K) have been measured.

## Theory

In the following, a continuum theory of the double layer capacitance of yttria-stabilised zirconia against an inert blocking electrode is given. It is assumed that, under conditions of ionic equilibrium at the interface, a redistribution of the diffuse layer formed by the mobile charge carriers takes place in response to a change in the electrochemically fixed interface potential, as devised by Gouy and Chapman [3]. The theory qualitatively fits the experimental voltage dependence of the capacitance. In the model, neither size effects of ionic charge carriers nor specific adsorption at the metal-solid oxide electrolyte interface are considered.

The mobile charge carriers in YSZ are electrons, electron holes and doubly ionised oxygen vacancies. Charge neutrality requires that $[Y_{Zr}']+n=p+2[V_O^{\cdot\cdot}]$, where $[Y_{Zr}']$ is the concentration of dopant ions, n the concentration of electrons, p the concentration of electron holes and $[V_O^{\cdot\cdot}]$ the concentration of oxygen vacancies. As long as experiments are performed in the electrolytic domain, a good approximation is that $n, p \ll [Y_{Zr}'], [V_O^{\cdot\cdot}]$, leaving oxygen vacancies as the single mobile ionic charge carriers.

The chemical potential of non-interacting oxygen vacancies in stabilised zirconia is given by [4],

$$\mu_{V_O^{\cdot\cdot}} = \mu^0_{V_O^{\cdot\cdot}} + k_B T \ln \frac{\left[V_O^{\cdot\cdot}\right]}{1-\left[V_O^{\cdot\cdot}\right]}, \tag{1}$$

where $[V_O^{\cdot\cdot}]$ is the molar fraction of oxygen vacancies, $\mu^0_{V_O^{\cdot\cdot}}$ a concentration-independent term and $k_B$ the Boltzmann constant. Under conditions of ionic equilibrium, the electrochemical potential of the oxygen vacancies in the zirconia phase, $\eta_{V_O^{\cdot\cdot}}$, is constant and independent of location. It follows that,

$$\eta_{V_O^{\cdot\cdot}} = \mu^0_{V_O^{\cdot\cdot}} + k_B T \ln \frac{\left[V_O^{\cdot\cdot}\right](x)}{1-\left[V_O^{\cdot\cdot}\right](x)} + q\phi(x), \tag{2}$$

where $q$ is the charge on oxygen vacancies ($q = 2e$, with $e$ the elementary charge) and $\phi(x)$ the local electrical potential. The implicit assumption made

here is that in equilibrium state, $\mu^0_{V_O^{\cdot\cdot}}$ at the surface is equal to that in the bulk. Eq. (2) can be rearranged into

$$\left[V_O^{\cdot\cdot}\right](x) = \frac{\left[V_O^{\cdot\cdot}\right]_{Bulk} e^{\frac{-2e\phi(x)}{k_B T}}}{1+\left[V_O^{\cdot\cdot}\right]_{Bulk}\left(e^{\frac{-2e\phi(x)}{k_B T}} - 1\right)}. \tag{3}$$

This expression is merely an extension of the regular Boltzmann distribution of charge carriers in the field of the interface, as it takes into account the effect of site exclusion [4]. The use of the simple Boltzmann form, often considered in liquid electrolytes, is not appropriate in ionic solids in view of the high defect concentration at the interface in conjunction with the limited number of available lattice sites. In the case of a negative potential, accumulation of positive charge carriers (oxygen vacancies) occurs at the interface. Similarly, a positive potential leads to depletion of oxygen vacancies at the interface, leaving the immobile negatively charged yttrium dopant ions behind. The zero potential has been taken at distances far from the electrode surface ($x \to \infty$), where the oxygen vacancy concentration reaches the bulk concentration, $[V_O^{\cdot\cdot}]_{Bulk}$. The latter postulate is valid provided that the thickness of the diffuse double layer is small compared with the sample dimensions.

The variation of the electrical potential in the electrolyte satisfies Poisson's equation, which in one dimension takes the form:

$$\frac{d^2\phi(x)}{dx^2} = -4\pi\frac{\rho(x)}{\varepsilon}, \tag{4}$$

where $\rho(x)$ is the local volume charge density and $\varepsilon$ the dielectric constant in the space-charge layer. The volume charge density at any point is formed by contributions from mobile and immobile charge carriers, i.e. oxygen vacancies and yttrium dopant ions,

$$\rho(x) = \sum_i q_i c_i(x) = c\left(2e\left[V_O^{\cdot\cdot}\right](x) - e\left[Y'_{Zr}\right]\right) = 2ce\left(\left[V_O^{\cdot\cdot}\right](x) - \left[V_O^{\cdot\cdot}\right]_{Bulk}\right), \tag{5}$$

where $c$ is the density of anionic lattice sites in YSZ. Combining Eqs. (3), (4) and (5) results in

$$\frac{d^2\phi(x)}{dx^2} = -\frac{8\pi ec}{\varepsilon}\left[\mathrm{V_O^{\cdot\cdot}}\right]_{\mathrm{Bulk}}\left(\frac{\mathrm{e}^{\frac{-2e\phi(x)}{k_\mathrm{B}\cdot T}}}{1+\left[\mathrm{V_O^{\cdot\cdot}}\right]_{\mathrm{Bulk}}\left(\mathrm{e}^{\frac{-2e\phi(x)}{k_\mathrm{B}\cdot T}}-1\right)}-1\right). \tag{6}$$

The boundary condition for the potential is

$$\lim_{x\to\infty}\frac{d\phi(x)}{dx} = 0\,. \tag{7}$$

In order to integrate Eq. (6) the definition of the electrical field strength $E(x)$ is used, given by $E(x)=-d\phi(x)/dx$, and

$$\frac{d^2\phi(x)}{dx^2} = -\frac{dE(x)}{dx} = -\frac{dE(x)}{d\phi(x)}\frac{d\phi(x)}{dx} = E(x)\frac{dE(x)}{d\phi(x)}\,. \tag{8}$$

Integration of Eq. (6) gives

$$\frac{d\phi(x)}{dx} = \pm\sqrt{\frac{16\pi ec}{\varepsilon}\left[\left[\mathrm{V_O^{\cdot\cdot}}\right]_{\mathrm{Bulk}}\phi(x)+\frac{k_\mathrm{B}T}{2e}\ln\left[1+\left[\mathrm{V_O^{\cdot\cdot}}\right]_{\mathrm{Bulk}}\left(\mathrm{e}^{\frac{-2e\phi(x)}{k_\mathrm{B}T}}-1\right)\right]\right]}\,, \tag{9}$$

where the plus or minus sign refers to a negative or positive value of $\phi(0)$, respectively. Eq. (9) cannot be solved analytically, but the surface charge density at the metal $\sigma^\mathrm{M}$ can be calculated using the Gauss theorem,

$$\sigma^\mathrm{M} = -\varepsilon\left(\frac{d\phi(x)}{dx}\right)_{x=0}\,. \tag{10}$$

The specific differential double-layer capacitance $C_\mathrm{diff}$ is defined as

$$C_\mathrm{diff}(\phi) = \frac{d\sigma^\mathrm{M}}{d\phi}\,. \tag{11}$$

From Eqs. (9)-(11) it then follows that

$$C_{\mathrm{diff}}(\phi_{\mathrm{b}}) = \mp \frac{\sqrt{4\pi\varepsilon e c}\left[\mathrm{V_O^{\cdot\cdot}}\right]_{\mathrm{Bulk}}\left(1 - \frac{\mathrm{e}^{\frac{-2e\phi_{\mathrm{b}}}{k_{\mathrm{B}}T}}}{1+\left[\mathrm{V_O^{\cdot\cdot}}\right]_{\mathrm{Bulk}}\left(\mathrm{e}^{\frac{-2e\phi_{\mathrm{b}}}{k_{\mathrm{B}}T}} - 1\right)}\right)}{\sqrt{\left[\mathrm{V_O^{\cdot\cdot}}\right]_{\mathrm{Bulk}}\phi_{\mathrm{b}} + \frac{k_{\mathrm{B}}T}{2e}\ln\left[1+\left[\mathrm{V_O^{\cdot\cdot}}\right]_{\mathrm{Bulk}}\left(\mathrm{e}^{\frac{-2e\phi_{\mathrm{b}}}{k_{\mathrm{B}}T}} - 1\right)\right]}}, \tag{12}$$

where $\phi_{\mathrm{b}}$ is the potential at the electrode/electrolyte interface. The variables influencing the capacitance are the applied electrode potential, temperature and bulk concentration of oxygen vacancies, hence, the dopant concentration of yttrium ions. In Eq. (12), $\varepsilon$ refers to the effective dielectric constant in the space charge region near the electrode. It is emphasised here that its value may deviate substantially from the corresponding bulk dielectric constant.

The differential capacitance at zero electrode potential can be obtained by Taylor expansion of Eq. (12). This leads to

$$C_{\mathrm{diff}}(0) = 4e\sqrt{\frac{\pi\varepsilon c}{k_{\mathrm{B}}T}\left[\mathrm{V_O^{\cdot\cdot}}\right]_{\mathrm{Bulk}}\left(1-\left[\mathrm{V_O^{\cdot\cdot}}\right]_{\mathrm{Bulk}}\right)}\,. \tag{13}$$

The overall capacitance $C_{\mathrm{overall}}$ of a symmetrical cell, with electrodes taken to be identical, can be regarded as a circuit consisting of two capacitances in series.

$$\frac{1}{C_{\mathrm{overall}}} = \frac{1}{C_+} + \frac{1}{C_-}\,. \tag{14}$$

Here $C_+$ and $C_-$ are the capacitances at the positively and negatively charged electrodes, respectively and the capacitance at the electrodes can be calculated with

$$C_+ = \frac{Q}{\phi_+} \quad \text{and} \quad C_- = \frac{Q}{\phi_-}\,, \tag{15}$$

where $\phi_+$ and $\phi_-$ are the potential at the positive and the negative electrode, respectively. $Q$ is the total charge stored at the electrodes. Rewriting the

definition of the differential capacitance results in an equation for the total charge

$$Q = A\int_0^{\phi_+} C_{\text{diff}}\,d\phi = -A\int_0^{\phi_-} C_{\text{diff}}\,d\phi\,, \tag{16}$$

where $A$ is the electrode surface area.

From Eq. (14) a capacitance $C_{\text{norm}}$, normalised with respect to the bulk concentration of oxygen, can be defined:

$$C_{\text{norm}} = \frac{C_{\text{overall}}}{\sqrt{\left[\text{V}_\text{O}^{\cdot\cdot}\right]_{\text{Bulk}}\left(1-\left[\text{V}_\text{O}^{\cdot\cdot}\right]_{\text{Bulk}}\right)}} = 2e\sqrt{\frac{\pi\varepsilon c}{k_\text{B}T}}\,. \tag{17}$$

## Experimental

Commercial yttria-stabilised zirconia powders (Tosoh Corporation, Tokyo, Japan), denoted as TZ-2Y, TZ-3Y and TZ-8Y for samples containing 2, 3 and 8 mol% yttria, respectively, were pressed into pellets under 400 MPa . The TZ-2Y and TZ-3Y pellets were sintered to more than 98% dense in air at 1400ºC for 4 h, while the TZ-8Y pellet was sintered to more than 99% dense at 1480ºC for 2 h. Prior to use the disks were polished using a 3 μm diamond emulsion.

For differential capacitance measurements the YSZ pellets were cut into discs (∅ 16.0 mm; thickness 4.0 mm). A circular notch was carved into the cylindrical side of the disc. Around the notch a platinum wire, serving as the reference electrode, was attached using platinum paste. One of the flat surfaces was painted with platinum paste to serve as the counter electrode. The platinum electrode was fired in air at 1200ºC and then cooled slowly. The Pt electrode was porous after this pre-treatment. The opposite flat surface was sputtered with a dense gold layer to serve as the working electrode.

A schematic drawing of the cell is shown in Fig. 1. Measurements were performed under a nitrogen atmosphere at a temperature of 822 K. The potential difference between the working and reference electrode was varied between -250 and +50 mV using a potentiostat (Potentiostat LB 75L, Bank Elektronik, Göttingen, Germany). Three-point impedance measurements were performed using a frequency response analyser (Solartron Instruments 1250 FRA, Schlumberger Technologies Ltd., Farnborough, Hampshire, England) at 10 mV rms in the frequency range of 10 mHz to 60 kHz. The experimental impedance dispersion curves were fitted to an equivalent circuit consisting of a constant phase element (CPE) and a resistance in series using the Equivalent Circuit software program [5]. The differential capacitance at zero frequency was calculated from the CPE values.

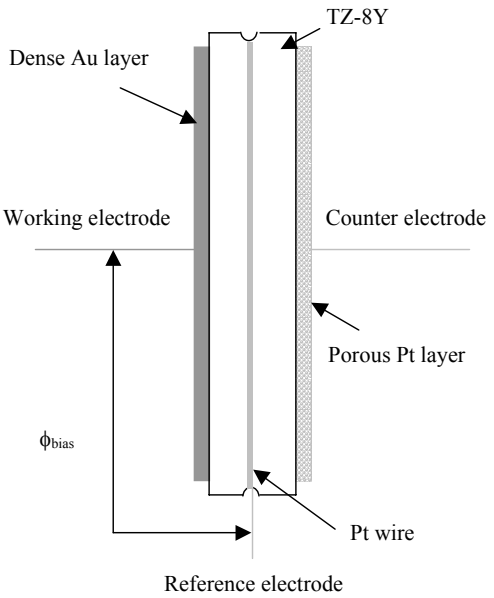


***Fig. 1:*** *Schematic picture of the experimental set-up for differential capacitance measurements.*

For dielectric constant and overall capacitance measurements, the compacts were cut into disks of 13.5 mm diameter and 2.0 mm thickness. A dense gold layer was sputtered on both sides. 2-point impedance measurements were carried out in the temperature range 298-873 K and the same frequency range as used in the differential capacitance measurements.

## Results and discussion

Results from 2-point impedance measurements at room temperature are shown in Table 1. The relative dielectric constants $\varepsilon_r$ were determined from

the high frequency behaviour (> 1 kHz) using the standard expression for the geometric capacitance $C=\varepsilon_0\varepsilon_r A/d$, where $\varepsilon_0$ is the permittivity of vacuum, $\varepsilon_r$ is the bulk dielectric constant, and $A$ and $d$ are the geometric surface area and thickness of the capacitor, respectively. The tetragonal zirconia samples (2 and 3 mol% yttria) show the highest relative dielectric constant, while the cubic zirconia sample (8 mol% yttria) has a slightly lower value. Thompson et al. [6] measured the relative dielectric constants of monoclinic, tetragonal and cubic zirconia, stabilised with different concentrations of various ions. Some of their results are listed in Table 1 for comparison. The value found in the present study for the stabilised zirconia containing 3 mol% of yttria is in close agreement with the value obtained by Thompson et al. Their suggestion that the relative dielectric constant is determined primarily by the crystallographic form, rather than by the nature or amount of the dopant, is supported by the results obtained in the present study.

***Table 1:*** *Dielectric constants of yttria-stabilised zirconia with varying yttria content; T = 298 K; f=1-60 kHz.*

| Mol% $Y_2O_3$ | Structure | $\varepsilon_r$ Experimental | $\varepsilon_r$ Thompson et al. [6] |
|---|---|---|---|
| 0 | Monoclinic | - | 23.0 |
| 2 | Tetragonal | 40.5 | - |
| 3 | Tetragonal | 39.5 | 39.5 |
| 6 | Tetragonal | - | 39.0 |
| 8 | Cubic | 28.7 | - |

The temperature dependence of the relative dielectric constant of cubic zirconia (TZ-8Y), calculated with the same expression as above from high frequency measurements, is shown in Fig. 2. A logarithmic dependence on temperature can be clearly seen. The activation energy of $\varepsilon_r$ is equal to $12.6 \pm 2.1$ kJ/mol. The magnitude of the activation energy is reasonably close to the value of approximately 19.2 kJ/mol reported by Jonscher and Reau [7] for the relative dielectric constant of lead fluoride**.**

The results from overall capacitance measurements performed at 822 K are listed in Table 2. In qualitative agreement with the model predictions, the capacitance increases with yttria concentration. The measured capacitances

were normalised to the bulk vacancy concentrations in accordance with Eq. (17). The results listed in Table 2 show that these normalised capacitances have similar values within the experimental error. This indicates that the oxygen vacancy concentration plays a decisive role in determining the dou-

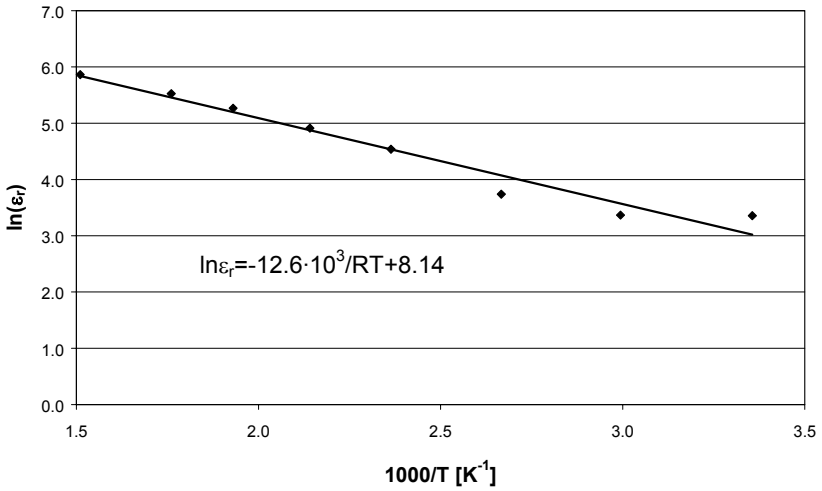


***Fig. 2:*** *Experimental dielectric constant of TZ-8Y as a function of temperature; f > 1 kHz.*

ble-layer capacitance at high temperature.

***Table 2:*** *Overall capacitances in YSZ with varying yttria content; T = 822 K; f < 10 Hz.*

| Mol% $Y_2O_3$ | $C_{overall}$ [F $m^{-2}$] | $C_{norm}$ [F $m^{-2}$] |
|---|---|---|
| 2 | 0.80 | 8.12 |
| 3 | 1.29 | 10.8 |
| 8 | 1.63 | 8.63 |

Overall capacitance measurements were performed on TZ-8Y in the temperature interval 700-900 K. At temperatures above approximately 700 K yttria-stabilised zirconia becomes significantly oxygen ion-conducting, and is therefore capable of forming a double-layer capacitance. At temperatures higher than 900 K the gold electrodes started to sinter, leading to irreproducible results. Fig. 3 shows the increase

of the overall capacitance with temperature. Eq. (15) was fitted to the experimental data using the relative dielectric constant as a fit parameter. In contrast to the high frequency data shown in Fig. 2, the low frequency (< 1 Hz) measurements show a different activation energy for the relative dielectric constant (116 ± 34 kJ/mol). This is due to the fact that the activation energy for the relative dielectric constant contains an additional ther-

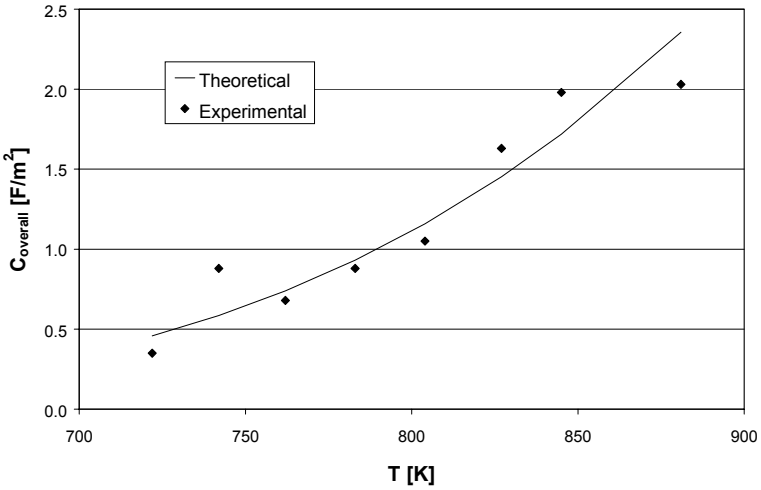


***Fig. 3:*** *Experimental and theoretical overall capacitances in TZ-8Y as a function of temperature; f < 100 Hz.*

mally activated component due to space-charge polarisation.

In Fig. 4 the experimental differential capacitances of TZ-8Y at 822 K are shown as a function of electrode bias potential. The trend predicted by Eq. (12) is also shown. The experimental data at $\phi_b$=0 were fitted to Eq. (12). This yielded a value $\varepsilon_r \sim 1$ for the relative dielectric constant in the double-layer region.

As is observed here, the value of the dielectric constant in the double layer can be significantly smaller than the bulk dielectric constant [8]. The qualitative agreement between the experimental and theoretically predicted curves in Fig. 4 is good. The experimental differential capacitance reaches a maximum value at approximately -125 mV, which is close to the maximum of -

143 mV predicted by the model. In view of Eq. (11), a maximum in the differential capacitance will occur at the bias potential $\phi_C$ at which the surface

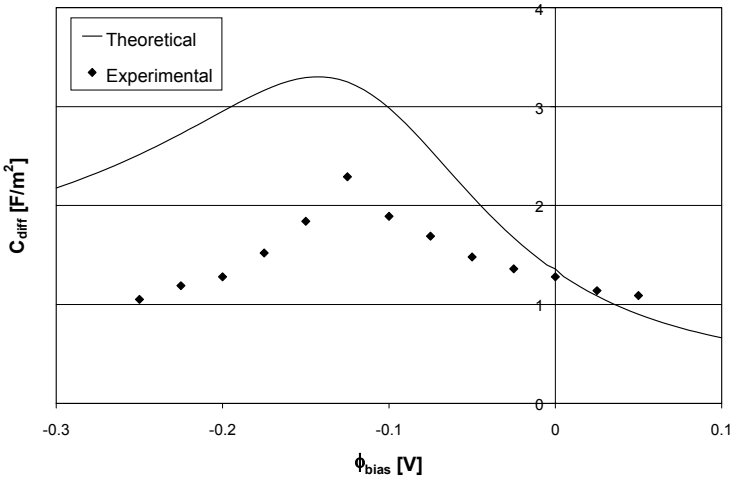


***Fig. 4:*** *Experimental and theoretical differential capacitances in TZ-8Y as function of bias potential; T = 822 K; f < 100 Hz.*

charge $\sigma^M$ changes most rapidly with changing potential.

To a first order of approximation, this potential coincides with the electrode bias potential at which the oxygen vacancy concentration $[V_O^{\cdot\cdot}]$ at the interface changes most rapidly with bias potential, or, when expressed mathematically, where $(d^2[V_O^{\cdot\cdot}]/d\phi^2)=0$. From Eq. (3) it can be calculated that

$$\phi_C \approx -\frac{k_B T}{2e} \ln\left(\frac{1-\left[V_O^{\cdot\cdot}\right]_{Bulk}}{\left[V_O^{\cdot\cdot}\right]_{Bulk}}\right). \qquad (15)$$

Using this approximation, $\phi_C \approx$-115 mV for TZ-8Y at 822 K. In contrast to these results, Robertson and Michaels [2], who measured the differential double-layer capacitance at an interface between a porous platinum electrode and YSZ at 828-968 K, did not observe a bias potential dependency of the differential capacitance. It is well possible that this is due to the reversible nature of the working electrode they employed.

Relatively large differences between the predicted and experimental data in Fig. 4 occur at large negative electrode bias potentials. This may be understood by considering that the model proposed here assumes that every oxygen site in the lattice can be occupied by an oxygen vacancy. In practice the oxygen vacancy concentration will most likely remain (much) smaller. Thus, the present model overestimates the differential double-layer capacitances at relatively low (negative) electrode potentials.

Using the results shown in Fig. 4, the capacitance at the electrodes can be calculated with Eqs. (15) and (16). The capacitance at the positively charged electrode is smaller than at the negatively charged electrode and decreases with increasing potential. According to Eq. (14) the overall capacitance thus decreases with increasing potential difference between the electrodes.

## Conclusions

At room temperature the relative dielectric constant of yttria-stabilised zirconia compacts with varying amounts of yttria depends on the crystal structure. Tetragonal zirconia has the highest value (~40), while the value for cubic zirconia is ~29. In the temperature interval 300-660 K the dielectric constant of cubic zirconia appears to be thermally activated (12.7 ± 2.1 kJ/mol).

At temperatures above 700 K, where the oxygen vacancies are mobile, contributions arise from space charge polarisation at the blocking electrolyte/electrode interface. The overall capacitance was found to increase with increasing oxygen vacancy concentration. The results are in fair agreement with model predictions based upon Gouy-Chapman theory. The differential capacitance reached a maximum at -125 mV, which is close to the value predicted by the model. The activation energy of the dielectric constant in the temperature interval 700-900 K was 116 ± 34 kJ/mol. The discrepancy between model predictions and experimental data at large negative bias potentials may be explained by considering that it is highly unlikely that all oxygen sites in the lattice can be occupied by vacancies, which was one of the underlying assumptions in the derivation of the model.

## References

[1] T. Kudo, in The CRC Handbook of Solid State Electrochemistry, Eds. P.J. Gellings and H.J.M. Bouwmeester, CRC Press, Boca Raton, 1997, p. 195.

[2] N.L. Robertson and J.N. Michaels, *J. Electrochem. Soc*., **138** [5], 1494, 1991.

[3] A.J. Bard and L.R. Faulkner, Electrochemical methods: Fundamentals and applications, John Wiley & Sons, New York, 1980, p. 488.

[4] M.H.R. Lankhorst, Thermodynamic and transport properties of mixed ionic-electronic conducting perovskite-type oxides, PhD thesis, University of Twente, Enschede, 1997.

[5] B.A. Boukamp, *Solid State Ionics*, **20**, 31, 1986.

[6] D.P. Thompson, A.M. Dickins and J.S. Thorp, *J. Mater. Sci*., **27**, 2267, 1992.

[7] A.K. Jonscher and J.M. Réau, *J. Mater. Sci*., **13**, 563, 1978.

[8] K. Natori, D. Otani and N. Sano, *Appl. Phys. Lett*., **73**, 632, 1998.

# Chapter 3
# The defect structure of the double layer in yttria-stabilised zirconia

*The space charge density of 2-10 mol% yttria-stabilised zirconia at the interface with a gold electrode was determined from differential capacitance measurements at 748-848 K. The oxygen vacancy fraction in the space charge layer was calculated as function of bias potential, temperature and composition by fitting experimental data at positive bias potential to a Boltzmann-type equation. The vacancy concentration in the space charge layer increases with decreasing bias potential and reaches a temperature-dependent maximum. This behaviour can be understood under the assumption that only a fraction of the oxygen sub-lattice is available for oxygen vacancy distribution. This volume fraction increases with temperature and yttria concentration. The activation energy for this process is in the range of 0.27 to 0.46 eV.*

## Introduction

Knowledge of the defect structure of solid oxides at the interface with the electrodes is of importance for the development of devices like oxygen sensors [1], oxygen separation membranes [2], and SOFCs [3]. In this chapter the space charge density of a solid oxide electrolyte at the interface with a blocking metal electrode is determined using differential capacitance measurements. With this method, changes in the near-surface concentrations of mobile charge carriers can be determined. The definition of the specific differential capacitance $C_{dif}$ is

$$C_{dif}(\varphi_b) = \left( \frac{d\sigma^M}{d\phi_b} \right), \tag{1}$$

where $\sigma^M$ is the surface charge density (C/m$^2$) on the metal and $\phi_b$ is the applied bias potential.
The space charge layer can be described using the Poisson equation

$$\left( \frac{d^2\phi(x)}{dx^2} \right) = -\frac{4\pi\rho(x)}{\varepsilon}, \tag{2}$$

with $\phi(x)$ the local electrical potential in the oxide at a distance $x$ from the interface, $\rho(x)$ the space charge density in the oxide, and $\varepsilon$ the dielectric constant ($=\varepsilon_0\varepsilon_r$, with $\varepsilon_0$ the permittivity of vacuum and $\varepsilon_r$ the relative dielectric constant of the oxide). In combination with the relationship between the surface charge on the metal and the potential gradient at the interface, i.e.,

$$\sigma^M = -\varepsilon \left( \frac{d\phi}{dx} \right)_{x=0}, \tag{3}$$

it can be established easily [4] that

$$\rho(0) = -\frac{\sigma^M}{4\pi\varepsilon} \left( \frac{d\sigma^M}{d\phi(0)} \right). \tag{4}$$

Using Eq. (1) and substituting $\phi_b$, the applied bias potential, for $\phi(0)$, it follows that

$$\rho(0) = -\frac{\sigma^{M} C_{dif}(\phi_b)}{4\pi\varepsilon}. \qquad (5)$$

In this chapter, results of differential capacitance measurements at yttria-stabilised zirconia (YSZ)/gold interfaces are reported. The only mobile charge carriers in this system are oxygen ions, which are mobile due to the presence of vacant sites in the oxygen sub-lattice. The space charge density in YSZ is determined by the concentrations of yttrium ions and oxygen vacancies, i.e.,

$$\rho(x) = \frac{e}{v_0}(2[V_O^{\cdot\cdot}](x) - [Y_{Zr}^{'}]) \qquad (6)$$

where $e$ is the absolute electron charge, $v_0$ the unit cell volume of YSZ, and $[V_O^{\cdot\cdot}]$ and $[Y_{Zr}']$ are the concentrations of oxygen vacancies and yttrium ions, respectively. The unit cell volume $v_0$ is taken equal to 136.4 $Å^3$ [5]. Under the conditions covered by the experiments, it can be assumed safely that the near-surface yttrium concentration $[Y_{Zr}']$ in Eq. (6) is equal to its bulk concentration [4]. Hence, changes of the space charge density are proportional to changes of the oxygen vacancy concentration.

## Experimental

Polycrystalline yttria-stabilised zirconia powders containing 2, 3, 8, and 10 mol% yttria, respectively, were obtained commercially (Tosoh Corp., Tokyo, Japan). Their nominal purities are 99.3%, 99.3%, 98.5% and 99.8%, respectively. The main impurities as reported by the supplier are $Al_2O_3$, $SiO_2$, $Fe_2O_3$ and $Na_2O$, all with impurity levels below 0.5%. The powders with 2 and 3 mol% yttria have a tetragonal structure, while the compositions with 8 and 10 mol% yttria have a cubic structure.

The powders were pressed uniaxially at 75 MPa, followed by isostatic pressing at 400 MPa. The green compacts were sintered in air at 1500ºC for 6 h to densities higher than 99% of theoretical. The grain sizes varied from 2-8 μm for 2 mol% $Y_2O_3$-doped YSZ to 3-10 μm for 10 mol% $Y_2O_3$-doped YSZ.

For the differential capacitance measurements the YSZ compacts were cut into discs (∅ 16.0 mm; thickness 4.0 mm) and polished with a 3 μm diamond emulsion. A circular notch was carved into the cylindrical side of the disc. Around the notch a platinum wire, serving as the reference electrode, was attached using platinum paste. One of the flat surfaces was painted with platinum paste and served as counter electrode. After firing at 1200ºC the Pt layer became porous, which is required to prevent polarisation at this electrode. The opposite flat surface was sputtered with a dense (ionically blocking) gold layer to serve as the working electrode [6]. This type of cell with a reversible and an irreversible electrode is commonly referred to as the Hebb-Wagner cell, and is normally used for measuring the partial electronic conductivity in mixed ionic-electronic conductors. The sample was kept at constant temperature in an atmosphere that was flushed with nitrogen.

A bias potential was applied between the reference and working electrode (Potentiostat LB 75L, Bank Elektronik, Göttingen, Germany). Three-point electrical impedance spectroscopy measurements were performed at 10 mV rms using a frequency response analyser (Solartron Instruments 1250 FRA, Schlumberger Technologies Ltd., Farnborough, Hampshire, England) in the frequency range from 10 mHz to 60 kHz. The experimental impedance frequency dispersion curves were interpreted in terms of a constant phase element (CPE) and a resistance in parallel. The differential capacitances were calculated from the CPE data. [7]. Experiments were performed in the temperature range 748-848 K. At lower temperatures, the oxygen vacancies are rendered immobile. At temperatures above 873 K, the effect of slow sintering of the gold electrode made reliable measurements impossible.

## Results and discussion

To prevent blistering of the working electrode, caused by the release of oxygen at high potentials, no measurements were performed at bias potentials $\phi_b$ larger than +50 mV. At low potentials, measurements were performed down to bias potentials at which the data could no longer be interpreted in terms of the equivalent circuit as described above. The lower limits for measurements were found to lie between –50 mV and -250 mV, depending on temperature and yttria concentration. Fig. 1 shows the measured differential capacitances

of 8 mol% $Y_2O_3$-doped YSZ at different temperatures. The following discussion is limited mainly to the analysis of these data. It should be stressed that similar trends were observed for the other compositions, and the analysis of those data is therefore similar to the one discussed below. In general it was observed that for all compositions the differential capacitance increases with temperature. Moreover, with increasing yttria concentration the absolute values of the differential capacitance increased and the maximum values of

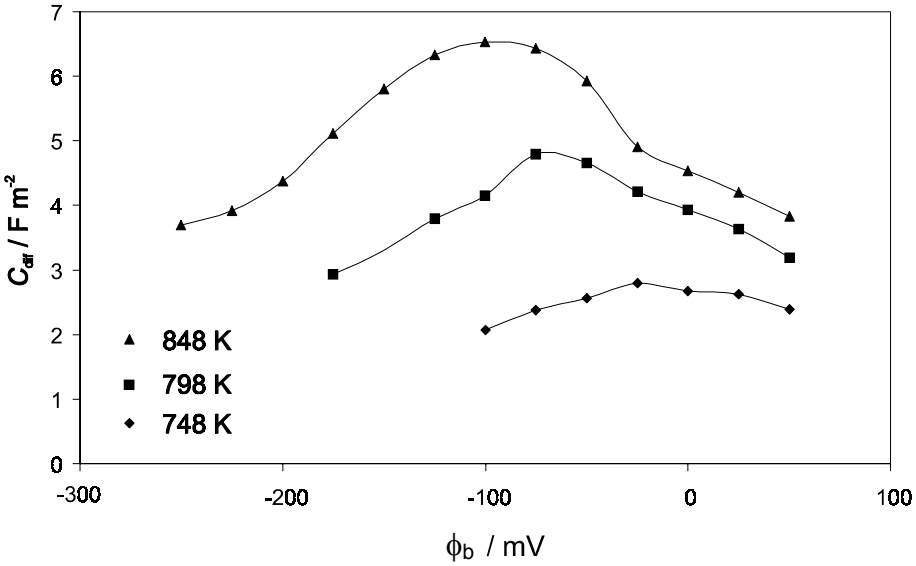


***Fig. 1:*** *Differential capacitances of 8 mol% $Y_2O_3$ doped YSZ versus bias potential.*

the differential capacitance shifted to lower bias potentials.

The absolute values of the differential capacitance varied from one sample to the other by factors up to 3, although the exhibited trends with respect to changes of bias potential were the same for all samples of similar composition. The variations are attributed to changes in the near-surface defect structure of YSZ. Since it is well known that the reproducibility in the measurement of double-layer capacitances is poor [8], no attempt was made to explain the absolute values.

Eqs. (5) and (6) can be used to calculate oxygen vacancy concentrations if the value of $\varepsilon_r$ in Eq. (5) is known. Bulk values of $\varepsilon_r$ at room temperature

reported in literature are 39-41 for tetragonal (2-6 mol% $Y_2O_3$) YSZ [6,9], and 23-30 for cubic YSZ [6,10-12]. However, the local dielectric constant near an interface can be much smaller than in the bulk [13]. This is due to

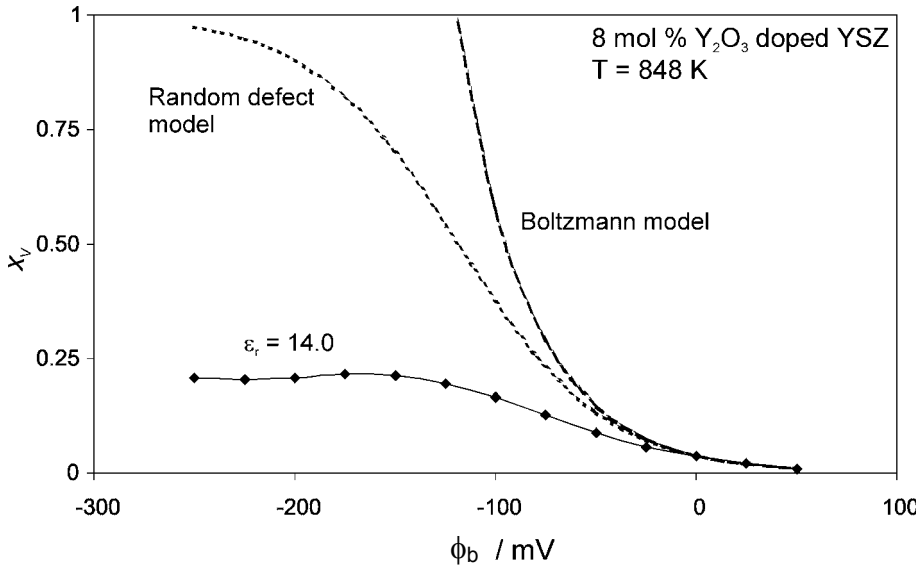


***Fig. 2:*** *Comparison of surface oxygen vacancy fractions of 8 mol% $Y_2O_3$ doped YSZ at 848 K as calculated from experimental data using Eq. (2) assuming $\varepsilon_r$=14.0, and predicted values according to Boltzmann-type equation and the random defect model.*

the reduction of the ionic polarisability.

To find an accurate $\varepsilon_r$ value for a sample at a given temperature, it is assumed that upon variation of the bias potential the oxygen vacancy fraction at low absolute concentration follows the trend predicted by the following Boltzmann-type expression [14-16]:

$$x_V = x_V^0 \exp\left(-z_V e\phi_b / k_B T\right). \qquad (7)$$

Here $x_V$ is the oxygen vacancy fraction in the oxygen sub-lattice, $T$ is the temperature, $z_V$ the formal charge of an oxygen vacancy (=2), $k_B$ the Boltzmann constant and $x_V^0$ the oxygen vacancy defect fraction at zero bias potential, which corresponds to the bulk concentration. The oxygen vacancy

fraction is related to the oxygen vacancy concentration by $x_V=[V_O^{\cdot\cdot}]/\chi_V$, where $\chi_V$ is the theoretically attainable defect concentration per unit cell. For the unit cell $(Zr,Y)_4O_8$, this value for $\chi_V$ is equal to 8. For the compositions under investigation the vacancy concentration is sufficiently low for Eq. (7) to yield reliable predictions when $\phi_b \geq 0$. Under these conditions the defect fraction is even decreased with respect to the fraction in the YSZ bulk. Hence, the value of $\varepsilon_r$ in Eq. (5) is chosen such that the oxygen vacancy concentration in Eq. (6) is in optimal agreement with the theoretical curve (Eq. (7)) for $\phi_b \geq 0$. In this manner, for each $C_{dif}$-$\phi_b$ isotherm the corresponding value of $\varepsilon_r$ is determined, under the assumption that $\varepsilon_r$ is independent of $\phi_b$.

Regarding the $C_{dif}$-$\phi_b$ isotherm of 848 K shown in Fig. 1, the best fit was obtained with $\varepsilon_r=14.0$. The experimental vacancy fractions, calculated using this value of $\varepsilon_r$, are shown in Fig. 2. The predictions of the Boltzmann-like model are shown for comparison. The same fitting procedure was also applied to the other $C_{dif}$-$\phi_b$ isotherms.

The simplest way to extend this Bolzmann-like model is to apply the restriction of site exclusion [17,18]. This yields the random defect model, in which all vacancies are distributed randomly over all oxygen sub-lattice sites. This model was used in the previous chapter [6]. A curve calculated on the basis of the random defect model is shown in Fig. 2 for comparison. The curve does not deviate significantly from the predictions of Eq. (7) at high $\phi_b$, but it does not explain the experimental behaviour at low potential.

The oxygen vacancy fractions at the interface in 8 mol% $Y_2O_3$ doped YSZ at several temperatures calculated using fitted $\varepsilon_r$ values are shown in Fig. 3. The $C_{dif}$-$\phi_b$ isotherms show similar behaviour at high $\phi_b$, but deviate at lower values. At low bias potentials a temperature-dependent plateau is reached. These plateaus are indicated by dotted lines. For the other compositions similar behaviour is observed. However, the height of the plateau increases with increasing yttria concentration in YSZ. This effect is not surprising since the bulk oxygen vacancy is proportional to the yttria concentration. The site exclusion principle alone can not explain the temperature depend-

ence of the maximum, since it assumes a finite and constant number of

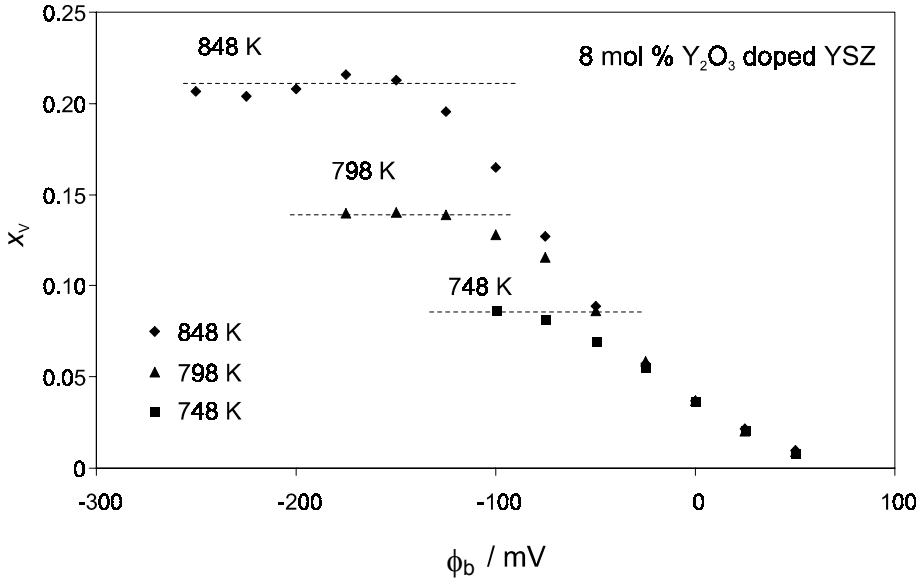


***Fig. 3:*** *Oxygen vacancy fractions in YSZ with 8 mol% $Y_2O_3$ as a function of temperature and bias potential, calculated using optimized values of $\varepsilon_r$.*

available oxygen lattice sites.

The temperature dependence of the experimentally determined maximum vacancy fraction $x_V^{max}$ was fitted to an Arrhenius-type equation

$$x_V^{max}(T) = A\exp\left(-E/k_B T\right), \tag{8}$$

where $E$ is an enthalpy-like parameter, and $A$ a pre-exponential factor. The values for $E$ and $A$ for different YSZ compositions are listed in Table 1. Both $E$ and $\ln A$ increase with yttrium concentration within the experimental error.

The observed behaviour can be explained if it is assumed that only a fraction of all oxygen sub-lattice sites are available for oxygen vacancy distribution and that this fraction increases with temperature. If $x_V^{max}(T)$ represents the temperature-dependent fraction of sites accessible for vacancy distribution, then the number of permutations $\Omega$ for distributing the actual fraction of vacancies ($x_V$) over a total number of $N$ oxygen sub-lattice sites, is equal to

$$\Omega = \frac{\left(x_{\mathrm{V}}^{\max}(T)N\right)!}{\left(x_{\mathrm{V}}^{\max}(T)N - x_{\mathrm{V}}N\right)!\left(x_{\mathrm{V}}N\right)!}. \tag{9}$$

In the random defect model that was mentioned above, $x_{\mathrm{V}}^{\max}$ is always equal to 1.

***Table 1:*** *Fitted parameters A and E from Eq. (8) for several YSZ compositions.*

| mol% $Y_2O_3$ | ln A | E (eV) |
|---|---|---|
| 2 | 0.58±2.03 | 0.29±0.15 |
| 3 | 0.76±1.17 | 0.27±0.09 |
| 8 | 4.81±0.24 | 0.46±0.02 |
| 10 | 5.76±1.67 | 0.45±0.11 |

The definition of the electrochemical potential of oxygen vacancies $\eta_{\mathrm{V}}$ reads

$$\eta_{\mathrm{V}} = \mu_{\mathrm{V}}^{0} - Ts_{\mathrm{V}} + z_{\mathrm{V}}e\phi, \tag{10}$$

where $\mu^{o}_{\mathrm{V}}$ is the standard chemical potential, φ is the electrical potential, and $s_{\mathrm{V}}$ is the configurational entropy, defined by

$$s_{\mathrm{V}} = \frac{k_{\mathrm{B}}}{N}\left(\frac{\mathrm{d}\ln\Omega}{\mathrm{d}x_{\mathrm{V}}}\right) = -k_{\mathrm{B}}\ln\left(\frac{x_{\mathrm{V}}}{x_{\mathrm{V}}^{\max}(T) - x_{\mathrm{V}}}\right). \tag{11}$$

Assuming chemical equilibrium between the oxygen vacancies in a surface layer and in the YSZ bulk, it follows that

$$\frac{1}{k_{\mathrm{B}}}\left(s_{\mathrm{V}}^{\ \mathrm{surface}} - s_{\mathrm{V}}^{\ \mathrm{bulk}}\right) = \frac{z_{\mathrm{V}}e\phi_{\mathrm{b}}}{k_{\mathrm{B}}T}. \tag{12}$$

In the bulk, $x_{\mathrm{V}}=x_{\mathrm{V}}^{\mathrm{bulk}}$, which is determined by the level of yttria doping. From Eqs. (10)-(12) the fraction of oxygen vacancies in the near-surface layer can be derived:

$$x_{\mathrm{V}} = \frac{x_{\mathrm{V}}^{\max}(T)\,x_{\mathrm{V}}^{\mathrm{bulk}}\exp\left(-z_{\mathrm{V}}e\phi_{\mathrm{b}}/k_{\mathrm{B}}T\right)}{x_{\mathrm{V}}^{\max}(T) + x_{\mathrm{V}}^{\mathrm{bulk}}\left(\exp\left(-z_{\mathrm{V}}e\phi_{\mathrm{b}}/k_{\mathrm{B}}T\right) - 1\right)}. \tag{13}$$

For YSZ with 8 mol% $Y_2O_3$, curves calculated using Eq. (13) are shown in Fig. 4. The curves are in good agreement with the experimental data. Using appropriate values for *A* and *E* in Table 1, the model also explains the behaviour of other compositions satisfactorily.

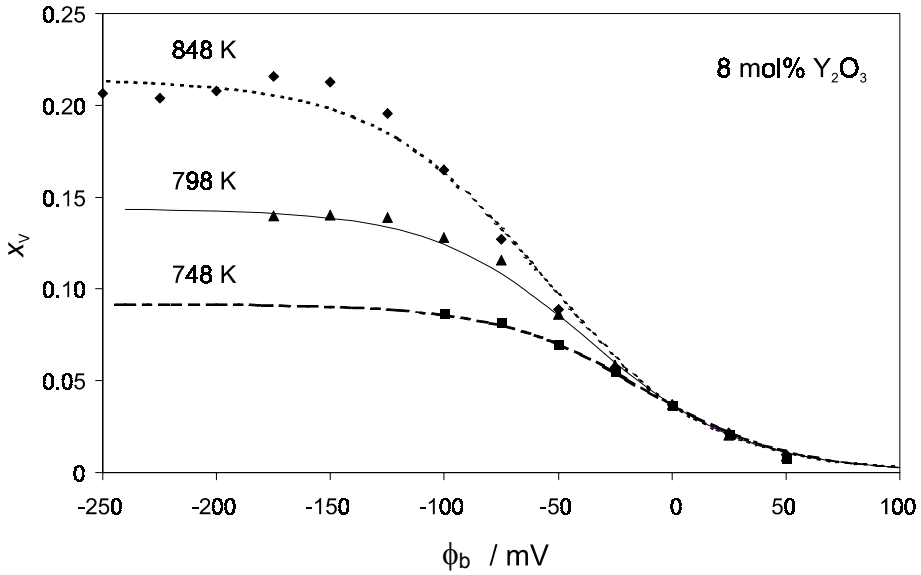


***Fig. 4:*** *Experimental oxygen vacancy fractions in YSZ with 8 mol% $Y_2O_3$, and predicted curves calculated from the thermodynamic model.*

An expression for the differential capacitance at high temperature can be derived following the same procedure that was applied in Ref. [6]. Using Eq. (13) as the expression for the vacancy fraction, the differential capacitance at zero bias potential reads

$$C_{\mathrm{dif}} = \sqrt{\frac{8\pi e^2 \chi_{\mathrm{V}} \varepsilon}{v_0 k_{\mathrm{B}} T} \frac{x_{\mathrm{V}}^{\mathrm{bulk}} \left( x_{\mathrm{V}}^{\max}(T) - x_{\mathrm{V}}^{\mathrm{bulk}} \right)}{x_{\mathrm{V}}^{\max}(T)}} \,. \tag{14}$$

When $x_{\mathrm{V}}^{\max}(T)=1$ is inserted in the above equation, the expression that was derived in Ref. [6] is obtained. The overall capacitance $C$ of a symmetrical cell, with electrodes taken to be identical, can be regarded as a circuit consisting of two capacitances in series. At zero potential difference, it follows that $C=\frac{1}{2}C_{\mathrm{dif}}$. In a double-layer capacitor using an electrolyte like YSZ the capacitance is proportional to $\varepsilon^{1/2}$, while for polarisable dielectric materials the capacitance is proportional to $\varepsilon$. In addition, in YSZ only one mobile charge carrier is present. Thus, compared to liquid electrolytes, where more than one mobile charge carrier is present, the differential capacitance be-

haves differently [19]. For YSZ it was shown that a maximum in the differential capacitance was obtained at negative bias potentials. However, for liquid electrolytes a minimum value for the differential capacitance is obtained at zero bias potential.

## Conclusions

Three-point differential capacitance measurements on oxide electrolyte/metal interfaces can be used to elucidate the near-surface defect structure of the electrolyte phase. By varying the differential capacitance with bias potential, the oxygen vacancy fractions in the surface layer of YSZ could be determined as a function of bias potential in the temperature range 748-848 K.

The near-surface relative dielectric constant of each sample was determined for each $C_{dif}$-$\phi_b$ isotherm by fitting the experimental data at high bias potential to a Boltzmann-type equation.

A thermodynamic model to describe the near-surface defect structure of YSZ was developed. The experimental behaviour could be understood by assuming that only a fraction of the oxygen sub-lattice in the near-surface layers is accessible for oxygen vacancy distribution. The vacancies are distributed randomly over the accessible lattice sites. The number of available sites increases with yttria concentration and temperature.

## References


1. A.M. Azad, S.A. Akhbar, S.G. Mhaisalkar, L.D. Birkefeld and K.S. Goto*, J. Electrochem. Soc.*, **139**, 3690, 1992.
2. H.J.M. Bouwmeester and A.J. Burggraaf, in CRC Handbook Solid State Chemistry. Editors P.J. Gellings and H.J.M. Bouwmeester, CRC Press, Boca Raton, 1996, p. 481.
3. N.Q. Minh, *J. Am. Ceram. Soc*., **76**, 563, 1993.
4. J.E. ten Elshof, M.G.H.M. Hendriks, H.J.M. Bouwmeester and H. Verweij, *Accepted for publication in J. Mater. Chem.*
5. D.W. Strickler and W.G. Carlson, *J. Am. Ceram. Soc*., **47**, 122, 1964.
6. M.G.H.M. Hendriks, J.E. ten Elshof, H.J.M. Bouwmeester and H. Verweij, *Submitted to Solid State Ionics*.
7. B.A. Boukamp, *Solid State Ionics*, **20**, 31, 1986.
8. R.D. Armstrong and R. Mason, *J. Electroanal. Chem*., **41**, 231, 1973.
9. D.P. Thompson, A.M. Dickens and J.S. Thorp, *J. Mat. Sci*., **27**, 2267, 1992.
10. M.A. Subramanian and R.D. Shannon, *Mater. Res. Bull*., **24**, 1477, 1989.
11. F.E.G. Henn, R.M. Buchanan, N. Jiang and D.A. Stevenson, *Appl. Phys. A: Mater. Sci Process.*, **60**, 515, 1995.
12. G.A. Samara, *J. Appl. Phys*., **68**, 4214, 1990.
13. K. Natori, D. Otani and N. Sano, *Appl. Phys. Lett*., **73**, 632, 1998.
14. J. Maier, *Prog. Solid St. Chem*., **23**, 171, 1995.
15. R.D. Armstrong and B.R. Horrocks, *Solid State Ionics*, **94**, 181 1997.
16. A. Many, Y. Goldstein and N.B. Grover, Semiconductor surfaces, North Holland, Amsterdam, 1965, p. 128.
17. R.E.W. Casselton, *Phys. Stat. Sol. A*, **2**, 571, 1970.
18. S. Jiang and J.B. Wagner, Jr., *J. Phys. Chem. Solids*, **56**, 1101 1995.
19. A.J. Bard and L.R. Faulkner, Electrochemical methods; Fundamentals and applications, John Wiley & Sons, New York, 1980, p. 488.

# Chapter 4
# Capacitance at ambient temperature and microstructure of Pt/YSZ composites

*The influence of microstructure on the capacitive behaviour in the dual-phase composite system platinum/cubic-yttria-stabilised zirconia (YSZ) was studied at ambient temperature. Three different synthesis methods were employed. The volume fraction of Pt metal in the composite was varied between 0 and 25 vol%. The resulting composites were characterised by scanning electron microscopy (SEM) and electrical impedance spectroscopy (EIS). The bulk capacitance increased with Pt content. Depending on the synthesis method, differences in microstructural homogeneity were observed by SEM. However, for samples prepared via different routes and with similar volume fractions of metallic Pt, no significant differences in capacitance were observed. A maximum increase in the capacitance of approximately 12.6 compared with pure cubic yttria-stabilised zirconia was obtained for a composite containing 25 vol% platinum, prepared via the sol-gel method. The percolation threshold for the platinum phase was estimated from a fit of the experimental data to normalised percolation theory and was found to be 31.1 ± 1.5 vol%.*

## Introduction

The fabrication of new, more efficient capacitors is in technological demand worldwide, especially in the computer and telecommunication industries [1]. State-of-the-art materials for such systems are the so-called multi-layered capacitors, which consist of thin layers of dielectric materials with a high dielectric constant (mostly barium titanate based ceramics) and layers of noble metals (Pd/Ag alloys). The main drawback of these capacitors is the additional cost involved with incorporating noble metals. In industry this disadvantage is partially addressed by forming thinner layers, less than 5 μm thick, resulting in an even larger capacitance. Miniaturised capacitors, with the ability to store the same charge can be produced in this manner with concomitant reduction of added noble metal and cost.

An alternative way to prepare capacitors with an increased electrode surface area is the production of composites with a randomly distributed metal phase in a dielectric matrix. Duan *et al.* [2] made Pt/PZT composites with a randomly distributed platinum phase via conventional solid state reaction and mixing methods. The dielectric constant of these composites increases with increasing volume fraction of platinum. A value for the percolation threshold ($p_c$) with respect to platinum (volume fraction at which the Pt phase forms a macroscopic network between the electrodes) was obtained via fitting the experimental data to the *General Effective Media* equation [3]. Next to this fit the experimental data were fitted to a scaling law: the *Normalised Percolation Theory* (NPT) [3], which indicated that extremely large dielectric constants can be reached in the vicinity of the percolation threshold. The percolation threshold in these PZT/Pt systems was estimated to be $33.2 \pm 1.0$ vol%. Compared with pure PZT an enhancement of approximately 4 times was reached for a composite containing 30 vol% platinum.

Pecharromán and Moya [4] reported an increase of the dielectric constant of a graded molybdenum/mullite composite by a factor of ~10,000 near the percolation threshold of the Mo phase. Pressure colloidal filtration of a slurry containing Mo and mullite resulted in a functionally graded composite. On one side of the compact a percolative Mo phase was obtained

and on the side other a non-percolative Mo phase. The percolation threshold (with respect to Mo) thus lies at some location between opposite sides. The dielectric constant in the graded composite was determined as a function of the local composition by employing 4-point impedance spectroscopy.

The increase in the dielectric constant near the percolation threshold of the metal phase is due to the formation of large clusters of metal particles, which effectively results in an enhancement of the electrode surface area when these clusters are connected to the electrodes. On the other hand, when the electrodes, of which the surface areas are enlarged by the connected clusters, are only separated by a thin barrier of the dielectric phase, the capacitance increases further.

The increase in dielectric constant of the material depends not only on the total volume fraction of conducting phase, but also on the microstructure and thus on the packing of the matrix, [5] shape of the particles [6, 7], and sizes of the particles in the composite [8, 9]. The value of the percolation threshold, however, is also influenced by these factors. For example, in random close packed systems with overlapping particles of both phases of equal size and shape $p_c$ equals 0.312, but can be decreased to approximately 0.09 when the ratio of particle sizes of matrix and metal is 10 [8, 9]. It can also decrease to approximately 0.16 when the metal particles have a volume equal to that of spherical particles but ellipsoidally shaped with an aspect ratio of 5 [6, 7]. The influence of a combination of these factors is not well understood and (reliable) model descriptions are lacking. Therefore the precise value of the percolation threshold in a real sample cannot be predicted *a priori*.

In addition to the presence of metal, the inclusion of pores also influences the dielectric behaviour. The presence of pores decreases the overall dielectric constant of the material, since it can be regarded as a dielectric phase with a dielectric constant that is low compared to YSZ. If we assume the pores to be spherical, the relative dielectric constant of porous YSZ ($\varepsilon_{r,\,MG}$) behaves according to the Maxwell-Garnett equation [10]:

$$\varepsilon_{r,\,MG} = \varepsilon_{r,\,YSZ}\frac{\varepsilon_{r,\,air} + 2\varepsilon_{r,\,YSZ} + 2f\left(\varepsilon_{r,\,air} - \varepsilon_{r,\,YSZ}\right)}{\varepsilon_{r,\,air} + 2\varepsilon_{r,\,YSZ} - f\left(\varepsilon_{r,\,air} - \varepsilon_{r,\,YSZ}\right)}, \qquad (1)$$

where $f$ is the porosity, and $\varepsilon_{r,\ YSZ}$ and $\varepsilon_{r,\ air}$ are the relative dielectric constants of YSZ and air, respectively. Eq. (1) is valid for composites with a porosity up to *ca.* 40% [10].

In a metal/insulator composite, a fraction of the metal particles is directly connected to the external electrode, thus leading to an effective increase in the electrode surface area. Since not all the metal particles are connected with the electrode surface, but effectively decrease the distance between the electrodes due to dispersion of these metal particles, a correction factor $(1-\phi_M)$ is required to describe the overall effect of the presence of the dispersed metallic phase. Hence the capacitance is given by

$$C = g(1-\phi_M)\frac{\varepsilon_0 \cdot \varepsilon_r \cdot A}{d}, \qquad (2)$$

with $g$ the increase of the capacitance, $\varepsilon_0$ the dielectric constant of vacuum, $\phi_M$ the volume fraction of metal, $A$ the surface area of the electrodes, and $d$ the distance between the electrodes.

The addition of metal particles to a dielectric phase influences the properties of the composite. In earlier work [11] it was shown that for palladium/yttria-stabilised zirconia composites, the capacitance increased with the amount of palladium added, leading to a maximum of *ca.* 4 times enhancement near the percolation threshold. In addition, for YSZ it is known that a double-layer capacitance is formed at elevated temperatures, where the oxygen vacancies are sufficiently mobile for fast diffusion through a zirconia lattice. The capacitance in this double layer can be increased to the order of 1-10 $F/m^2$, depending on temperature, yttrium concentration and applied potential [12]. As explained above, one way to increase the capacitance even further is to produce disordered composites with a noble metal dispersed in the electrolyte matrix.

In the present study the room temperature capacitive behaviour of platinum-metal/cubic yttria-stabilised zirconia composites prepared by different synthesis methods and varying in Pt concentration was investigated. At room temperature a double layer of oxygen vacancies is not formed and YSZ behaves as a normal dielectric phase. Next to the addition of platinum to a

YSZ matrix, the influence of the microstructure on the capacitive behaviour of the Pt/YSZ composites was investigated.

## Experimental

Three different synthesis routes were used to determine the effect of synthesis method and resulting microstructure on the capacitive behaviour of Pt/YSZ composites. Two methods start from commercially available cubic-phase zirconia, while the third method is based on sol-gel chemistry. The structural properties of the composites were investigated with a JSM-5800 Scanning Microprobe, JEOL Ltd. (Tokyo, Japan) scanning electron microscope (SEM) operating at 20 kV. Samples were polished using 3000-mesh diamond paste. The microstructure was revealed by 15 min thermal etching at 30ºC below sinter temperature. On the sample with a 13.5 mm diameter and 2.0 mm thickness a conductive gold layer was sputtered. The composition of non-etched samples was investigated using field emission SEM (S-800 FE-SEM, Hitachi Ltd., Tokyo, Japan) with EDX (Delta V system- Kevex Ray, Foster City, CA) operating at 20 kV. A conductive carbon layer was sputtered on the polished samples.

The capacitive behaviour of the composites was investigated by electrical impedance spectroscopy (EIS) at room temperature using a frequency response analyser (Solarton Instruments 1250 FRA, Schlumberger Technologies Ltd., Farnborough, UK) in the frequency range of 1 Hz to 65 kHz. The experimental frequency dispersion curves were fitted to an equivalent circuit consisting of a capacitance and a resistance in series using the Equivalent Circuit software program [13]. From the capacitance, the geometric increase of the electrode surface was calculated using Eqs. (1) and (2).

*Synthesis routes*

In the synthesis routes the initial amount of platinum varied between 10 and 25 volume percent. A few compacts remained porous after sintering which reduced the final volume percentages of platinum in the compacts.

Method 1

Commercially available cubic yttria-stabilised zirconia, denoted as TZ-8Y (Tosoh Corp., Tokyo, Japan), was milled in a mortar and then sieved (38 μm). An aqueous solution of $H_2[PtCl_6]$ at *ca.* 0.5 M concentration (obtained via Pt metal dissolution in aqua regia) was added to the powder at room temperature. A film evaporator was utilised to remove water and to keep the suspension as homogeneous as possible. The dried powder was reduced in a hydrogen gas atmosphere (5% $H_2$ in $N_2$ at 1 bar) at 400ºC for 2 h. The resulting powder was uniaxially pre-pressed into compacts at *ca.* 20 MPa and isostatically pressed at 400 MPa. The resulting compacts were sintered at 1480 (method 1a) or 1250ºC (method 1b) in air for respectively 2 and 4.5 h, heating and cooling rates were respectively 2 and 4ºC/min.

Method 2

The same commercial zirconia powder (15 wt%) as used in Method 1, was dispersed in water, after which 15 wt% of the stabiliser/binder Darvan C (ammonium polymethacrylic acid, R.T. Vanderbilt Co., Norwalk, USA) was added. The suspension was milled for 24 h using 2 mm zirconia milling balls, because particle size analysis (Microtrack X-100, Leeds+Northrup, St. Petersburg, FL) on prior milling experiments indicated that these experimental conditions resulted in the smallest mean volume diameter. An aqueous solution of $H_2[PtCl_6]$ adjusted to *ca.* 0.5 M was added to the milled suspension at room temperature and the suspension immediately flocculated. For reasons mentioned, the water was also removed with a film evaporator. The stabiliser was burnt-out at 550ºC after which the powder was reduced in a hydrogen gas atmosphere at 400ºC (see above). The final powder was uniaxially pre-pressed into compacts at *ca.* 20 MPa and isostatically pressed at 400 MPa and then sintered at 1480ºC in air for 6 h with heating and cooling rates of 2 and 4ºC/min., respectively.

Method 3

This method was first described by Shiga et al. [14]. Cubic yttria-stabilised zirconia, ZY17 ($Zr_{0.83}Y_{0.17}O_{1.915}$), was formed by dissolving the precursor $Zr(OC_4H_9)_4$ in iso-propanol at a concentration of 0.1 M. The zirconia was hydrolysed by drop-wise addition of a 1 M $HNO_3$ solution in the same

volume of iso-propanol as in the precursor solution. The final concentration of the $HNO_3$ reached 2 mM and the molar ratio of acid:ZY17 was 200. After 24 h stirring, 5 l water was added drop-wise for each mole of zirconium. The iso-propanol was removed by evaporation at 75ºC. A gel was formed after subsequent additions of aqueous $Y(NO_3)_3$ and $H_2[PtCl_6]$ solutions at 0.23 M and 0.5 M, respectively. The gel was dried at 40ºC and simultaneously calcined and reduced in a hydrogen-containing atmosphere (5% $H_2$ in $N_2$ at 1 bar) at 600ºC for 2 h. The resulting powder was uniaxially pre-pressed into compacts at *ca.* 20 MPa and isostatically pressed at 400 MPa. The compact was subsequently sintered at 1480ºC in air for 6 h with heating and cooling rates of 2 and 4ºC/min., respectively.

The density of all samples was measured with the Archimedes technique in water.

## Results and discussion

The porosities of the compacts, *f*, calculated from Archimedes density measurement data are shown in Table 1. Samples prepared via method 1a (sintered at 1480ºC) and method 2 were sintered to compacts exceeding 97% of the theoretical density, while the samples prepared via method 1b (sintered at 1250ºC) and method 3 showed increased porosity with increasing platinum content. The sinter activity may not be sufficient to obtain dense compacts when 'method 1' powders are sintered at 1250°C.

*Microstructural analysis*

Due to thermal etching pores were formed on the surface at positions where three or more Pt and/or zirconia grains are connected with each other. In a few cases it appears as if the compacts are highly porous (see Fig. 1b), but in reality the compacts are relatively dense, as explained above. Platinum metal produces more secondary electrons than zirconia [15], and therefore in a SEM investigation it will appear as a bright phase, while the zirconia phase is dark. It can be seen from Fig. 1a that composites prepared via method 1 and sintered at 1480ºC resulted in a compact with an inhomogeneously distributed platinum phase.

***Table 1:*** *Porosity and dielectric constants of compacts produced using the different methods with correlating increase in capacitance.*

| Method | Initial vol% Pt | $T_{sint}$ [ºC] | *f* [%] | $\varepsilon_{r, MG}$ | g |
|---|---|---|---|---|---|
| - | 0 | 1480 | <1 | 28.7 | 1.00 |
| 1 | 10 | 1480 | <1 | 28.7 | 1.6 |
| 1 | 15 | 1480 | 1.0 | 28.2 | * |
| 1 | 20 | 1480 | 1.1 | 28.1 | 5.0 |
| 1 | 25 | 1480 | 2.5 | 27.4 | * |
| 1 | 10 | 1250 | <1 | 28.7 | 1.5 |
| 1 | 15 | 1250 | 8.6 | 24.8 | * |
| 1 | 20 | 1250 | 7.0 | 25.3 | 4.7 |
| 1 | 25 | 1250 | 10.2 | 23.6 | * |
| 2 | 10 | 1480 | 2.7 | 27.5 | 1.5 |
| 2 | 15 | 1480 | 3.1 | 27.2 | 3.2 |
| 2 | 20 | 1480 | <1 | 28.7 | 4.7 |
| 2 | 25 | 1480 | 1.1 | 28.1 | * |
| 3 | 10 | 1480 | 6.0 | 26.1 | 1.7 |
| 3 | 15 | 1480 | 11.7 | 23.5 | 3.9 |
| 3 | 20 | 1480 | 12.9 | 22.8 | * |
| 3 | 25 | 1480 | 19.3 | 19.8 | 12.6 |

*Composites are conducting at room temperature (< 100 Ω).

From EDX analysis on a composite with 20 vol% Pt, it could be estimated that the dark-grey regions have a low platinum concentration of *ca.* 15 vol%. The light grey regions are platinum enriched, containing *ca.* 30 vol% of Pt,

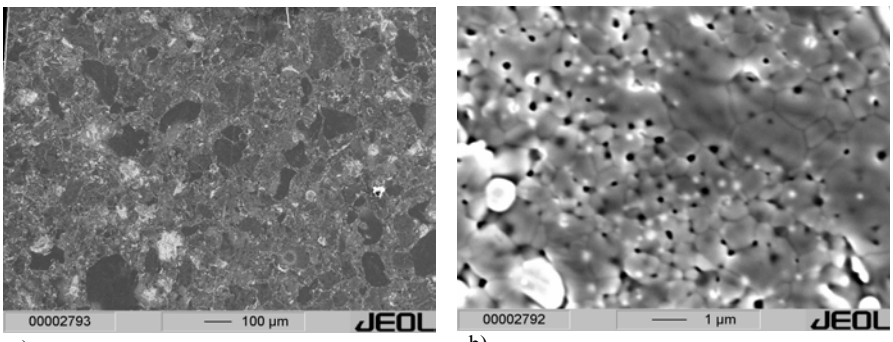


a) b)

***Fig. 1:*** *SEM pictures of Pt/TZ-8Y composites prepared with method 1; $T_{sint}$=1480ºC; a) 20 vol% Pt and b) 25 vol% Pt.*

while the bright areas are platinum clusters.

In Fig. 1b the grain boundaries can be observed. The grain sizes of the TZ-8Y phase vary between 0.3 and 1.5 μm. The platinum phase appears to have a bimodal particle size distribution. The majority of Pt particles have grain sizes between 0.2 and 0.5 μm, although some particle sizes in the range 1-2 μm are observed. Composites sintered at 1250ºC (not shown) have a similar microstructure to those sintered at 1480ºC, with the exception of the average

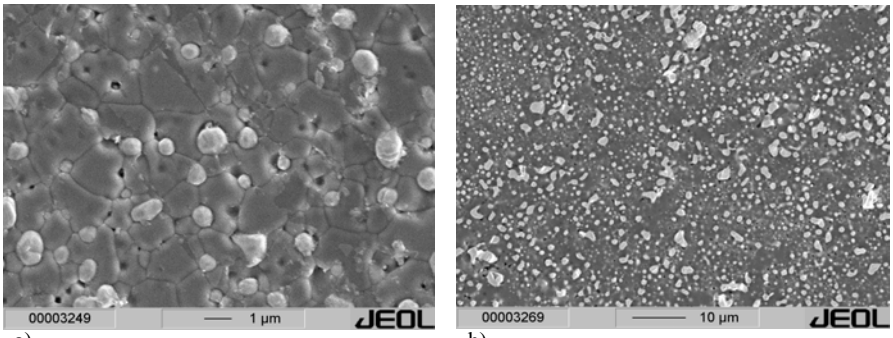


a) b)

***Fig. 2:*** *SEM pictures of a Pt/TZ-8Y composite containing 25 vol% Pt prepared by method 2.*

grain sizes of the zirconia phase, which are slightly larger in the latter case.

A SEM micrograph of the compact surface formed through method 2 is shown in Fig. 2a. The TZ-8Y composite grain sizes vary from 1 to 3 μm. The platinum grain sizes vary from 0.5 to 1 μm and Fig. 2b shows that the platinum particles reach a size up to 8 μm.

From the observation that the TZ-8Y grains are slightly larger at lower levels of platinum in the composite, it appears that platinum acts as a grain growth inhibitor for TZ-8Y. This is expected, since the presence of a metallic phase increases the average distance over which diffusion of oxide material must take place in order to sinter. In addition, the platinum particles are somewhat smaller in composites with lower platinum content. Compared to method 1, the compacts prepared via method 2 have a much more homogeneously distributed platinum phase. However, the smallest platinum particles are

larger than those in obtained in method 1 and this may be most likely attributed to the addition of the stabiliser Darvan C.

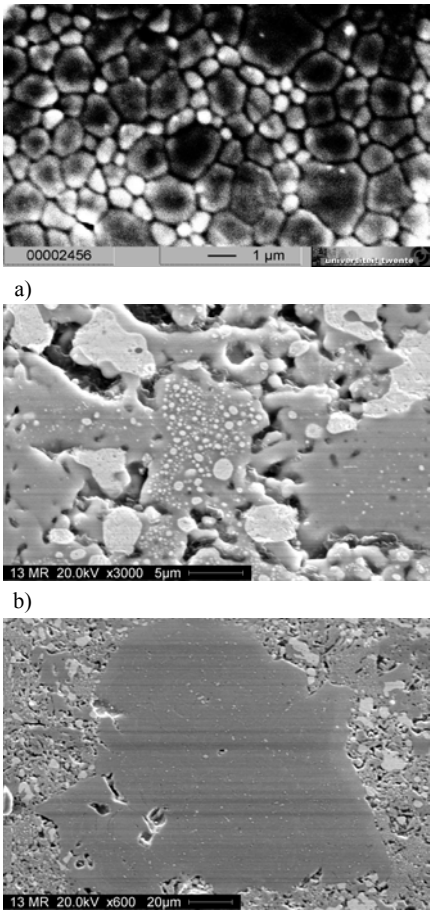


***Fig. 3:*** *SEM pictures of Pt/ZY17 composites prepared by method 3; a) 10 vol% Pt, b) and c) 25 vol% Pt, non-etched.*

Following addition of the $H_2[PtCl_6]$ solution, the milled suspension flocculated. The Pt(IV) species complexed with Darvan C, possibly reduced, and became insoluble in the water phase [16]. The precipitated complex could not infiltrate the pores of the zirconia phase effectively, with the result that no small particles could be formed, unlike method 1.

The microstructure of composites produced by method 3 is shown in Fig. 3. The grain boundaries are shown in Fig. 3a. The platinum grain sizes vary in the range 0.3 to 0.5 µm, while the ZY17 grains vary from 0.7 to 2 µm. Small zirconium hydroxide particles were formed during the condensation step in the sol-gel synthesis.

After addition of $H_2[PtCl_6]$ a stable gel was formed. It is likely that acidic $H_2[PtCl_6]$ interacts with basic zirconium hydroxide particles, thereby functioning as a gelating agent. After evaporation of the solvent this results in zirconium hydroxide particles coated with the platinum salt. The distribution of Pt around zirconium hydroxide particles remains after reduction and calcination. Sintering therefore occurs primarily between the Pt-coated surfaces. This eventually results in small, connected strings of

platinum particles, which coat the ZY17 particles after sintering. In Fig. 3b it is shown from non-etched samples with a platinum concentration of *ca*. 25 vol% Pt that larger platinum particles (up to 5 μm in diameter) are also formed. Moreover, micro-cracks are formed next to these large Pt particles. The platinum phase probably has a higher sinter activity than the zirconia particles, leading to the formation of micro-cracks. From Fig. 3c it can be seen that large relatively dense domains up to approximately 150 μm are formed upon sintering. From EDX measurements the amount of platinum in these domains is estimated to be approximately 10 vol%. The remainder of the composite contains a relatively large platinum concentration of approximately 35 vol%. At relatively large volume concentrations of platinum method 3 results in composites with an inhomogeneous distributed platinum phase.

*Electrical impedance spectroscopy*

In Fig. 4 the capacitance representation of the electrical impedance spectrum of a composite containing 15 vol% platinum prepared via method 2 is shown. It is a typical spectrum for non-conducting composites with a zirconia matrix. The imaginary capacitance is plotted against the real capacitance and semi circle is obtained, indicating that in the frequency range investigated, a pure capacitive behavior is measured in these composites. From the electrical impedance spectroscopy data the enhancement in the capacitance, *g*, was calculated from Eqs. (1) and (2). Their values are shown graphically in Fig. 5. The capacitance increases with increasing platinum content for all samples obtained from the three synthesis methods. A maximum of approximately 12.6 times enhancement for the capacitance is obtained for a composite containing 25 vol% platinum prepared via method 3.

The obtained data were fitted to an expression we derived from the Normalised Percolation Theory (NPT) [3]:

$$g = \left( \frac{p_c - \phi_M}{p_c} \right)^{-s} \tag{3}$$

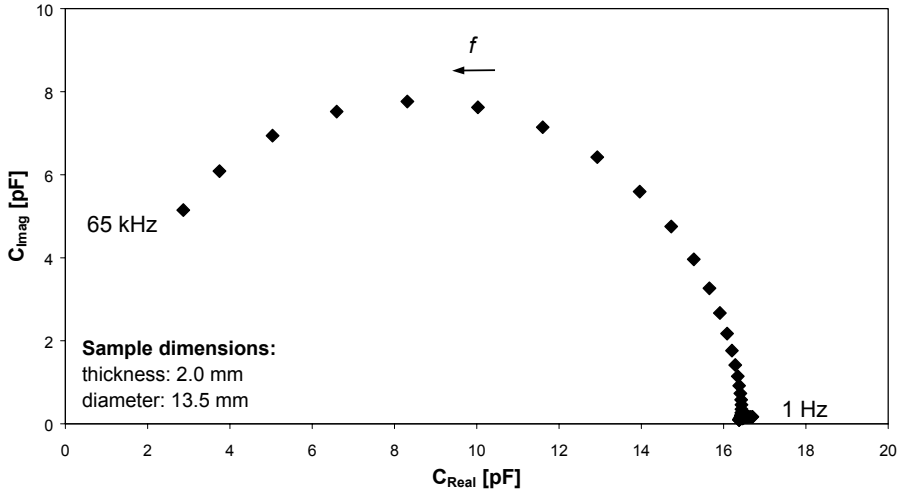


***Fig. 4:*** *Capacitance representation of an impedance spectrum of a composite containing 15 vol% Pt prepared via method 2.*

The fitting parameters are $s = 1.56 \pm 0.18$ and $p_c = 0.311 \pm 0.015$. The s-value is relatively large compared with typical values, which are in the range 0.76 – 0.89 [3]. NPT predicts a large increase of the capacitance just below the percolation threshold. The experimentally obtained value for the percolation threshold is in good agreement with the theoretical value for random packed overlapping particles of uniform size and shape ($p_c = 0.312$) [8]. Although the particle sizes in our samples vary between the different particles and amongst the three different methods, the composites can be considered randomly packed.

In practice it is very difficult to reproducibly prepare composites with a metal volume fraction sufficiently close to the percolation threshold ($|p_c-\phi_M| < 0.1$), because during each subsequent step in the synthesis procedure, an uncontrollable amount of the starting materials is inevitably lost. Therefore no large increase in capacitance is measured experimentally.

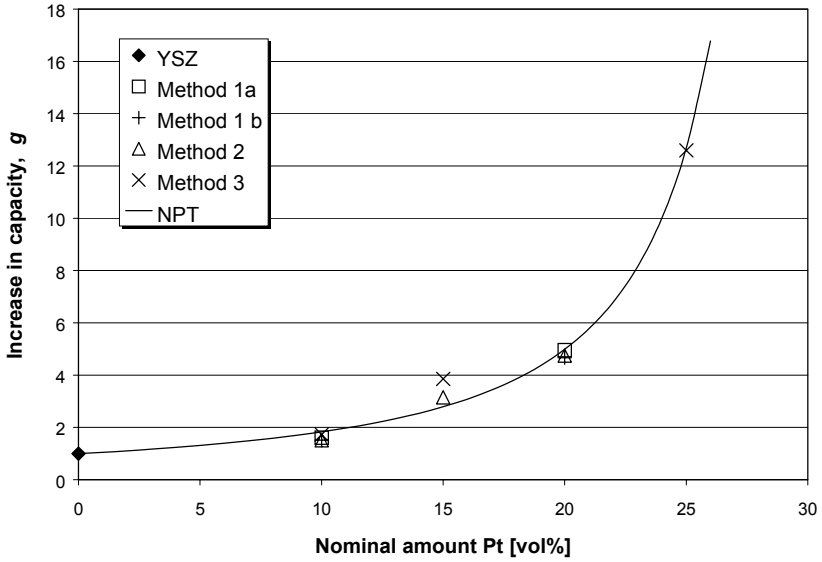


***Fig. 5:*** *Enhancement of the capacitance, g, as function of Pt volume fraction; continuous line represents the NPT fit to the measurements.*

The enhancement in capacitance appears not to depend on grain size, because the values obtained from method 1a and 1b are in good agreement. Moreover, the microstructure has no influence on the capacitive behaviour, since the enhancement in capacitance of composites prepared by the different methods are in close agreement, as shown in Fig. 5.

Although all compacts contain a volume fraction of platinum below the percolation threshold as predicted by NPT, some of the samples are conducting as is evident by their bulk resistivity of <10 Ω, as determined by impedance measurements. In particular, composites prepared by method 1 and 3 have a less homogeneously distributed platinum phase. The inhomogeneity increases the chance to form a conductive electron path from Pt metal grains, resulting in an electrically conducting sample.

## Conclusions

All three synthesis methods result in inhomogeneous composites. The most homogeneously distributed platinum phase is obtained with method 2.

For each method, the capacitance increases with increasing volume fraction of platinum in the composite. However, no significant changes are observed between the different methods, indicating that in these samples grain size and homogeneity apparently do not affect the capacitive behaviour to a significant extent. A maximum enhancement factor of about 12.6 was obtained for a composite containing 25 vol% platinum. The experimental data were fitted with the Normalised Percolation Theory and resulted in a predicted percolation threshold of approximately 31 vol% Pt for this type of composite.

Although all composites containing a volume fraction of platinum below the percolation threshold as predicted by NPT, some of them contain a conductive platinum network. Apparently it is difficult to reproducibly prepare non-conducting composites.

## References


1. B.W. Peace, *Ceram. Ind*. 32, 1994.
2. N. Duan, J.E. ten Elshof and H. Verweij, *J. Eur. Ceram. Soc.*, in press 2001.
3. D.S. McLachlan, *Mat. Res. Soc. Symp. Proc.* **411**, 309, 1996.
4. C. Pecharromán and J.S. Moya, *Adv. Mater.* **12** [4], 294, 2000.
5. D. Stauffer, and J.G. Zabolitzky*, J. Phys. A: Math. Gen.* **19**, 3075, 1986.
6. E.J. Garboczi, K.A. Snyder, J.F. Douglas and M.F. Thorpe, *Phys. Rev. E*, **52**, 819, 1995.
7. E.T. Gawlinski and H.E. Stanley, *J. Phys. A: Math. Gen.* **14** [8], L291, 1981.
8. A. Maillaris and D.T. Turner, *J. Appl. Phys*. **42**, 614, 1971.
9. F. Lux, J. Mater. Sci., 28 (1993) 285-301.
10. P.A.M. Steeman, in Interfacial phenomena in polymer systems; A dielectric approach, Ph.D. Thesis, Delft, The Netherlands, 1992.
11. M.G.H.M. Hendriks, M.P. Timmerman-Oude Wolbers and H. Verweij, in Electronic ceramic materials and devices. Editors K.M. Nair and A.S. Bhalla, Vol. 106 Ceramic Transactions, Westerville, Ohio, 2000.
12. M.G.H.M. Hendriks, J.E. ten Elshof, H.J.M. Bouwmeester and H. Verweij, *Submitted to Solid State Ionics.*
13. B.A. Boukamp, *Equivalent Circuit* software, 2nd edition, University of Twente, Enschede, The Netherlands, 1989.
14. H. Shiga, T. Okubo and M. Sadakata, *Ind. Eng. Chem. Res.*, **35**, 4479, 1996.
15. L. Reimer and G. Pfefferkorn, Raster-Elektronenmikroskopie, 2nd Edition, Springer-Verlag, Berlin, Germany, 1977, pp.41.
16. D.R. Lide, Handbook of Chemistry and Physics, 75th Special student edition, CRC Press, Inc., Boca Raton, USA, 1994, p. 4-82.

# Chapter 5
# Microstructural homogeneity and capacitance correlations in Pd/YSZ composites

*Voronoi tessellation was applied for quantifying microstructural homogeneity of palladium particles in random Pd/cubic yttria-stabilised zirconia (YSZ) composites. The palladium concentration ranged from 0 to 30 vol%. Room temperature impedance measurements were used to investigate the capacitance in the composites. The enhancement in capacitance increased to a maximum near the percolation threshold of Pd, which was estimated at approximately 30 vol% Pd with the Normalised Percolation Theory (NPT). Data obtained from Voronoi diagrams resulted in a quantitative measure for the homogeneity of the dual-phase composite. The homogeneity was found to decrease with increasing Pd concentration in the composites. Near the theoretical value of the percolation threshold, the Pd phase was found distributed too inhomogeneously for preparing insulating composites. No extreme increase in capacitance as predicted by NPT could therefore be experimentally obtained.*

## Introduction

Ceramic/metal composites (cermets) are widely used materials with technological applications in the areas of electrocatalysis, charge transport, optics, chemical sensors and related solid state devices. According to percolation theory, the electrical properties (e.g. conductivity and dielectric constant) of disordered systems change strongly with composition when one phase in the mixture approaches its percolation threshold ($p_c$). The interpretation of the resulting properties can be analysed via different theories [1]. The composite undergoes a transition from insulating to conducting at the percolation threshold of the metal phase. Near the percolation threshold metallic clusters are separated by thin dielectric regions, and as the composition of the compacts approaches the percolation threshold, the calculated dielectric constant increases asymptotically to a large value [2]. This feature may be exploited in capacitors with anomalously high capacitances and used in a variety of applications such as electromagnetic shieldings, solid state ionic devices, and antenna systems.

The increase in dielectric constant of the material depends not only on the total volume fraction of the conducting phase, but also on the microstructure and thus the packing of the matrix [3], shape of the particles [4, 5], and sizes of the particles in the composite [6, 7]. However, the position of the percolation threshold is closely related to the microstructure and thus also influenced by the above-mentioned factors. For example, in randomly close packed systems consisting of overlapping particles of equal size and shape, $p_c$ equals 0.312 [3], but can be decreased to 0.09 when the ratio of particle sizes between matrix and metal equals 10 [6, 7]. It can also decrease to 0.16 when the metal particles are ellipsoidally shaped with an aspect ratio of 5 [4, 5]. The influence of these combined factors is not well understood, and (reliable) model descriptions are lacking. The exact position of the percolation threshold in an authentic sample and thus the electrical properties can therefore not be predicted *a priori*.

Since all ceramic properties are ultimately related to their microstructure (including composition), scanning electron microscopy (SEM)-analysis is widely used in research endeavours to determine microstructural homogene-

ity. Comparing pictures with different microstructures gives an indication of the relative homogeneity of the composite samples [8-10]. Placement of a grid over the image and counting the grains of one phase within each cell [11] or the mean intercept length [12] of the grains can give a more descriptive measure for homogeneity. However, in these cases the homogeneity is very sensitive to the size of the grid chosen and visual inspection is time consuming and susceptible to human error. The utilisation of Voronoi diagrams [13] as a method for quantification of homogeneity was applied in this study to give a quantitative indication of the homogeneity of different phases in a composite. However, homogeneity is a dimensionless and abstract property that is system and scale dependent and can therefore not be used to compare properties of different types of materials with different compositions. The quantification of the homogeneity in composite materials is rarely taken on as is evident from the paucity of this topic in literature.

In the present study the influence of palladium metal concentration (from 0 to 30 vol%) in Pd/YSZ composites and its role in subsequent capacitance enhancement was investigated. In addition, the homogeneity parameters for area, perimeter and number of sides of the Voronoi cells were determined using SEM micrographs of all compacts. Finally, the increase in capacitance was related to the homogeneity of the palladium distribution in the composites.

## Theory

The principle of a Voronoi diagram resulting from a distribution of points in a Euclidian space is as follows: space is divided up into cells, each consisting of the positions closer to one particular point than to any other as depicted in Fig. 1. The boundaries of each cell are the perpendicular bisectors between the closest neighbouring points. The number of points in the Voronoi diagram is larger than 1 but finite. The points are distinct, thus every location in the plane is assigned to the closest member of the point set and every member of this set forms its own region with locations assigned to it. Each location is assigned to at least one member.

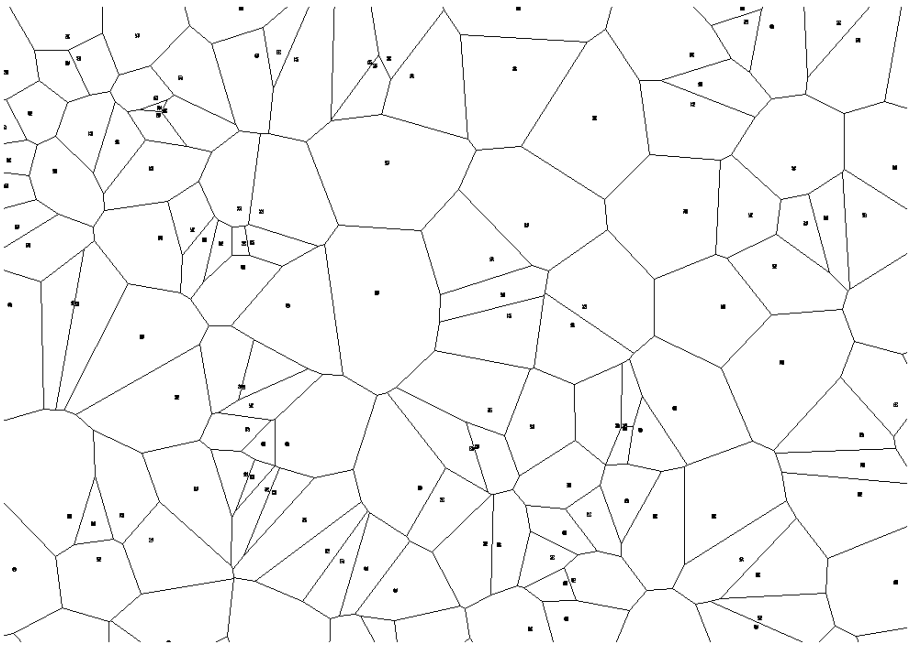

***Fig. 1:*** *Typical Voronoi diagram constructed from a distribution of points.*

In the 2D case the tessellation thus obtained, is referred to as a planar Voronoi diagram and the regions are called Voronoi polygons [14]. In theory the size of the diagram is infinite, but in practice the dimensions are confined by the edges of a SEM micrograph. The convex hull of a Voronoi diagram is the collection of outer boundaries of all closed Voronoi polygons and thus the cells in contact with the edges of the micrograph are excluded from the analysis.

The relevant characteristics of Voronoi polygons are their area, perimeter and number of sides. For an ideally regular lattice, the distribution of one of these characteristics would show a single peak, with the height of this peak corresponding to the number of polygons within the convex hull. For real samples a distribution curve is obtained for the different parameters and the area below the curve corresponds to the number of the polygons. The decreasing width of the distribution curve and thus the standard deviation ($\sigma$), gives a measure for the increasing degree of homogeneity [15].

Using image analysis it was possible to differentiate between individual phases and the centres of mass of these phases could be determined. The centers of mass can be used to construct a Voronoi diagram and the homogeneity of the distribution of a second phase could be determined. A major advantage of using Voronoi diagrams is that the average number of neighbouring grains can be measured directly.

## Experimental

*Sample preparation*

Cubic yttria-stabilised zirconia (YSZ) containing 8 mol% yttria (TZ-8Y, Tosoh corporation, Tokyo, Japan) and palladium oxide (Alfa®, Johnson Matthey GmbH, Karlsruhe, Germany) powders were suspended separately in water containing 15 wt% Darvan C (ammonium polymethacrylic acid, R.T. Vanderbilt Company, Inc., Norwalk, U.S.A). The powder loadings were taken optimal (15 wt%) to prevent agglomeration during the milling step. The suspensions were milled with zirconia milling balls with a diameter of 2 mm for 24 h. Particle size experiments (Microtrack X-100, Leeds+Northrup, St. Petersburg, Florida, U.S.A) prior to milling of the powders indicated that the milling period used above resulted in the smallest particle sizes. The mean volume diameters of the powders were 0.35 and 0.74 μm for YSZ and PdO, respectively. After milling, the suspensions were diluted to approximately 5 wt% of the powder. The YSZ and PdO suspensions were added to a stirring vessel and mixed at approximately 1000 rpm for 1 h. The amount of each suspension was chosen such that in the post-sintering composition the palladium metal concentration ranged from 0 to 30 vol%.

The powder was obtained by spray drying (Büchi 190 Mini Spray Dryer, Büchi Laboratoriums-Technik AG, Flawil, Switserland) of the mixed suspension, after which it was powdered in a ceramic mortar. The dry powder was subsequently heated at 550ºC in air for 2 h, with heating and cooling rates 5ºC/min to remove all organic residues. The powder was uniaxially pre-pressed at 75 MPa into discs after which it was isostatically pressed at 400 MPa. Dilatometry (Netzsch 402E Dilatometer, Netzsch Gerätebau GmbH, Selb/Bayern, Germany) experiments revealed that the optimum sin-

tering conditions were 6 h at 1480ºC to obtain compact densities above 98 % of the theoretical value. The obtained compacts were cut into discs (diameter 13.5 mm, thickness 2 mm). Both sides of the discs were polished and sputtered with palladium to obtain a dense layer, serving as an electrode.

Quantitative X-Ray Fluorescence (XRF) (Philips PW1480 Spectrometer, Nederlandse Philips Bedrijven B.V., Almelo, The Netherlands) measurements were performed to verify the composition of the powders as obtained after removal of organic residues. The concentrations of the respective elements in the powder were calculated using COMBI [16].

*Electrical impedance spectroscopy*

Two-point impedance measurements (Solartron® Instruments 1250 FRA, Schlumberger Technologies Ltd., Farnborough, Hampshire, England) were performed at room temperature in the frequency range 1 Hz to 60 kHz at 10 mV rms. The experimental impedance plots were interpreted in terms of a capacitance [17]. The increase in capacitance ($g$) was calculated from this data, using:

$$C = g\left(1-\phi_m\right)\frac{\varepsilon_0 \cdot \varepsilon_r \cdot A}{d}, \qquad (1)$$

with $C$ the capacitance of the sample, $\phi_m$ the volume fraction of palladium, $\varepsilon_0$ the permittivity of vacuum, $\varepsilon_r$ the relative dielectric constant, $A$ the electrode surface area and, $d$ the distance between the electrodes.

*Image analysis*

The microstructure of polished cross-sections of the compacts was investigated with SEM (JSM-5800 Scanning Microscope, JEOL Ltd., Tokyo, Japan ), using an electron beam of 17 kV. The micrographs were taken with increased contrast level to better distinguish between Pd and YSZ phases. Each sample was analysed at 5 different and randomly selected locations. All micrographs had identical size, resolution (number of pixels) and scale. The micrographs were analysed using Image-Pro® Plus 3.0 (MediaCybernetics®, Silver Spring, MD, USA) software. Since palladium was dispersed in the zirconia matrix, the homogeneity of only the distribution of the Pd phase

was calculated. To this end the centers of mass of the Pd phase were determined from the SEM pictures.

A computer software program was used to construct a Voronoi diagram from the centers of mass of the Pd phase. The program also calculated the area, the perimeter, and the number of sides of each Voronoi polygon. The respective standard deviations were calculated from the data obtained from this computer software program [18]. For these calculations only the polygons within the convex hull were used. The standard deviation for the respective parameters, $\sigma_i$, can be calculated according to:

$$\sigma_i^2 = \frac{\sum_{i=1}^{n}(x_i - \bar{x})^2}{n-1} \tag{2}$$

with $n$ the number of polygons, $x_i$ the parameter of interest, and $\bar{x}$ its average value. The number of polygons was different for pictures from various locations in the sample and from various sample compositions. To correct for these effects the standard deviation was normalised for the number of polygons [19].

$$\bar{\sigma}_i = \frac{\sigma_i}{\sqrt{n}}, \tag{3}$$

where $\bar{\sigma}_i$ is the mean standard deviation. In this chapter the mean standard deviations of area, perimeter, and number of sides of the polygons are considered as the homogeneity parameters.

## Results and discussion

The results of powder XRF analyses are listed in Table 1. The amount of palladium in the final composition of the powders was found to be close to the initial amount.

***Table 1:*** *XRF results.*

| Sample | $Pd_{Nominal}$ [vol%] | $Pd_{Detected}$ [vol%] |
|---|---|---|
| 1 | 10.0 | 10.0 ± 0.2 |
| 2 | 23.0 | 22.4 ± 0.4 |
| 3 | 25.2 | 24.6 ± 0.5 |

In Fig. 2 the capacitance representation of the impedance spectrum of a composite with a Pd concentration of 23 vol% is shown. This behaviour corresponds to a true capacitance and is typical for Pd/YSZ composites. However, on composites with a Pd concentration of 25.2 and 30 vol%, respectively, a small resistance (<10 Ω) was measured, indicating that a conducting

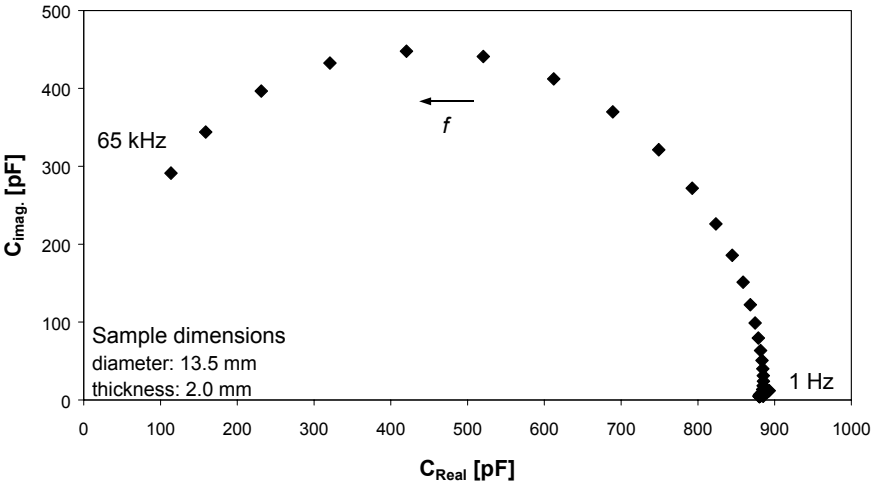


***Fig. 2:*** *Capacitance representation of an electrical impedance spectrum of a Pd/YSZ composite with a Pd concentration of 23 vol%.*

Pd network was formed in these composites.

The increase in capacitance of non-conducting composites that ranged in palladium concentration is shown in Fig. 3. The experimental data were fitted with an expression for increase in capacitance derived from the normalised percolation theory (NPT) [20]:

$$g = \left( \frac{p_c - \phi_m}{p_c} \right)^{-s} . \qquad (4)$$

The fitting parameters are s = 0.823 ± 0.095 and $p_c$ = 0.298 ± 0.014. The s value (~0.8) is in accordance with the typical value (normally 0.76 – 0.89)

[20], which further indicates that the system has a microstructure without a preferential orientation. A value for $p_c = 0.30$ is in accordance with theoretical value of 0.312 for randomly distributed composites with overlapping

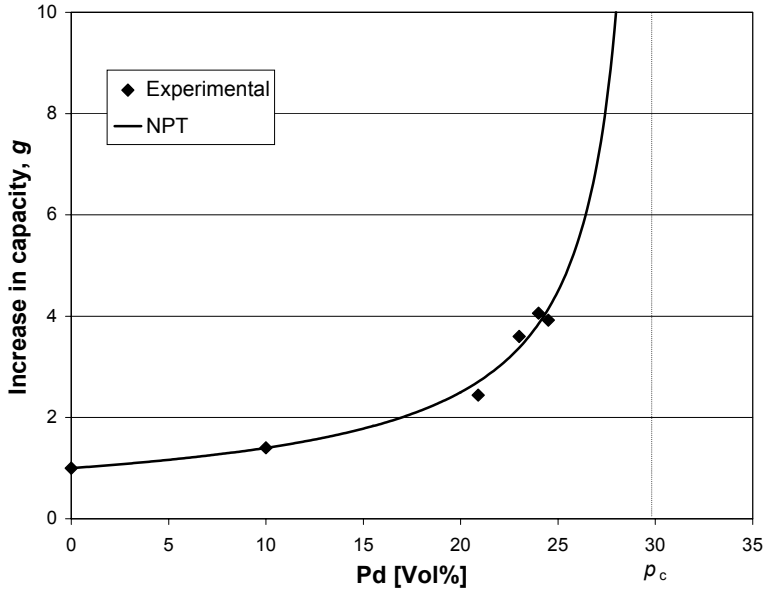


***Fig. 3:*** *The room temperature enhancement in capacitance as function of Pd concentration in the composites. The dots represent the experimental data, while the line represents the fit from NPT.*

particles of equal size and shape [21].

It can be seen from Fig. 3 that near the percolation threshold, NPT calculations can result in a high *g*-value, but that these large values were not experimentally verified. Samples with a Pd concentration close to the percolation threshold ($|\phi_m - p_c| < 0.1$ vol%) are difficult to prepare, since during each of the synthesis steps an uncontrollable amount of the starting materials is inevitably lost. Moreover, below theoretical values of the percolation threshold for Pd, electrically conductive composites were already formed. This was probably due to a very inhomogeneously distributed Pd phase in these samples, which caused the formation of conducting Pd networks. The relation

between Pd concentration and phase distribution and quantitative homogeneity is described in the next section.

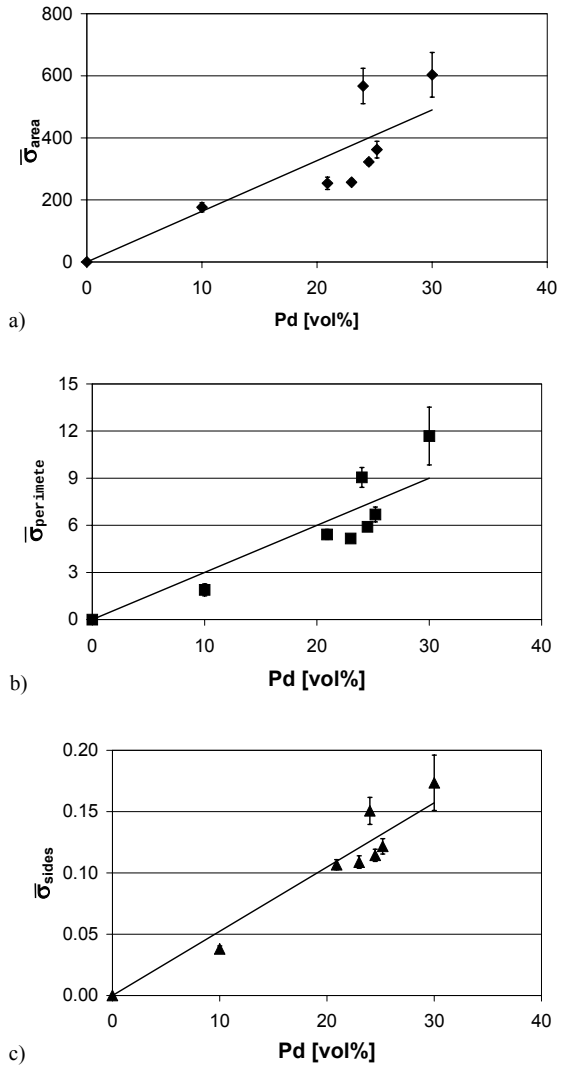


***Fig. 4:*** *Normalised standard deviations of the homogeneity parameters; a) area, b) length of the perimeter and c) number of sides.*

*Image analysis*

The mean standard deviations of the perimeter and area size distributions as well as the number of sides of the Voronoi cells are shown in Figs. 4a to 4c. In all figures the experimentally obtained data points were fitted with a first order "trendline" through the origin, because at zero concentration Pd, a homogeneous Pd distribution is obtained and thus the mean standard deviation is equal to zero. The conformity of the trendline was tested with the *F*-distribution function [22]. The number of data points used in the fit is equal to 7. However, in this case the trendline is fitted through the origin, which limits the number of degrees of freedom to 6. The obtained *F*-values for the trendline in all graphs are listed in Ta-

ble 2 and are all above the critical $F_{95}$-value of 5.99, indicating that there is at least a 95% probability that the trendlines are accurate. In the case of the mean standard deviation for the number of sides the $F$-value even exceeds the critical $F_{99}$-value of 13.74, which means that for this parameter a 99% probability for a linear trendline exists. For each Pd particle, the number of closest neighbouring Pd particles and thus the number of sides of the Voronoi cell is equal to approximately 6 and does not deviate much with changing Pd concentration in the composite. This observation probably explains the high certainty of a linear trendline for the concentration dependence of the mean standard deviation for the number of sides of the polygons. Considering all homogeneity parameters it can be concluded that the homogeneity of the Pd distribution decreases roughly linear with the Pd concentration in the composites.

***Table 2:*** *F-values obtained from the F-distribution function test on the trendlines for the homogeneity parameters as function of the Pd concentration in the composites.*

| | $F$-value* |
|---|---|
| Area | 6.90 |
| Perimeter | 12.9 |
| Sides | 35.9 |

*$F_{95}$-critical = 5.99, $F_{99}$-critical = 13.74.

It should be noted that the determination of the homogeneity parameters using Voronoi cells constructed from the centers of mass of the palladium particles mainly gives information about the *positional* distribution of Pd particles rather than their *size* distributions.

The normalised standard deviations for the distributions of area, perimeter, and the number of sides of the Voronoi polygons exhibit a positive correlation with the concentration of Pd particles. Thus a positive correlation between the level of microstructural inhomogeneity of the Pd distribution and the Pd concentration in the composites was obtained.

*Evaluation*

From normalised standard deviations of Voronoi polygon size, perimeter and the number of sides obtained from image analysis on Pd/YSZ composites, it was concluded that the homogeneity of the Pd distribution decreased with increasing Pd concentration. The data for the homogeneity of the Pd/YSZ

composites obtained in this study are based on the positional distribution of the Pd particles. During sintering of the materials, clustered Pd particles fused together, resulting in larger particles. These particles in turn were considered as single particles. In this study the particle size was not (yet) included. However, including the particle size would provide additional information, since homogeneity is a function of both particle size and phase dis-

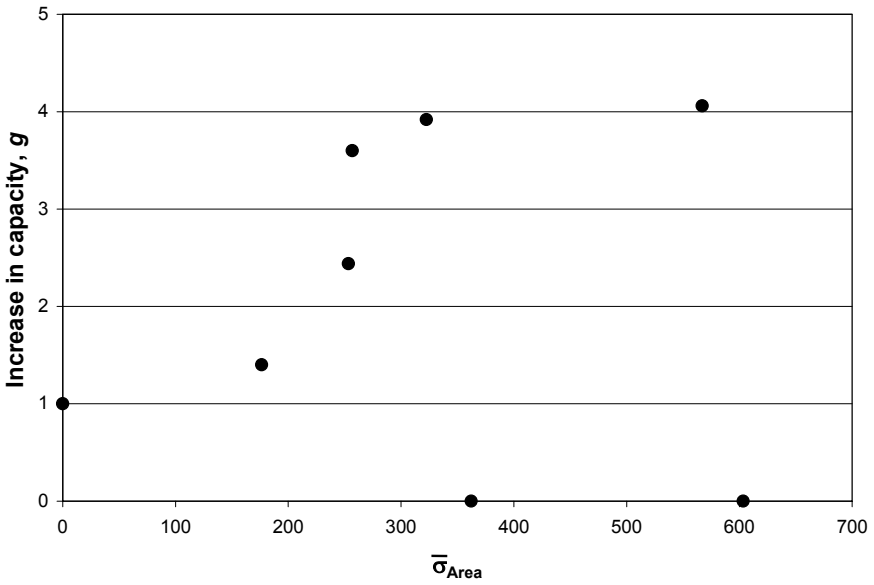


***Fig. 5:*** *The increase in capacitance as function of the mean standard deviation for the area of the polygons in the Voronoi diagram.*

tribution.

To investigate the influence of the homogeneity of the Pd distribution on the capacitance of the composites, the latter is shown in Fig. 5 as function of the mean standard deviation of the area of the polygons in the Voronoi diagram. For the other homogeneity parameters similar graphs were constructed. A positive correlation between the increase in capacitance and the positional homogeneity of Pd was obtained to a certain extent. At high values for the inhomogeneity ($\sigma_{Area}$>350), with the Pd concentration near the percolation threshold, electronic conductive composites were obtained in some cases.

Apparently in that case the Pd phase was distributed too inhomogeneously, also indicating increasing difficulty to prepare insulating Pd/YSZ composites with a Pd concentration near the theoretical value of the percolation threshold. Therefore no large increase in capacitance could be obtained experimentally with state-of-the-art preparation techniques.

## Conclusions

For Pd/YSZ composites, the room temperature capacitance measured with impedance spectroscopy increases with Pd concentration. According to a fit from the Normalised Percolation Theory the percolation threshold was equal to approximately 30 vol% Pd, which indicated that the palladium distribution did not have a preferential orientation and that the Pd particles were distributed randomly.

The mean standard deviation of area, perimeter, and number of sides of the polygons in the Voronoi diagrams, constructed from SEM micrographs of the composites, increased roughly linearly with a certitude of >95% with palladium concentration in the composites. Thus with increasing concentration Pd, the distribution of Pd becomes more inhomogeneous, probably due to clustering/aggregation of the Pd particles during sintering.

With decreasing homogeneity of the Pd distribution the probability of preparing an electrically conducting composite below the theoretical value for the percolation threshold for random composites increases. Therefore, no gigantic increase in capacitance as predicted by NPT was obtained experimentally upon approaching the Pd percolation threshold. This may change when fundamentally different synthesis methods that insure a certain homogeneity up to the percolation threshold are employed, resulting in insulating composites.

## References


1. S. Kirkpatrick, *Rev. Mod. Phys.*, **45** [4], 574, 1973.
2. A.L. Efros and B.I. Shklovskii, *Phys. Stat. Sol. B*, **76**, 475, 1976.
3. D. Stauffer, and J.G. Zabolitzky, *J. Phys. A: Math. Gen.*, **19**, 3705, 1986.
4. E.J. Garboczi, K.A. Snyder, J.F. Douglas and M.F. Thorpe, *Phys. Rev. E*, **52**, 819, 1995.
5. E.T. Gawlinski and H.E. Stanley, *J. Phys. A: Math. Gen.*, **14** (8), L291, 1981.
6. A. Maillaris and D.T. Turner, *J. Appl. Phys.*, **42**, 614, 1971.
7. F. Lux, *J. Mater. Sci.*, **28**, 285, 1993.
8. B. Kerkwijk, L. Winnubst, E.L. Mulder and H. Verweij, *J. Am. Ceram. Soc.*, **82** [8], 2087, 1999.
9. R. Guo, Z. He, Z. Yang, Q. Yuan and Y. Chen, *J. Eur. Ceram. Soc.*, **16**, 1345, 1996.
10. H.H.D. Lee, *J. Mater. Sci.*, **27,** 6673, 1992.
11. A. Krell, P. Blank and T. Weiss, *J. Mater. Sci.*, **22**, 3304, 1987.
12. M. Sajko, T. Kosmac, R. Dirscherl and R. Janssen, *J. Mater. Sci.*, **32**, 2647, 1997.
13. G.F. Voronoi, *J. Reine Angew. Math.,* **136**, 47, 1908.
14. A. Okabe, B. Boots and K. Sugihara, Spatial tessellation concepts and applications of Voronoi diagrams, John Wiley and Sons, New York, 1992, p. 405.
15. H. Tanake, T. Hayashi and T. Nishi, *J. Appl. Phys.*, **65** [12], 4480, 1990.
16. M. Bos and J.A.M. Vrielink, *Anal. Chim. Acta*, **373**, 291, 1998.
17. B.A. Boukamp, *Solid State Ionics*, **20**, 31, 1986.
18. M.J.G.W. Heijman, N.B. Benes, J.E. ten Elshof and H. Verweij, *Submitted to Mat. Sci. Eng. A.*
19. E.E. Underwood, in Quantitative stereology, Addison-Wesley Publishing Company, Reading, Massachusetts, USA, 1970, p. 23.
20. D.S. McLachlan, *Mat. Res. Soc. Symp. Proc.*, **411**, 309, 1996.
21. D. Stauffer and J.G. Zabolitzky, *J. Phys. A: Math. Gen.*, **19**, 3705, 1986.
22. E. Kreyszig, Introductory mathematical statistics; Principles and methods, John Wiley and Sons, New York, 1970, p. 215.

# Chapter 6
# The electrical behaviour of platinum impregnated porous YSZ

*Porous sintered cubic yttria-stabilised zirconia samples were impregnated with a platinum salt solution and subsequently reduced to Pt metal to enhance the capacitance. Two impregnation methods were applied: 1) immersion of porous YSZ in a Pt salt solution, followed by reduction of the platinum salt, and 2) deposition of Pt at an electrode by means of electrolysis during impregnation. The samples were investigated by impedance spectroscopy. The capacitance of samples prepared by the first method was up to 4 times larger than that of porous YSZ, while an increase in capacitance of ~20× was observed with method 2. Compared to dense composites with a randomly dispersed platinum phase, the preparation of impregnated samples, with an enhancement of the capacitance comparable to or larger than that in the random composites, resulted in a reduction of the amount of noble metals of at least one order of magnitude. At temperatures above 400°C YSZ is oxygen-ion conducting so that a double layer can be formed at low frequencies at the metal/electrolyte interfaces. From the measured double-layer capacitance, which amounts to ~2.6·10$^2$ F/m$^2$ at 551°C, it was determined that the specific electrode/electrolyte interfacial surface area of electrolytically impregnated samples was in the range of 80 - 300 m$^2$/m$^2$.*

## Introduction

Ceramic capacitors are widely used for electronic applications, *e.g.* in the computer and telecommunication industries [1]. In general, these capacitors are layered composites consisting of a dielectric phase with a very large dielectric constant and noble metal (Pd/Ag alloys) electrodes. Capacitors have to follow the general trend of miniaturisation of electronic appliances [2]. To decrease the total volume of a capacitor, the capacitance per unit volume has to be increased, which can be realised by increasing the electrode surface area and at the same time by decreasing the distance between the electrodes.

In commercial applications multi-layered structures consisting of a noble metal and a dielectric medium with a high dielectric constant are used. This leads to an increase in electrode surface area and thus an increase in capacitance. A 50% reduction of the layer thickness at constant volume leads to a factor 4 increase in the total capacitance. This is due to the combined effect of reduction in the distance between the electrodes and increase in electrode surface area [1]. Layer thicknesses of less than 5 μm have been achieved previously [3]. Smaller capacitors with the ability to store the same charge can be produced in this manner, which reduces the amount of noble metals needed. However, up to 50 vol% of noble metals are used during the processing of multi-layered capacitors [2].

An alternative way to prepare capacitors with an increased electrode surface area and a decreased distance between electrodes is the use of metal/dielectric composites with a random distribution of the metal phase. At the percolation threshold of the metal phase, $p_c$, the composite undergoes a transition from an isolating to a conducting material. Efros and Shklovskii [4], McLachlan [5], and Dubrov *et al.* [6] described the behaviour of such a composite near its percolation threshold. In general, the relative dielectric constant of the composite $\varepsilon_{r,c}$ can be approximated by [4]

$$\varepsilon_{r,c} = \frac{\varepsilon_r}{\left|\phi_M - p_c\right|^q}, \qquad (1)$$

where $\varepsilon_r$ is the relative dielectric constant of the dielectric matrix and $\phi_M$ the volume fraction of metal in the composite and the index $q > 0$. The dielectric

constant of the composite increases with the volume fraction of metal and diverges in the immediate vicinity of the percolation threshold.

Pecharromán and Moya [7] reported an increase of the dielectric constant of a graded molybdenum/mullite composite by a factor of ~10,000 near the percolation threshold ($p_c$) of the Mo phase. Mo/mullite composites were prepared by pressure colloidal filtration of a slurry containing Mo and mullite. This resulted in a functionally graded composite. On one side of the sample a percolative Mo phase was obtained and on the other a non-percolative Mo phase. As a result, the percolation threshold (with respect to Mo) lies at some location between these two opposite sides. The dielectric constant in the graded composite was determined as a function of the local composition by employing 4-point impedance spectroscopy.

In contrast, for Pt/YSZ composites with randomly distributed phases and prepared by conventional mixing and processing methods, an increase in the capacitance by a factor of only 12.6 was achieved [8]. The data followed an expression derived from the normalised percolation theory [5], which also predicts a large increase in the dielectric constant near the percolation threshold of the metal phase. However, the values obtained were much lower since the concentration of Pt was well below the percolation threshold in these samples. In general, using present state-of-the-art preparation methods for disordered metal/ceramic composites, a metal concentration very close to the percolation threshold cannot be realised, as an uncontrollable amount of the starting materials is inevitably lost during each process step. In addition to this effect, the composites may possess a somewhat inhomogeneously distributed Pt phase, which increases the statistical chance of obtaining conducting composites below the theoretical percolation threshold for randomly distributed dual phase systems.

The amount of noble metal needed in the synthesis of composites with a randomly distributed metal phase is close to the volume concentration at the percolation threshold. The percolation threshold of the metallic phase in a disordered composite is 31.2 vol% [9] under the assumption that both phases consist of particles of equal size and shape. This still is a high volume fraction.

Metal/insulator composites can also be made by impregnation of a porous dielectric matrix with a metal solution. Impregnation of the dielectric phase using a metal solution will result in a random distribution of metal in the matrix provided the latter consists of a connected pore network. The increase in capacitance will be similar to that of dense metal/insulator composites [8]. On the other hand, electrolytic impregnation will result in metal deposition at the electrode only. Hence, no metal becomes dispersed in the remainder of the porous matrix. The electrode surface area can grow until a situation is reached where the electrodes are isolated by a thin barrier of the dielectric material only. The resulting composite microstructure may differ greatly from that obtained upon regular mixing of two phases such as described in Chapter 4. Hence the percolation threshold may have distinctly different values.

In the study presented here, porous zirconia was impregnated with platinum-containing solutions and the dielectric properties at ambient temperature were investigated. The system platinum/cubic yttria-stabilised zirconia (YSZ) was used here as a model system, since YSZ can form a double-layer capacitance at elevated temperatures (>400°C) and low frequency (<1 Hz). In case of oxygen vacancy-blocking electrodes, a double layer of oxygen vacancies can be formed at the interface between electrolyte and electrode at high temperatures. The double-layer capacitance differs from the normal expression for the room temperature capacitance of a dielectric medium. For electrolytes with an oxygen vacancy-conducting mechanism, the double-layer capacitance $C_{dl}$ can be calculated [10] from

$$C_{dl} = 2e\sqrt{\frac{\pi\varepsilon c}{k_B T}\left[V_O^{\cdot\cdot}\right]_{Bulk}\left(1-\left[V_O^{\cdot\cdot}\right]_{Bulk}\right)}, \qquad (2)$$

with $e$ the electron charge, ε the local dielectric constant in the double-layer of the oxide, $c$ the concentration of oxygen sites, $k_B$ the Boltzmann constant, $T$ the temperature, and $[V_O^{\cdot\cdot}]_{Bulk}$ the oxygen vacancy concentration in the bulk of the oxide. An important difference between the capacitance of a dielectric medium and the high temperature double-layer capacitance is that in the latter case the space charge layer is built up over the entire interfacial surface area, while at room temperature only the geometric surface area of

the capacitor influences the total capacitance. The capacitance of this double layer has been shown to reach values of approximately 1.6 $F/m^2$ at 550ºC [10].

Based on the effective medium theory Gluzman *et al.* [11] predicted an enhancement of 4 to 6 orders of magnitude increase in the dielectric constant of a metal/solid electrolyte composite at the percolation threshold of the metal phase. However, Abel and Kornyshev [12] showed that using random network simulations, in contrast to metal/dielectric composites, no giant enhancement in capacitance could be obtained near the percolation threshold of metal/electrolyte composites. The maximum increase of the double-layer capacitance was shown to be proportional to the ratio of the sample size over the individual grain size. Typically, this results in an enhancement of the capacitance by a factor < 1000.

In this chapter the room temperature capacitance of porous Pt/YSZ obtained via regular impregnation of a platinum salt is compared with that of porous Pt/YSZ after impregnation and electrolytic reduction of Pt inside the pores. In addition the high temperature double-layer capacitance of electrolytically impregnated Pt/YSZ is investigated. The latter samples still contain porosity after deposition, processes such as gas phase diffusion and oxygen exchange take place at the triple phase boundary at high temperatures. To distinguish between electrode and bulk processes, the electrochemical is investigated behaviour at elevated temperatures in a nitrogen atmosphere with changing $p(O_2)$.

## Experimental

Pt/YSZ composites were prepared via two routes. The first method involved regular impregnation of porous samples with a platinum salt solution, followed by reduction of the platinum salt by $H_2$ treatment. The second method involved immersion of the sample in a platinum-containing solution, after which the platinum was deposited at the electrode through electrolytic reduction.

Commercially available cubic yttria-stabilised zirconia (TZ-8Y, Tosoh Corporation, Tokyo, Japan), containing 8 mol% yttria, was uniaxially pre-

pressed at approximately 25 MPa and isostatically pressed at 400 MPa. The green samples were sintered at temperatures ranging from 1200 to 1300ºC for 1 h, with heating and cooling rates of 2 and 4ºC/min, respectively. The densities of the sintered samples ($\rho_s$) were determined using the Archimedes technique in mercury.

*Impregnation*

Porous discs sintered at temperatures between 1200 and 1300ºC were immersed in a 0.5 M aqueous $H_2[PtCl_6]$ solution, after which they were dried at 140ºC in air. At this temperature the platinum salt was transformed to $PtCl_4$ [13]. Reduction to metallic Pt took place at 400°C for 2 hours in a hydrogen containing (5 mol% $H_2$, 95 mol% $N_2$) atmosphere at ambient pressure. The cycle of impregnation and reduction was repeated up to 8 times. Finally, after drying the external electrodes were made by sputtering a platinum layer on opposite sides of the samples.

*Electrolytic impregnation*

A platinum electrode was sputtered on one of the flat sides of the zirconia discs sintered at 1200ºC. A platinum strip was attached to this Pt layer to serve as a cathode. The platinum electrode and the cylindrical side of the disc were sealed with beeswax to ensure net mass transport of Pt ions in the direction parallel to the applied electric field. Another platinum strip was placed on the other flat side of the disc to serve as the anode. A schematic representation of the sample is shown in Fig. 1. The distance between positive and negative electrode was kept as small as possible (± 2 mm, which corresponds to the sample thickness) in order to obtain a low cell resistance. This was achieved by placing the sample together with the electrodes between clips. The sample and electrodes were then immersed in an aqueous 0.5 M $H_2[PtCl_6]$ solution and a potential of 2.1 V was applied. This resulted in $Cl_2$ (*g*) formation at the anode and deposition of Pt at the cathode. The measured current was ≈1 mA. After a period of up to 15 h the metal strips were removed and the sputtered platinum layer was removed by polishing to obtain a porous surface. A platinum layer was then sputtered on the other side of the disc.

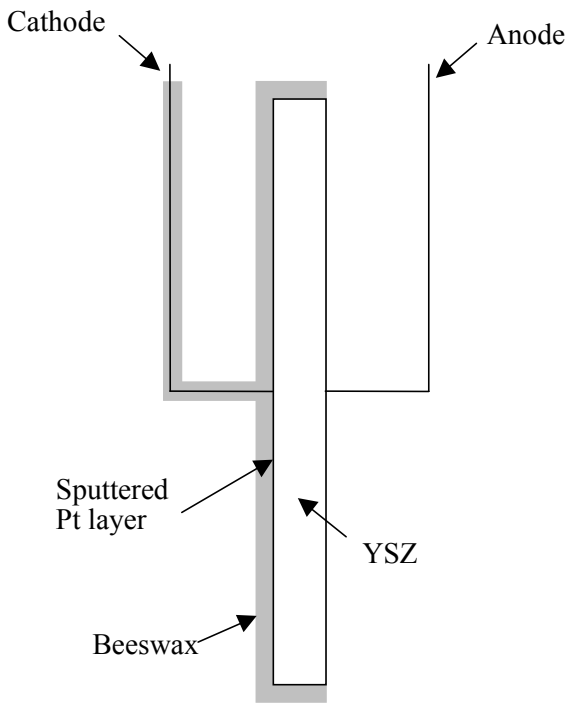


***Fig 1:*** *Schematic representation of a sample prepared for electrolytic impregnation.*

Platinum strips were placed on both sides of the disc as described above, and the cylindrical side and the sputtered layer were again covered with beeswax. The electrolytic deposition of Pt was performed for the same period as for the other. The platinum salt solution, which still remained in the pores after impregnation, was removed by ultrasonic treatment of the sample in water. Finally, after drying a new Pt electrode was sputtered on the side of the disc where the first electrolytic deposition of the Pt occurred.

*Electrical impedance spectroscopy*

The room temperature capacitance of the samples was determined by standard two-electrode impedance spectroscopy. The capacitance measurements were conducted at room temperature, using a frequency response analyser (Solartron® Instruments 1250 FRA, Schlumberger Technologies Ltd., Farnborough, Hampshire, England) in the frequency range from 1 Hz to 60 kHz at 10 mV rms. Using the equivalent circuit software program [14], the experimental impedance plots could be interpreted in terms of a resistance in series with a capacitance.

To determine the double-layer capacitance the impedance of the sample that had been impregnated electrolytically for 15 h was investigated at 551ºC by 2-point impedance spectroscopy. The electrochemical properties were de-

termined from equilibrium measurements in the frequency range from 10 mHz to 65 kHz at 10 mV rms. The initial measurements were performed in a 5% oxygen-containing nitrogen atmosphere. After ending the oxygen supply, several measurements were conducted to investigate the electrochemical behaviour over time until equilibrium had been reached and a double-layer capacitance was formed.

## Results and discussion

The densities and relative porosities of samples sintered at temperatures between 1200 and 1300ºC are listed in Table 1. The density of YSZ increases with sintering temperature, and thus the porosity decreases. At the highest sintering temperature the samples remain 6 % porous after pressureless sintering.

***Table 1:*** *Sintering behaviour of porous zirconia.*

| $T_{sint}$ [ºC] | $\rho_{sint}$ $\cdot 10^{-3}$ [kg/m$^3$] | f [%] |
|---|---|---|
| 1200 | 3.8 | 36 |
| 1220 | 4.1 | 31 |
| 1240 | 4.3 | 28 |
| 1260 | 4.7 | 20 |
| 1280 | 5.2 | 13 |
| 1300 | 5.6 | 6 |

Porous YSZ can be regarded as a two-phase composite consisting of dense YSZ and air. Assuming that all pores have an equal size and are spherically shaped, the Maxwell-Garnett equation can be applied to calculate the dielectric constant ($\varepsilon_{r,\,MG}$) [15]:

$$\varepsilon_{r,\,MG} = \varepsilon_{r,\,YSZ}\frac{\varepsilon_{r,\,air} + 2\varepsilon_{r,\,YSZ} + 2f\left(\varepsilon_{r,\,air} - \varepsilon_{r,\,YSZ}\right)}{\varepsilon_{r,\,air} + 2\varepsilon_{r,\,YSZ} - f\left(\varepsilon_{r,\,air} - \varepsilon_{r,\,YSZ}\right)}, \qquad (3)$$

where $\varepsilon_{r,\,YSZ}$ is the relative dielectric constant of zirconia, $\varepsilon_{r,\,air}$ the relative dielectric constant of air and *f* the porosity. This equation is valid up to a porosity of approximately 40 % [15]. In Fig. 2 it is shown how the dielectric constant decreases with increasing porosity. The experimental data are in reasonable accordance with the predictions from the Maxwell-Garnett equation taking a dielectric constant of $\varepsilon_{r,\,YSZ} = 28.7$ for cubic YSZ [10].

The capacitance of the impregnated samples varies with the concentration of platinum according to Eq. 1. An emperical enhancement of the capacitance, *g*, resulting from percolation effects due to the presence of Pt, can be obtained from the expermentally obtained value for the capacitance ($C_{exp}$):

$$C_{exp} = g\frac{\varepsilon_0 \varepsilon_{r,MG} A}{d}, \tag{4}$$

Here $\varepsilon_0$ is the permittivity of vacuum, $A$ the geometric surface area of the sputtered electrode and $d$ the geometric distance between the electrodes.

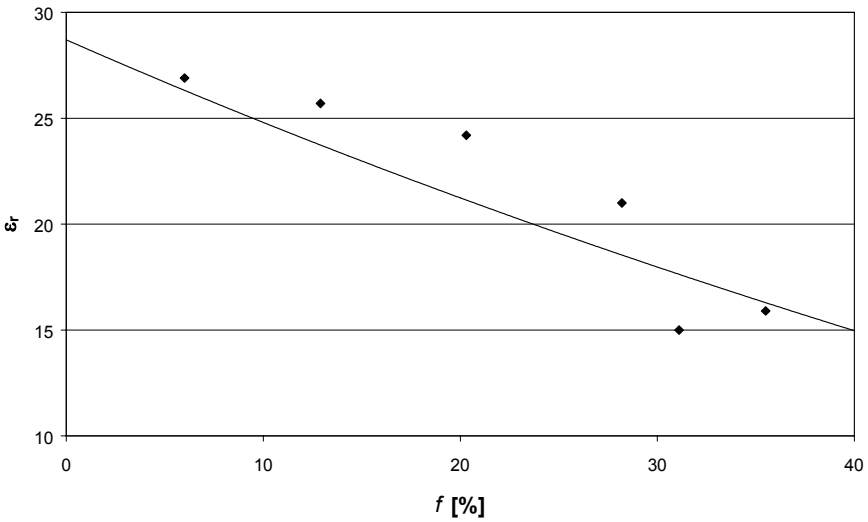


***Fig.2:*** *The dielectric constant of 8 mol% $Y_2O_3$ doped YSZ as a function of porosity; ♦ experimental data, - Maxwell-Garnett equation.*

*Regular impregnation*

In Fig. 3 the increase in capacitance as function the deposited Pt concentration is shown. For samples with a porosity of 6 vol %, the capacitance of the sample remains constant, since almost no Pt is deposited in the pores. It is likely that at this porosity no continuous pore structure was present and therefore no 3D platinum structures was formed. For samples with a porosity of 13 % the increase in capacitance reached a final value of approximately a

factor 3 compared to its original value. Most likely, this sample also does not contain a percolative pore structure: after 7 impregnation steps the platinum phase still has not formed a conductive path through the zirconia matrix. Moreover, the capacitance does not increase further upon additional impregnation steps. At higher porosities the samples apparently contain a connected pore structure, since only a few impregnation steps already led to the formation of a percolative platinum phase. The largest increase in capacitance was obtained for a YSZ sample with a porosity of 20 vol %. In this case *g* is

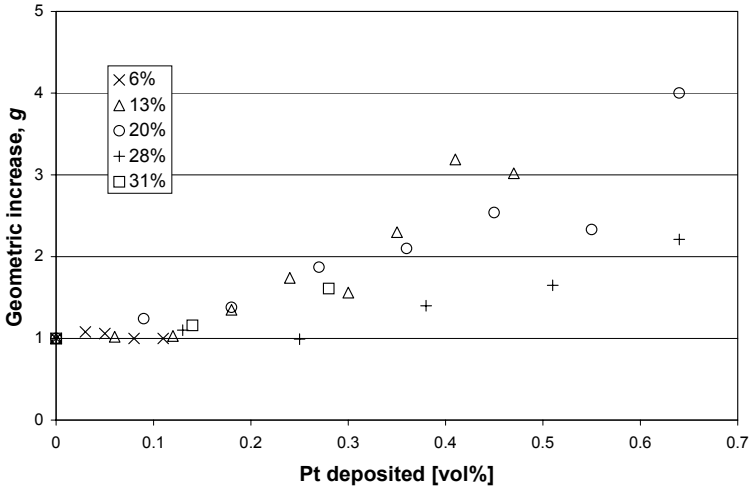


***Fig. 3:*** *Enhancement factor g of Pt/YSZ composites with varying porosity as function of the deposited Pt concentration.*

equal to approximately 4 after 7 impregnation steps.

The optimal porosity can be found where the pores barely form a connected network. At this composition the highest chance of the formation of internal Pt networks, formed at both external electrodes, but not connected to each other, emerged. Here it is expected to lie between 13 and 20 vol %. The largest amount of platinum in regularly impregnated YSZ was obtained after 7 impregnation steps of a sample with a porosity of 20 %. From the pore volume, number of impregnation steps and the precursor concentration it

was estimated that the concentration of Pt in this composite amounts to approximately 0.7 vol%.

*Electrolytic impregnation*

Samples with a porosity of about 38 vol % were used to ensure that the pores would be completely filled with the platinum-containing solution during electrolytic impregnation. Moreover, such a highly porous structure also ensures continuous diffusion of Pt(IV) towards the cathode. In Fig. 4 the enhancement of the capacitance of electrolytically impregnated samples as a function of impregnation time is shown. The capacitance increased with the amount of Pt deposited. After deposition of 1.6 vol% Pt (after 15 h of electrolytic impregnation at each electrode), the capacitance was enhanced by a factor of approximately 20. Impregnating for an even longer period resulted

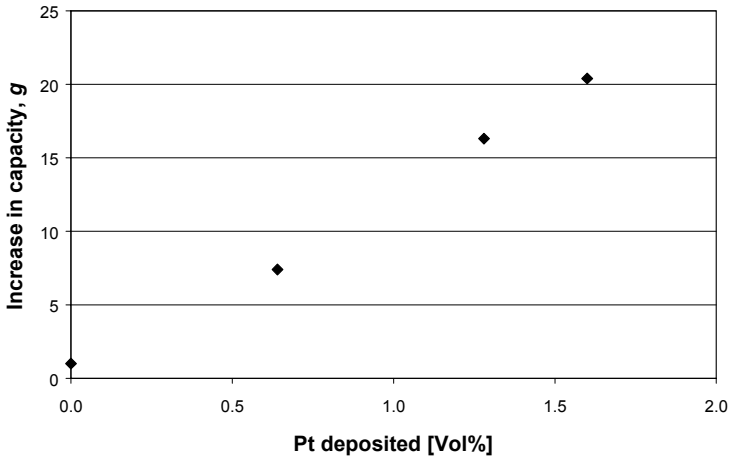


***Fig. 4:*** *Enhancement factor g of Pt/YSZ composites sintered at 1200ºC as function of Pt concentration during electrolytic impregnation.*

in short-circuiting of the electrodes.

Assuming 100% efficiency of the electrolytic impregnation process, the theoretical maximum concentration of platinum in the electrolytically impregnated sample can be calculated from the applied electrical current.

Hence, an electrolytically impregnated sample, where each electrode was allowed to grow for 15 h, contained *ca.* 1.6 vol% Pt. For dense composites with a randomly distributed Pt phase, a maximum enhancement of $g = 12.6$ at a volume percentage of approximately 25 vol% Pt was obtained [7]. Hence, regular impregnation of porous YSZ did not result in a larger increase in capacitance in comparison with dense composites with a randomly distributed platinum phase. On the other hand, it decreased the required amount of platinum by more than one order of magnitude. For electrolytically impregnated YSZ, the increase in capacitance was larger than that of the formerly mentioned dense composites. And in this case the amount of

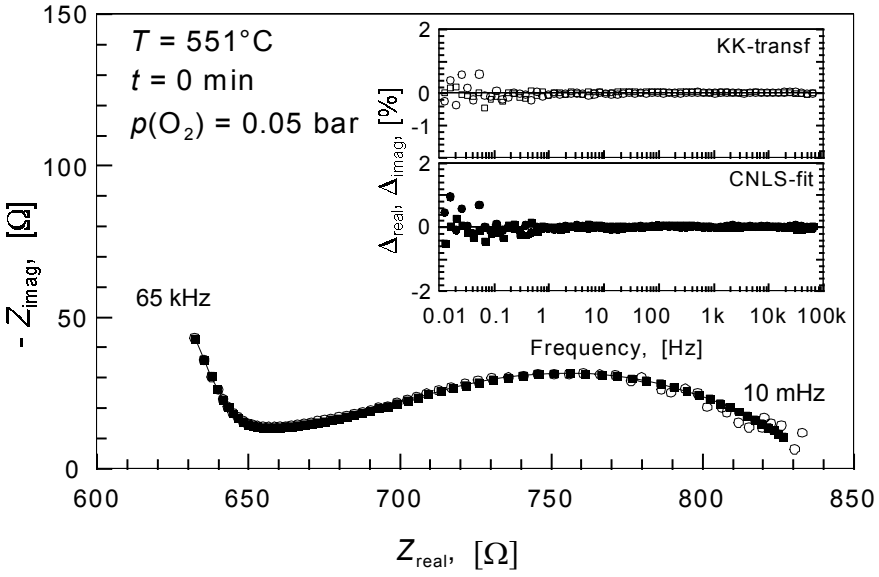


***Fig. 5:*** *Impedance of YSZ-Pt composite. (○) measurement, (-■-) CNLS-fit model based on a (RQ)(RQ)(RQ) equivalent circuit. Insert: residuals plot for the K-K test and the CNLS-fit.*

platinum required was also drastically decreased.

The electrochemical behaviour of a sample electrolytically impregnated for 15 h was investigated at 551ºC. The impedance measured in a 5% oxygen atmosphere ($p(O_2) = 0.05$ bar) is presented in Fig. 5. The inset shows the

residuals plots for the CNLS-fit and for the Kramers-Kronig transform test [16]. The data could be modelled with a (*RQ*)(*RQ*)(*RQ*) equivalent circuit, which is a symbolic representation of an equivalent circuit as described in ref [14]. The residuals obtained with both the CNLS-fit and the K-K test show close agreement in the error distribution, which indicated that the proposed equivalent circuit was realistic.

***Table 2:*** *Results of CNLS-fit of impedance data presented in Fig. 4. Equivalent circuit used: $(RQ)_1(RQ)_2(RQ)_3$.*

| Element | Value | Error |
|---|---|---|
| $R_1$ | 636 [Ω] | 0.9 % |
| $Q_1$-$Y_0$ | $1.1 \cdot 10^{-9}$ [$S \cdot s^n$] | 50 % |
| ,, n | 0.885 | 4 % |
| $R_2$ | 44 [Ω] | 29 % |
| $Q_2$-$Y_0$ | $3.7 \cdot 10^{-4}$ [$S \cdot s^n$] | 51 % |
| ,, n | 0.46 | 18 % |
| $R_3$ | 160 [Ω] | 6 % |
| $Q_3$-$Y_0$ | $2.30 \cdot 10^{-3}$ [$S \cdot s^n$] | 7 % |
| ,, n | 0.458 | 3 % |
| $\chi^2_{CNLS}$ | $1.5 \cdot 10^{-6}$ | |
| $\chi^2_{K\text{-}K}$ | $2.8 \cdot 10^{-6}$ | |

The high frequency CPE element ($Q_1$) was close to a capacitance with a *n*-value of 0.885. The magnitude of the $Y_0$-value of the CPE ($\sim 10^{-9}$) seemed to indicate that it is related to a grain boundary impedance.

The low frequency part was dominated by a diffusion related process as the CPE *n*-value was close to 0.5 ($n = 0.46$). Between these two readily distinguishable sub-circuits, a third semi-circle is found from the data analysis. Again, this sub-circuit must be related to a diffusion type of response as the *n*-value of the corresponding CPE is close to 0.5 (see Table 2). The error estimates for this sub-circuit are rather large, which is due to the small contribution to the overall dispersion.

Upon a change to a $N_2$ atmosphere ($p(O_2) \sim 10^{-5}$ bar) a rapid change in the impedance was observed. A time sequence of the observed impedance is presented in Fig. 6. Within a relatively short time, an important low frequency diffusion dispersion (straight 45° line) develops. The question arises what part of the dispersion relates to electrode response and what part is related to the bulk properties of the Pt/YSZ composite. A full CNLS-fit results in significant scatter between parameters. On visual inspection it seems that the (*RQ*)(*RQ*)(*RQ*) circuit, observed at $t = 0$ and $p(O_2) = 0.05$ bar, remains to some extent unaffected by the drastic change in $p(O_2)$.

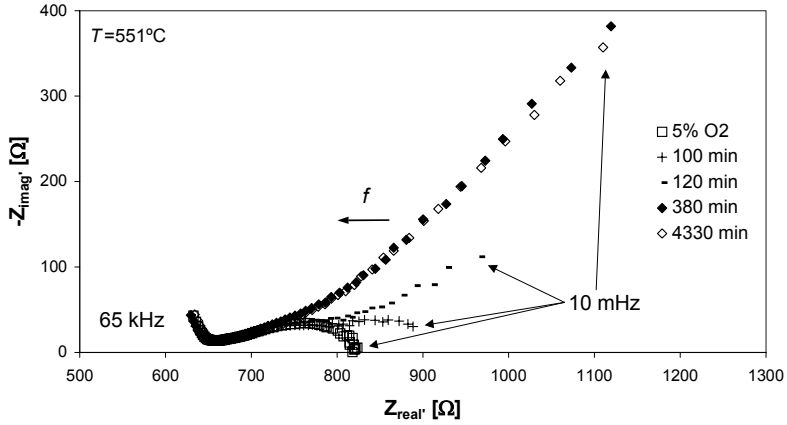


***Fig. 6:*** *Development of impedance with time upon a $p(O_2)$ change from 0.05 bar to ~$10^{-5}$ bar.*

To test the hypothesis, this particular circuit was subtracted from the disper-

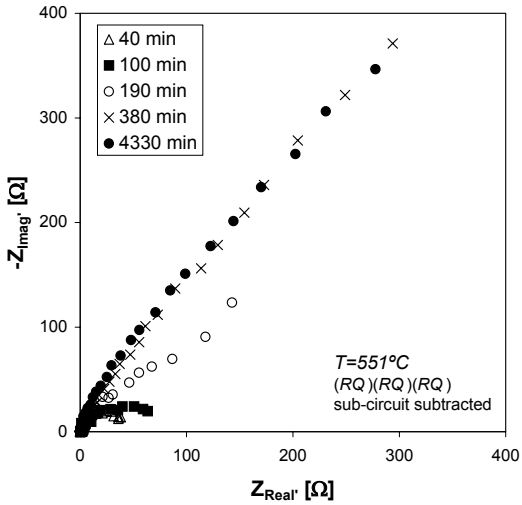


***Fig. 7:*** *Evolution with time of the low frequency dispersion after subtraction of the $p(O_2)$ independent (RQ)(RQ)(RQ) circuit.*

sions measured after the change to $N_2$. The resulting low frequency dispersions are presented in Fig. 7. This figure shows a clear evolution of the electrode response of the Pt/YSZ composite. No strong deviations are observed at the high frequency end. As possible deviations should be due to the subtraction of an incorrect dispersion model, one can safely assume that the (*RQ*)(*RQ*)(*RQ*) circuit is not affected by $p(O_2)$ changes. Hence it must represent a bulk property.

At intermediate time-frames, it is not possible to obtain a good fit to the subtracted dispersion. This is understandable as the system is still moving towards a new equilibrium situation following the step in $p(O_2)$. The slow change affects especially the lowest frequencies. After about 6 h the system had reached thermodynamic stability. The low frequency tail can then be modelled with capacitance in parallel with a semi-infinite diffusion element (Warburg). The fit results are presented in Table 3.

The capacitance could be interpreted as the double-layer capacitance associated with the Pt/YSZ interface. It is more difficult to ascribe the Warburg element to a physical process. One possible option is surface diffusion of adsorbed oxygen species on the Pt surface, while another option could be gas phase diffusion of oxygen through the pores of the (porous) YSZ-Pt composite.

***Table 3:*** *CNLS-fit results of the low frequency tail after subtraction of the (RQ)(RQ)(RQ) sub-circuit. The data is fitted with a R(C[RW]) circuit. The first resistance is due to minor subtraction errors and has no significance.*

| Parameter | 1440 min. | 2985 min. | 4330 min.* |
|---|---|---|---|
| range [Hz] | 0.01 - 3 | 0.01 - 10 | 0.01 10 |
| $\chi^2_{CNLS}$ | $9 \cdot 10^{-4}$ | $1 \cdot 10^{-3}$ | $2.4 \cdot 10^{-3}$ |
| $R_1$ [Ω] | 2.9 [9%] | 2.1 [6%] | 1.7 [7%] |
| $C_2$ [F] | $4.1 \cdot 10^{-3}$ [2%] | $5.2 \cdot 10^{-3}$ [5%] | $6.4 \cdot 10^{-3}$ [2.3%] |
| $R_3$ [Ω] | -- | 12 [60%] | 42 [20%] |
| $W_4$, $Y_0$ [$S \cdot s^{0.5}$] | $7.0 \cdot 10^{-3}$ [1.2%] | $7.0 \cdot 10^{-3}$ [1.6%] | $7.4 \cdot 10^{-3}$ [3%] |

*equilibrium is reached

From the magnitude of the double-layer capacitance $C_2$, a prediction of the total electrode surface area can be given. The average capacitance calculated

from the equilibrium $C_2$ value (~ $6.4 \cdot 10^{-3}$ F) and the geometric electrode surface area ($A = 0.25$ cm$^2$) amounts to a specific capacitance $C = C_2/A_g = 2.6 \cdot 10^2$ F/m$^2$. From the work described in Chapter 2 it is known that the double-layer capacitance of dense cubic YSZ with polished flat electrode/electrolyte interfaces at 549ºC is $C_{YSZ} \approx 1.6$ F/m$^2$ [10]. Hence the specific electrode/electrolyte interfacial surface area $A_{spec}$ of the sample under investigation here is $A_{spec} = C/C_{YSZ} = 1.6 \cdot 10^2$ m$^2$/m$^2$. The *total* specific Pt surface area $A_t$ can be estimated to be $A_t \approx A_{spec}/(1-f) = 2.6 \cdot 10^2$ m$^2$/m$^2$, where $f = 0.38$ is the porosity of the sample. Since the measurement of absolute double-layer capacitances is not very accurate [17], $A_{spec}$ probably lies somewhere in the range 80 – 300 m$^2$/m$^2$.

During electrolytic impregnation Pt(IV) species diffuse into the direction parallel to the electric field strength. Platinum is deposited at the cathode, so it can be assumed that the internal electrode network grows preferentially in a direction that is parallel, but opposite to the electric field vector. In this manner a large interfacial area between Pt and YSZ can be obtained. Its specific surface area can be determined from impedance measurements at elevated temperatures. The specific electrode surface area calculated from these measurements was not measured at room temperature. At room temperature only the component of the electrode surface area that is perpendicular to the electric field contributes to the polarisation of the dielectric phase. Hence, the effective electrode surface area is smaller and the main increase in capacitance of approximately 20 times can be attributed to percolation effects. On the other hand, at elevated temperatures the total interfacial surface area between electrolyte and electrode contributes to the formation of the electrochemical double-layer.

## Conclusions

For porous Pt/YSZ composites the relative dielectric constant decreases with increasing porosity. The trend could be described satisfactorily in terms of the Maxwell-Garnett theory. Upon regular impregnation, the capacitance of samples containing a connected pore structure was increased up to ~4 times before the electrodes short-circuit. The capacitance of electrolytically im-

pregnated YSZ sintered at 1200ºC, was enhanced by a factor of up to ~20 after deposition of platinum at both electrodes.

The main advantage of electrolytic impregnation over conventional processing methods is that only a small amount of noble metals is necessary to obtain a capacitance enhancement. A larger increase in capacitance compared to random composites was obtained, while the volume fraction of Pt was reduced with more than an order of magnitude. On the other hand, the porosity of the matrix, necessary for impregnation, led to a reduction of the effective dielectric constant of the oxidic matrix by a factor of 1.1-1.9.

Electrochemical impedance measurements at 551ºC in air in the frequency range 10 mHz – 65 kHz on a sample electrolytically impregnated for 15 h could be interpreted as a series of bulk and grain boundary processes. The formation of an oxygen vacancy double-layer at the Pt/YSZ interface was investigated by changing the atmosphere surrounding the sample from 0.05 bar $O_2$ to pure nitrogen and measuring a number of impedance spectra over time until equilibrium was reached. The double layer capacitance could be determined at $C=2.6\cdot10^2$ F/m$^2$ (geometric surface area). The double layer was formed over the entire interface between electrode and electrolyte. The specific electrode/electrolyte interfacial surface area lies in the range 80 – 300 m$^2$/m$^2$.

## References


1. B.W. Peace*, Ceram. Ind*., 32, 1994.
2. A. Morell and J.-C. Niepce, *J. Mater. Educ*. **13**. 173, 1991.
3. R. Höppener and A. Daemen, in CARTS-EUROPE '94, *Electron. Components Inst. Int., 1995. Proc. 8th Eur. Pass. Comp. Symp*., Crowborough, UK, October 17-20 (1994) p. 47.
4. A.L. Efros and B.I. Shklovskii, *Phys. Stat. Sol*., (b) **76**, 475, 1976.
5. D.S. McLachlan, *Mat. Res. Symp. Proc*., **411**, 309, 1996.
6. V.E. Dubrov, M.E. Levinshtein and M.S. Shur, *Zh. Eksper. Teor. Fiz*., **70**. 2014, 1976.
7. C. Pecharromán and J.S. Moya, *Adv. Mater*., **12** [4], 294, 2000.
8. M.G.H.M. Hendriks, W.E. van Zyl, J.E. ten Elshof and H. Verweij, *Accepted for publication in Mater. Res. Bull*.
9. D. Stauffer and J.G. Zabolitzky, *J. Phys. A: Math. Gen*., **19**, 3705, 1986.
10. M.G.H.M. Hendriks, J.E. ten Elshof, H.J.M. Bouwmeester and H. Verweij, *Submitted to Solid State Ionics*.
11. S. Gluzman, A.A. Kornyshev and A.V. Neimark, *Phys. Rev. B*, **52** [2], 927, 1995.
12. J. Abel and A.A. Kornyshev, *Phys. Rev. B*, **54** [9], 6276, 1995.
13. D.R. Lide, Handbook of chemistry and physics, 75th Special student edition, Boca Raton, U.S.A., 1994, p. 4-82.
14. B.A. Boukamp, *Solid State Ionics*, **20**, 31, 1986.
15. P.A.M. Steeman, Interfacial phenomena in polymer systems; A dielectric approach, PhD Thesis, Delft, The Netherlands, 1992.
16. B.A. Boukamp, *J. Electrochem. Soc*., **142** [6], 1885, 1995.
17. R.D. Armstrong and R. Mason, *J. Electroanal. Chem*., **41**, 231, 1973.

# Chapter 7
# Layered structures of YSZ sandwiched between Pt/YSZ composites

*Layered structures of cubic yttria-stabilised zirconia (YSZ) sandwiched between two layers of platinum/YSZ composites with the platinum concentration varying between 20 and 55 vol% were prepared to obtain large double-layer capacitances. The capacitances were due to the presence of large 3-dimensional electrode surface areas in the composite layers. The composite layers were subjected to image analysis on SEM micrographs. It is demonstrated that the specific surface area of the platinum particles decreased from ~$17 \cdot 10^3$ to ~$13.5 \cdot 10^3$ $cm^2/cm^3$ with increasing Pt concentration. The image analyses obtained with an in-lens detector with the possibility to distinguish potential differences, revealed that the effective surface area of the Pt particles that were part of a conducting percolative network increased with Pt concentration to approximately $11 \cdot 10^3$ $cm^2/cm^3$ at a Pt metal volume fraction of 0.50. From impedance spectroscopy measurements performed at 550°C it was determined that the capacitance increased with Pt concentration in the composite layer and may become as high as $4.3 \pm 1.3$ $kF/m^2$ at 50 vol% Pt. The specific electrode surface area calculated from this data was in good agreement with the data obtained from image analysis.*

## Introduction

Supercapacitors exhibit the unique property that large quantities of electrochemical energy can be stored in the double layer near the electrodes. Typical capacitances of 1-10 F can be obtained with supercapacitors compared to $10^{-10}$–$10^{-3}$ F for conventional capacitors [1]. The capacitance obtained with conventional capacitors finds its origin in the electronic and ionic polarisation of the dielectric medium. For ideal capacitors the capacitance is constant and linearly proportional to the component of the electrode surface area perpendicular to the electric field strength. Supercapacitors make use of an ion-conducting medium instead of a dielectric. In these materials mobile charge carriers can accumulate or deplete near the interface between the electrode and electrolyte resulting in a space charge layer. In such electrochemical capacitors the double-layer capacitance can reach values up to ~100 $\mu F/cm^2$ depending on the nature of the electrolyte [2]. Next to the double-layer itself, supercapacitors can have electrodes that possess an enormous electrode surface area on the order of $10^3$ $m^2/g$ on which space-charge build-up can take place [3]. The appropriate combination of space-charge layers and large surface areas are important factors in designing state-of-the-art supercapacitors.

Commonly used materials for the electrolyte phase are ion-conducting polymers [4, 5] or aqueous KOH solutions [2,6], while large surface area carbon [7], electron-conducting oxides like $In_2O_3$ or $RuO_2$ [2, 3, 8, 9], or electron-conducting polymers [7, 10, 11] are used for the electrodes.

In previous work the double-layer capacitance of yttria-stabilised zirconia (YSZ) was investigated [12]. Compared with liquid electrolytes, which have two or more mobile charge carriers, YSZ only possesses one mobile charge carrier, namely oxygen ions. At elevated temperatures (>400ºC), oxygen ions become mobile and may diffuse through the oxygen sub-lattice through a hopping mechanism to neighbouring vacant lattice sites. At electrodes that block transport of oxygen, a double-layer capacitance can be formed and can amount to approximately 1-10 $F/m^2$, depending on temperature and yttria dopant concentration and thus on oxygen vacancy concentration [12].

The electrode surface area can be increased, for instance, by using composite materials consisting of an ionic conductor and a metallic phase. The elec-

tron-conducting particles that are in contact with the electrode increase the electrode surface area. In porous YSZ a large effective electrode surface area (~260 $m^2/m^2$) was grown by electrolytic impregnating of the compact with $H_2[PtCl_6]$ salt solutions, followed by reduction to metallic Pt [13]. Another possibility to increase the electrode surface area is to prepare cermet electrodes, with the concentration of both the metal and electrolyte phase above the percolation threshold. De Boer [14] obtained a large triple phase boundary on the anode of a solid oxide fuel cell by forming porous composites of YSZ and nickel where both materials in the composite were fully percolative. A percolative pore structure was also obtained.

The aim of this study was to prepare dense layered structures consisting of YSZ sandwiched between two Pt/YSZ composite layers with a varying Pt concentration, and to determine the influence of the Pt concentration on the capacitance and thus the electrode surface area to which it relates. When the metal fraction is above its percolation threshold in the composite layers, a 3-dimensional metallic network is expected, leading to a large electrode surface area. The structure of the composite electrodes was investigated with image analysis performed on SEM-micrographs. Capacitance measurements were performed at 550ºC.

## Experimental

Commercially available cubic yttria-stabilised zirconia containing 8 mol% yttria (TZ-8Y, Tosoh Corporation, Tokyo, Japan) was milled in a mortar after which it was sieved using a 38 μm mesh. An aqueous 0.5 M $H_2[PtCl_6]$ solution was added to the powder and mixed. A film evaporator was utilised to remove water while keeping the suspension as homogeneous as possible. The dried powder was reduced in a hydrogen-containing atmosphere (5% $H_2$ in $N_2$ at 1 bar) at 400ºC for 2 hours [15]. Layered structures, which consisted of the resulting dual-phase powders and sieved YSZ powder were obtained. The YSZ phase was sandwiched between two composite powders and the three successive layers were uniaxially pressed at 15, 20 and 25 MPa, respectively. The green compacts were sintered between two alumina plates at 1480ºC for 6 h with heating and cooling rates of 1 and 2ºC/min, respectively. The final density after sintering exceeded 93% of the theoretical value. On

both flat sides of the disc dense gold electrodes were provided by dc-sputtering. A schematic representation of a capacitor obtained by the above procedure is shown in Fig. 1. The layer thickness' of both the YSZ layer and the composite layers was ~0.6 mm.

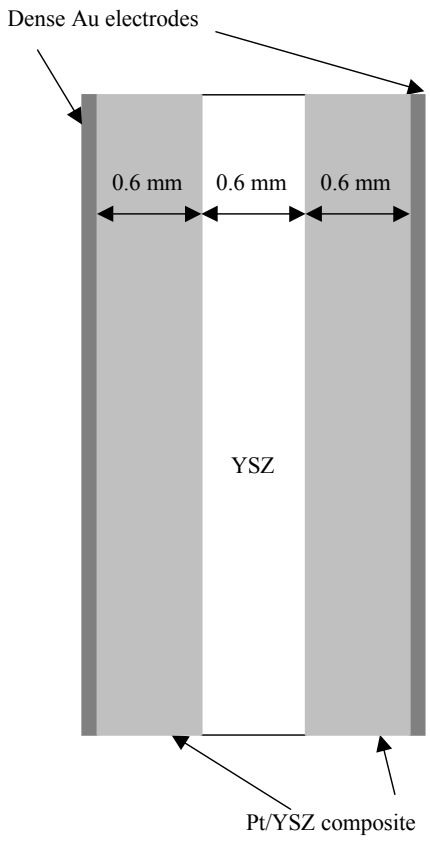


***Fig. 1:*** *Schematic representation of a capacitor consisting of a YSZ layer sandwiched between 2 Pt/YSZ composite layers.*

On the as-prepared samples two-point electrical impedance spectroscopy measurements were performed in a nitrogen atmosphere at 550ºC using a frequency response analyser (Solartron Instruments 1250 FRA, Schlumberger Technologies Ltd., Farnborough, Hampshire, England) at 10 mV rms in the frequency range of 1 mHz to 60 kHz. The experimental impedance plots were fitted to an equivalent circuit consisting of a constant phase element (CPE) in series with a resistance using the Equivalent Circuit software program [16]. The double-layer capacitance of these composites was calculated from the CPE values. The response time of compacts with a high Pt concentration (>45 vol%) in the composite layer was too large to determine the double layer capacitance within applied the frequency range. For that purpose potential step response (Autolab® PGSTAT20, ECO Chemie, Utrecht, The Netherlands) measurements were performed on the latter samples. The potential was set at a constant value of

10 mV while the decrease in current was measured as a function of time. The double-layer capacitance could be calculated by integration of the current over time.

The microstructures of the samples were observed by SEM (JSM-5800 Scanning Microscope, JEOL Ltd., Tokyo, Japan) using a 17 kV electron beam. After sputtering of a conducting gold layer on polished cross-sections of the samples, micrographs of the composite electrodes were taken with an increasing contrast level. Non-sputtered polished cross-sections were investigated with SEM (LEO 1500 Series, LEO Electron Microscopy Ltd., Cambridge, England) using an in-lens detector perpendicular to the sample surface and an electron beam operating at 2 kV. Using this detector, differences in potential due to charging could be detected to distinguish isolated Pt particles from the grounded 3-dimensional Pt network.

## Image analysis

In SEM investigations of sputtered Pt/YSZ composites with a standard SE detector, platinum appears as a bright phase, while the YSZ phase is dark [15]. The average platinum grain sizes estimated from the SEM pictures are listed Table 1. The majority of the platinum grains in the composite with a Pt concentration of 20 vol% had a grain size of *ca*. 0.5 μm. However, a few larger particles with a grain size up to 10 μm were also present. The average platinum grain size increased to 1.9 μm with increasing Pt concentration in the composite. At concentrations >40 vol% the Pt particles formed large clusters.

***Table 1:*** *Pt particle size in the composite layer estimated from SEM micrographs.*

| $\nu_{Pt}$ | $d_p$ [μm]* |
|---|---|
| 0.20 | 0.6 |
| 0.25 | 0.8 |
| 0.30 | 1.0 |
| 0.35 | 1.2 |
| 0.40 | 1.4 |
| 0.45 | 1.6 |
| 0.50 | 1.7 |
| 0.55 | 1.9 |

*Error estimate: 5.7%

In Fig. 2a a picture of a composite layer containing 40 vol% Pt is shown. Using the computer software program Image Pro® Plus 3.0 (MediaCyber-

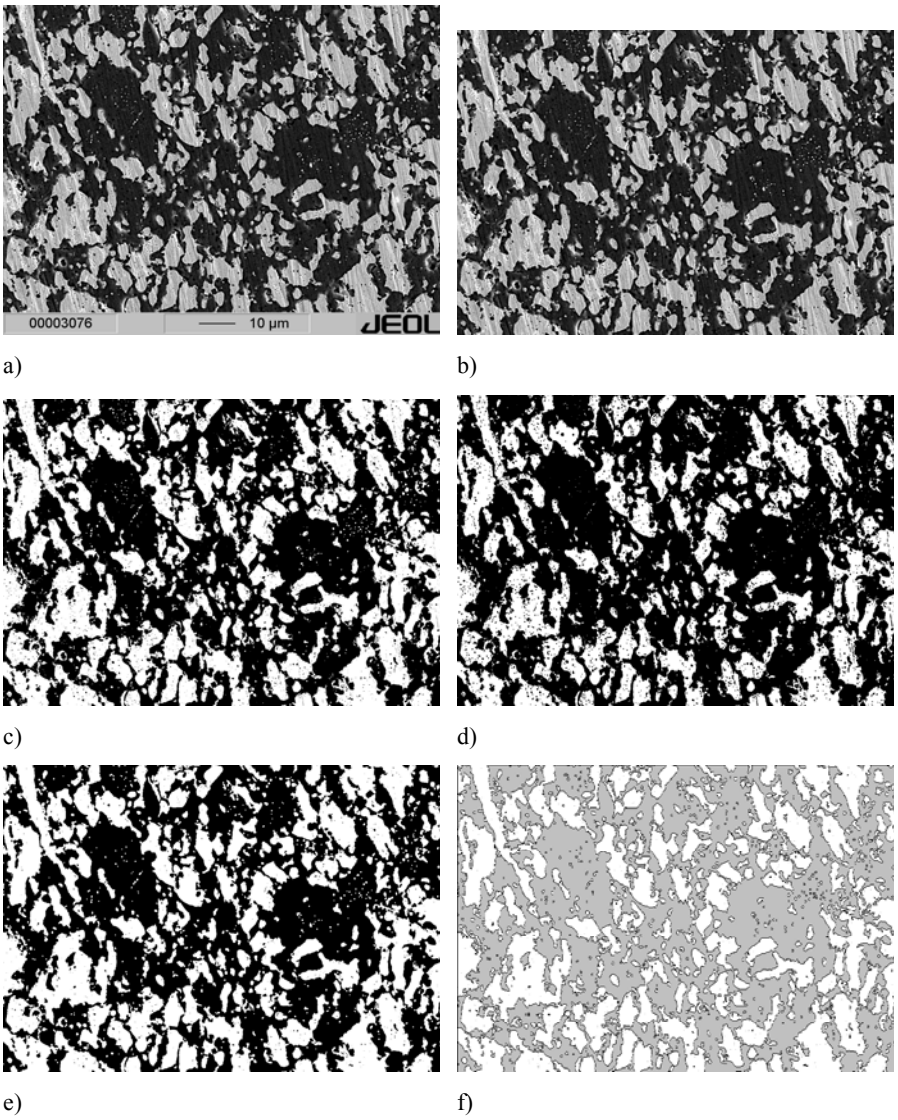


***Fig. 2:*** *Image analysis procedure on a SEM micrograph of a Pt/YSZ composite electrode containing 40 vol% Pt; a) SEM photo, b) SEM photo without scale bar, c) thresholding step, d) first smoothing step; eroding the white particles, e) second smoothing step; enlarging the white particles and f) counting of the perimeter.*

netics®, Silver Spring, MD, U.S.A.), image analysis of the SEM pictures was performed. The scale of the pictures was not changed during the analysis. Since the porosity of the sample resulted in a decrease in the volume fraction of Pt compared to the composition of the starting materials, a correction for this effect was incorporated.

In Fig. 2c the picture was converted to a black and white binary image by thresholding at a value between 0 and 255 in such a way that the fraction of white pixels was equal to the volume fraction of Pt in the composite. In this manner the pores are seen to be imbedded in the YSZ matrix.

Due to the intrinsic properties of the image analysis program white noise was obtained at the edges of the bright particles, resulting in a rough interface with the YSZ matrix. The edges were smoothed in two sequential steps. First the white particles were eroded (Fig. 2d), which yielded smaller Pt particles and thus the corresponding surface area was also smaller. This effect was corrected in a second step namely the enlarging of bright particles (dilation) until the surface area of the bright particles was equal to the initial volume fraction of Pt. This resulted in a further smoothing of the interface (Fig. 2e). In the final step (Fig. 2f) the number of pixels at the perimeter of the platinum particles was counted.

To obtain a satisfactory visual contrast between the YSZ phase and the drawn perimeter of the Pt particles, the YSZ phase was coloured grey in Fig. 2f.

By counting the total number of pixels in the picture the specific surface area of platinum in the composite ($A_{\mathrm{spec}}$) was calculated by the following expression derived from quantitative stereology theory [17]:

$$\left(\frac{L_{\mathrm{perimeter}}}{A_{\mathrm{picture}}}\right)_{2\mathrm{D}} = \left(\frac{A_{\mathrm{particles}}}{V_{\mathrm{composite}}}\right)_{3\mathrm{D}} = A_{\mathrm{spec}}\,, \tag{1}$$

where $L_{\mathrm{perimeter}}$ is the length of the perimeter visible on the micrograph, $A_{\mathrm{picture}}$ the area of the SEM micrograph, $A_{\mathrm{particles}}$ the total surface area of the platinum particles in the composite, and $V_{\mathrm{composite}}$ the volume of the composite. Quantitative stereology relates 1- and 2-dimensional observations to the true 3-dimensional structure and characterises the geometrical aspects of the mi-

crostructure numerically. In this case the specific surface area of the platinum particles is of interest.

In situations where Pt particles in the composite layer are spheres of equal size, one would expect the specific surface area of such particles to be proportional to $\nu_{Pt}(1-\nu_{Pt})$, where $\nu_{Pt}$ is the Pt fraction in the composite layer. However, the average Pt particle size, $d_p$, listed in Table 1, shows an increase with increasing Pt content. The specific Pt surface area can be calculated from the average particle size, using the relationship

$$A_{spec} = \frac{2\pi}{d_p} \nu_{Pt} (1 - \nu_{Pt}) . \qquad (2)$$

Eq. (2) was derived by following the procedure for calculating the specific surface area of randomly dispersed cubes as outlined by Sahimi et al. [18]. The specific surface area with varying Pt concentration is shown in Fig. 3. The specific surface area was quite large, up to *ca.* $17 \cdot 10^3$ $cm^2/cm^3$ and de-

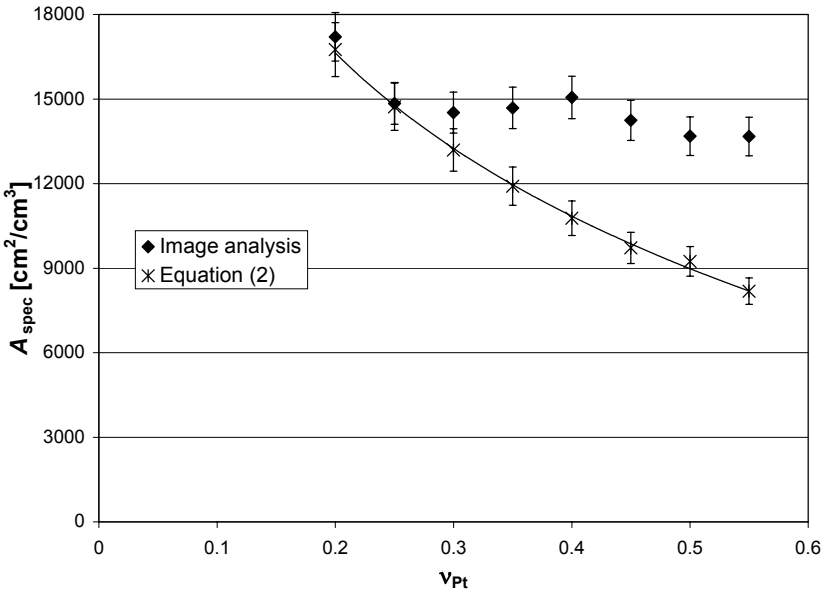


***Fig. 3**: Specific surface area of the platinum particles in the composite layer as function of the platinum concentration in the layer. ♦ obtained with image analysis, ∗ theoretical predictions from Eq. (2).*

creases to ~$13.5 \cdot 10^3$ $cm^2/cm^3$ with increasing Pt concentration in the composite layer. In Fig. 3 the specific surface area calculated from Eq. (2) is shown. At low concentration of Pt in the composite layer, the experimental and theoretical values were in good agreement. At larger Pt concentrations, however, the theoretical specific surface areas calculated using the estimated Pt particle sizes were up to 30% lower than the experimentally observed specific surface areas. The discrepancy between the predicted and experimental curves increased with Pt concentration. This can be explained by the fact that in Eq. (2) it was assumed that the Pt particles were spherical. In Fig. 2a it can be seen that non-spherical particles were formed during the preparation of the materials which, compared with spherical particles, increased the specific surface area.

On non-sputtered sample cross-sections, differences in potential between Pt particles that were part of the infinite 3-dimensional network and Pt particles isolated in the YSZ matrix were distinguished with an in-lens detector.

In Fig. 4 two SEM pictures obtained with the LEO-SEM are shown. On the right side the composite was investigated with a standard SE detector, while on the left side the same area investigated with the in-lens detector. Using the in-lens detector resulted in less bright spots for some Pt particles. These particles do not participate in the formation of a 3D Pt network and are thus isolated in the YSZ matrix. The effective interface area of the conducting Pt network using pictures obtained with the in-lens detector could be estimated by applying the same image analysis procedure for the specific surface area of all Pt particles as described above with the only difference that the isolated particles were converted to black similar to the YSZ matrix by using a different threshold. Since the volume fraction of Pt that formed a connected network can not be predicted *a priori*, the threshold value must be set visually. This procedure is somewhat less accurate, since it does not allow to correct for the porosity.

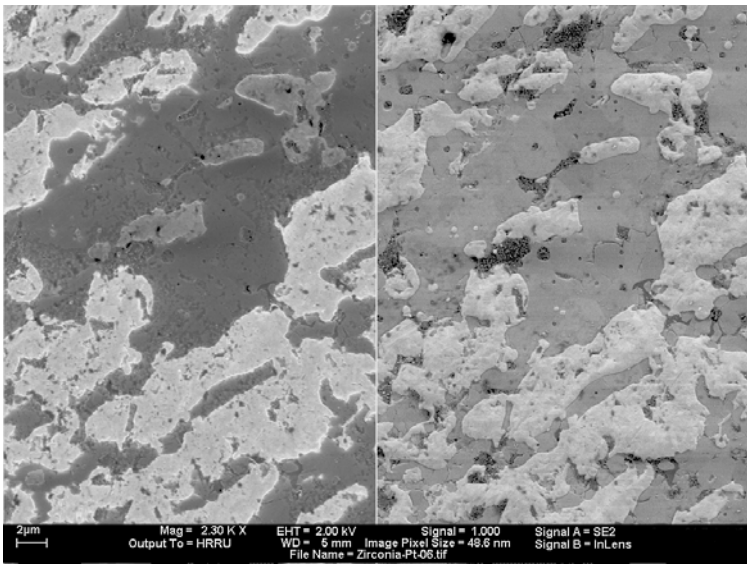


***Fig. 4**: SEM micrographs of a composite layer with a platinum concentration of 40 vol%; left: in-lens detector, right: regular detector.*

The effective surface area of Pt that formed a connected 3-dimensional network as determined with image analysis of the non-sputtered samples is shown in Fig. 5. The effective surface area increased exponentially with the Pt concentration, with the constant in the exponent having a value of 16.0±1.0. The highest value for the effective surface area was determined to be approximately $11 \cdot 10^3$ $cm^2/cm^3$ at a Pt volume fraction of 0.50. This value was close to the specific surface area of all platinum particles, implying that at high platinum concentrations in the composite layer, almost all particles participate in the formation of a conducting network. However, at low concentrations, beneath the so-called percolation threshold [19], no network was formed. The percolation threshold, which lies at approximately 31 vol% for a randomly dispersed metal phase with particles of equal size and shape [20], is the concentration at which a transition from an isolating to conducting composite is obtained. Below the percolation threshold the number of isolated particles is equal to the total amount of Pt particles in the YSZ matrix. Above the percolation threshold the fraction of isolated particles rapidly decreases to zero [18].

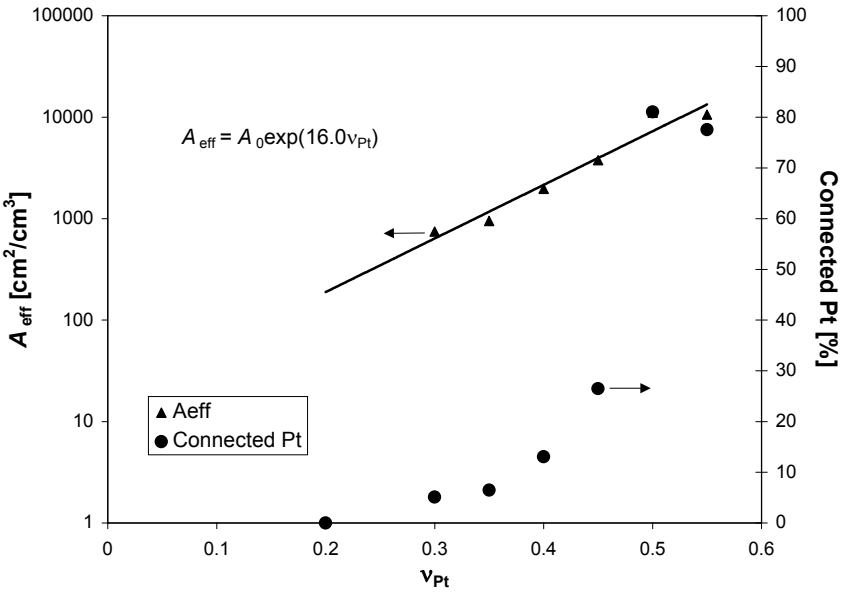


***Fig. 5**: Effective surface area and fraction of platinum particles that form a 3D network.*

It can be seen from the results of the calculations shown in Fig. 5 that above 30 vol% Pt in the composite layer a connected 3-dimensional network was easily formed. The fraction Pt that contributed to the formation of this network increased rapidly with Pt concentration to approximately 80% of the platinum particles in the matrix at 50 vol% Pt.

## Electrical impedance spectroscopy

An oxygen vacancy double layer was formed in the YSZ phase at the interface between the electrode and electrolyte at elevated temperatures (>400ºC). At this temperature the total capacitance was completely determined by the charge stored in the double layer and was therefore not influenced by the distance between the electrodes. The entire electrode surface area participates in the storage of charge.

The double-layer capacitance could be calculated from the CPE obtained at low frequencies, since the value of the exponent *n* varied from 0.85 to 0.95,

which indicated that a true capacitance was obtained. For samples with a platinum concentration of 20 vol% in the composite layer, the CPE was determined from frequencies lower than 3 Hz. With increasing platinum concentration (up to 45 vol%) the frequency range from which the CPE was determined, shifted to lower values (<50 mHz). For a capacitor with 45 vol% Pt in the composite layer the charging time was approximately 60 times larger than for a compact with 20 vol% Pt in the composite layer. Since the ionic resistance of the sample was constant for all compositions ($R \approx 1.5 \cdot 10^2\ \Omega$), the shift was most likely due to the increased electrode surface area, which was responsible for a longer charging time of the double-

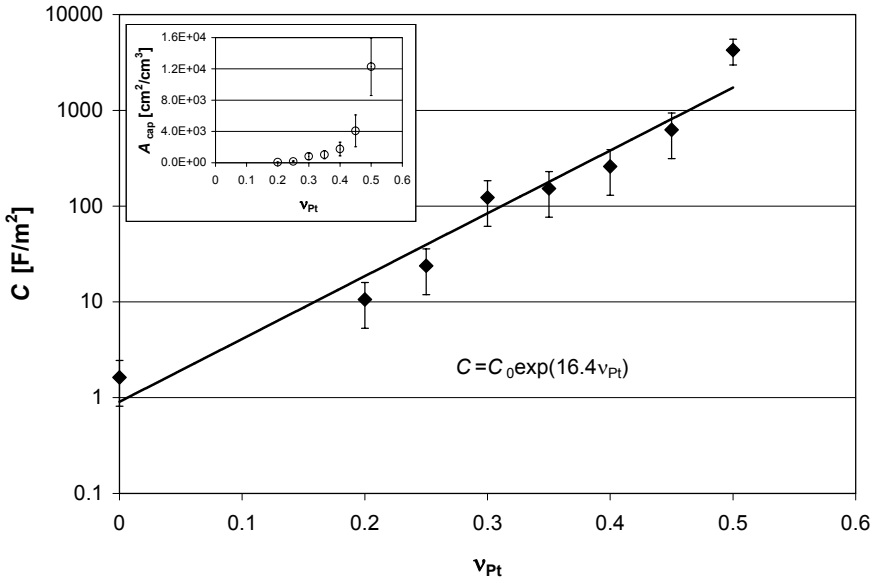


***Fig. 6:*** *Double-layer capacitance as function of platinum concentration in the composite layers; inset shows the specific electrode surface area calculated from the capacitance.*

layer.

The inset in Fig. 6 shows the effective electrode surface area calculated by dividing the enhancement in capacitance compared to pure YSZ by the volume of the composite layer. From the values shown in Fig. 6 it can be cal-

culated that the effective electrode surface area increased approximately 55 to 60 times if the Pt concentration increased from 20 to 45 vol%, which was in close agreement with the increase in charging times for the corresponding composites.

The double-layer capacitance normalised for the geometric electrode surface area is shown graphically in Fig. 6. In the experiments presented here it was observed that the estimated error in the absolute values of the double-layer capacitance was quite large, ~30% for the potentiostatic measurements and ~50% for the impedance measurements. However, an impressive exponential increase in capacitance with platinum concentration in the composite layer was obtained with the constant in the exponent having a value of 16.4±0.9. The exponential increase in capacitance is thus in agreement with the exponential increase of the effective platinum surface area as determined with image analysis on the not coated composite layers. Moreover, the values for the specific electrode surface areas calculated from the capacitance data were close to those determined from image analysis, which indicates that the capacitance data were reliable. The largest capacitance obtained amounted to 4.3±1.3 $kF/m^2$ and was obtained at a 50 vol% Pt concentration in the composite layers.

## Conclusions

The specific platinum surface area in Pt/YSZ composite layers estimated from image analysis on SEM micrographs, decreased from $\sim 17 \cdot 10^3$ to $\sim 13.5 \cdot 10^3$ $cm^2/cm^3$ with increasing concentration of Pt in the composite layers in the concentration range of 20 to 55 vol% Pt. When a SEM with an in-lens detector was used, a difference between isolated Pt particles and Pt particles that form a connected network could be observed. Image analysis on these micrographs revealed an exponential increase of the effective electrode surface area with Pt concentration in the composite layer when the Pt concentration was above its percolation threshold. A maximum value of approximately $11 \cdot 10^3$ $cm^2/cm^3$ was obtained at a Pt concentration of 50 vol%. At low concentrations no conducting network was formed, while up to 80% of the Pt particles contributed in the formation of a conducting network at the highest concentrations.

From high temperature impedance spectroscopy measurements it was determined that with increasing concentration of Pt in the composite layers, the capacitance of the layered compacts increased exponentially to 4.3±1.3 $kF/m^2$. This exponential increase is similar to the exponential increase in the effective surface area of the connected Pt particles.

## References


1. M. Wixom, L. Owens, J. Parker, J. Lee, I. Song and L. Thompson, Proc. Electrochem. Soc., **96** [25], 63 (1997).
2. S. Trassatti and P. Kurzweil, Platinum Metals Rev., **38**, 46 (1994).
3. J.P. Zheng and T.R. Jow, J. Electrochem. Soc., **142**, L6 (1995).
4. M. Adlsissi, R.H. Baughman, F.M. Ginder, H.H. Kuhn, H. Neidlinger and S. Ventura, Crit. Rev. Surf. Chem., **3**, 13 (1993).
5. S. Panero, E. Spila and B. Scrosati, J. Electroanalytical Chem., **396**, 385 (1995).
6. J.P. Zheng, J. Huang and T.R. Jow, J. Electrochem. Soc., **144**, 2026 (1997).
7. C. Arbizzani, M. Mastragostino, L. Meneghello and R. Paraventi, Adv. Mater., **8**, 331 (1996).
8. S. Sarangapani, B.V. Tilak and C.-P. Chen, J. Electrochem. Soc., **143**, 3791 (1996).
9. J.P. Zheng and T.R. Jow, J. Power Sources, **62**, 155 (1996).
10. C. Arbizzani, M. Catellani, M. Mastragostino and C. Mingazzini, Electrochim. Acta, **40**, 1871 (1995).
11. S. Panero, A. Clemente and E. Spila, Solid State Ionics, **86-88**, 1285 (1996).
12. M.G.H.M. Hendriks, J.E. ten Elshof, H.J.M. Bouwmeester and H. Verweij, *Submitted to Solid State ionics.*
13. M.G.H.M. Hendriks, B.A. Boukamp, J.E. ten Elshof, W.E. van Zyl and H. Verweij, *Submitted to Solid State Ionics.*
14. B. de Boer, SOFC anode; hydrogen oxidation at porous nickel and nickel/yttria-stabilized zirconia cermet electrodes, Ph.D. Thesis, University of Twente, Enschede, 1998.
15. M.G.H.M. Hendriks, W.E. van Zyl, J.E. ten Elshof and H. Verweij, *Accepted for publication in Mater. Res. Bull.*
16. B.A. Boukamp, Solid State Ionics, **20**, 31 (1986).
17. E.E. Underwood, Quantitative Stereology, Addison-Wesley Publishing Company, Reading, Massachusetts, USA, 1970, p. 23-47.
18. M. Sahimi, G.R. Gavalas and T.T. Tsotsis, Chem. Eng. Sci., **45**, 1443 (1990).
19. S. Kirkpatrick, Rev. Mod. Phys., **45**, 574 (1973).
20. D. Stauffer and J.G. Zabolitzky, J. Phys. A: Math. Gen., **19**, 3705 (1986).

# Chapter 8
# Conclusions and outlook

*In this chapter, the work described in this thesis is summarised and the results and the accomplishments are evaluated. In addition, some recommendations for further research and development regarding the preparation of electrolyte and electrode materials is given.*

## Introduction

As described in Chapter 1 of this thesis, the principal goal of the project was to prepare an all solid state supercapacitor. Since yttria-stabilised zirconia (YSZ) conducts oxygen at elevated temperatures (>400ºC) it was used as the electrolyte phase, while the electrodes were prepared from noble metals. Due to the mobility of the oxygen vacancies an electrochemical double layer of these vacancies is formed in the electrolyte at the interface with a charged electrode. This results in a large capacitance.

To increase the capacitance further, large electrode surface areas were developed by preparing noble metal/YSZ composites with a randomly dispersed metal phase using conventional preparation and compaction techniques.

In YSZ different polarisation effects were measured. At room temperature YSZ behaves like a normal dielectric medium. The contribution of the electronic and ionic polarisation was measured at high frequencies (>1 kHz). At elevated temperatures YSZ is an electrolyte in which the space charge polarisation was measured in the low frequency regime (<1 Hz).

## Electrolyte phase

A general model for describing the (differential) capacitance in oxygen conducting materials was derived on a thermodynamic basis. This model is based on the assumption of a random distribution of all oxygen vacancies in the lattice. It can qualitatively predict the double-layer capacitance.

Based on differential capacitance measurements on YSZ a defect structure for the near-surface layer was proposed. Under the assumption that part of the oxygen sub-lattice is inaccessible for mobile oxygen vacancies, a prediction for the maximum oxygen vacancy fraction, contributing to the double-layer formation can be made. Applying this maximum resulted in an improved model for describing the differential capacitance in YSZ.

The near-surface dielectric constant of YSZ was fitted to a Boltzman type equation, which appeared to result in values lower than reported in literature for the YSZ bulk. According to the developed model, the double-layer capacitance is proportional to $\varepsilon_r^{0.5}$, while for dielectric materials the capaci-

tance is proportional to $\varepsilon_r$. Unfortunately, elevated temperatures are required for the formation of the double-layer capacitance, since at room temperature the mobility of the oxygen ions is insufficient.

## Dispersed metal phase

For composites with a randomly dispersed metal phase the preparation technique does not have a significant influence on the room temperature properties. The capacitance of the composites increases with concentration of the metal phase. The component of the electrode surface area perpendicular to the electric field strength contributes to the enhancement of the capacitance. This contribution is rather small. The increase in capacitance is merely attributed to a decrease in the distance between the electrodes. The normalised percolation theory was applied for fitting the data points. For the random composites a percolation threshold close to the value for random dual-phase composites with overlapping particles of equal size and shape was obtained. However comparable values for the enhancement in capacitance were not experimentally verified. Most likely this is due to a very inhomogeneously distributed metal phase near the theoretical percolation threshold, resulting in conducting paths in the compacts. If other than conventional methods are employed which can assure a high homogeneity up to the percolation threshold, values for the capacitance comparable to values as calculated in percolation theories might be obtained.

In the preparation of random composites a large amount of noble metals, up to 30 vol% was used. This makes these composites less attractive from an economical point of view. To decrease the concentration of the noble metals, a porous YSZ matrix was impregnated with a Pt salt solution. Only a fraction of Pt compared to the random composites was used. However, impregnated and afterwards reduced compacts did not result in a larger enhancement of the capacitance. In contrast, porous YSZ impregnated with a Pt salt solution from which Pt was electrolytically deposited at the electrodes, resulted in a relatively large enhancement of the capacitance at room temperature. Platinum was deposited at the electrodes in a direction parallel to the electric field strength, resulting in an increase of the electrode surface area and in a decrease in distance between the electrodes at the same time. At

550ºC the effective electrode surface area was determined to increase to 260 times the geometric surface area, due to the formation of three dimensional Pt structures that are connected to the electrodes.

A large disadvantage of porous YSZ, however, is that at this temperature no pure double-layer capacitance is obtained and other diffusion and/or surface exchange processes occur at or in the vicinity of the electrodes. Therefore the preparation of dense compacts is required and might be achieved by impregnating the pores with a ceramic paste or a polymer that can withstand high temperatures.

A large electrode surface area is obtained in dense compacts consisting of YSZ sandwiched between two layers of Pt/YSZ composites. At a Pt concentration above its percolation threshold, large 3-dimensional structures are formed when connected to the electrodes result in large capacitances.

## Perspectives

Several industrially available supercapacitors are listed in Table 1 [1]. The capacitance of these materials varies from $1.6 \cdot 10^{-3}$ to 5.3 F/g. The highest capacitance obtained with a layered structure of YSZ sandwiched between two layers of Pt/YSZ composites described in Chapter 7 of this thesis, amounts to approximately 0.5 F/g. This value is reasonably close to those listed in Table 1. Since YSZ is oxygen ion conducting only at elevated temperatures, these layered structures can not be used in room temperature applications as discussed in Chapter 1. Due to their high working temperature these materials might be used to compensate for peak-cut of power that can emerge during SOFC operation.

***Table 1:*** *Comparison of various commercial supercapacitors [1].*

| | Capacity [F/g] |
|---|---|
| Maxwell ultracapacitor | 2.6-3.2 |
| Panasonic | 2.5-3.5 |
| Superfarad | $16 \cdot 10^{-3}$ |
| Saft (Gen) | 4.8-5.3 |
| PowerStor | 0.67 |

Prospects regarding the applied materials of the solid state supercapacitor can be found on both electrolyte as electrodes. For room temperature applications alternative

electrolytes have to be utilised. By increasing the electrode surface area, the capacitance can be increased further. However, the charging time is proportional to the electrode surface area. Thus another requirement for the electrolyte is a large mobility of the charge carriers.

Possible materials that are suitable for room temperature ceramic electrolytes are solid-state lithium ion-conducting materials. Since 1996 lithium doped borophosphates are used as solid-state electrolytes in lithium ion batteries due to their high room temperature lithium conduction [2]. More recent Li ion conductors at room temperature were found in oxides with a perovskite related structure with the general formula $La_{2/3-x}Li_{3x}TiO_3$ [3]. A disadvantage of these electrolytes is that lithium forms a solid solution with most metals. However, nickel is a suitable possibility as electrode material, since the Li solubility in Ni is negligible [4].

As described in a previous section, the amount of noble metal used in random composites described in this thesis is still quite large. The percolation threshold and thus the noble metal concentration can be decreased if non-spherical metal particles with a volume much smaller than the electrolyte particles are used [5-8]. Moreover, a possible method to avoid aggregation of the metal particles during sintering may be by employing a powder with a core-shell morphology, where the metal phase forms the core and the oxidic phase the shell. As the metal particles are entirely encapsulated by the oxidic phase, aggregation can be hampered and sintering occurs predominantly in the outer oxidic shells. This may finally result in a more homogeneous distribution of the metal phase and in a large room temperature capacitance.

The electrode surface area can be increased by the preparation of multi-layered structures of electrolyte and metal/electrolyte composite as is commonly applied in the production of multi-layer ceramic capacitors [9]. Another possibility for increasing the electrode surface area is to decrease the metal grain size. This might be achieved by using preparation techniques like emulsion precipitation [10].

## References


1. A. Burke, *J. Power Sources*, **91**, 37, 2001.
2. E.M. Kelder, M.J.G. Jak, F. de Lange and J. Schoonman, *Solid State Ionics*, **85**, 285, 1996.
3. A. Várez, M.L. Sanjuán, M.A. Laguna, J.I. Peña, J. Sanz and G.F. de la Fuente, *J. Mater. Chem.*, **11**, 125, 2001.
4. F.A. Shunk Constitution of binary alloys, Second supplement, McGraw-Hill Book Company, New York, USA, 1969.
5. E.J. Garboczi, K.A. Snyder, J.F. Douglas and M.F. Thorpe, *Phys. Rev. E*, **5**, 819, 1995.
6. E.T. Gawlinski and H.E. Stanley, *J. Phys. A: Math. Gen.,* **14** [8], L291, 1981.
7. A. Maillaris and D.T. Turner, *J. Appl. Phys*., **42**, 614, 1971.
8. F. Lux, *J. Mater. Sci*., **28**, 285, 1993.
9. A. Morell and J.-C. Niepce, *J. Mater. Educ.*, **13**, 173, 1991.
10. F.C.M. Woudenberg, Nanostructured oxide coatings via emulsion precipitation, PhD Thesis, University of Twente, Enschede, 2001.

# Summary

Conventional capacitors use a dielectric medium that becomes polarised in the high frequency regime and are commonly used in ac and dc applications. In contrast, supercapacitors make use of an electrolyte in which space-charge polarisation takes place at low frequencies (<1 Hz). The electrical behaviour of supercapacitors can be found between that of conventional capacitors and batteries. The space-charge layer can store an enormous amount of charge and since the space charge layer is formed at the complete interface between electrolyte and electrode, a large electrode surface area can be used to increase the capacitance. The work described in this thesis deals with the preparation of supercapacitors from metal/yttria-stabilised zirconia (YSZ) composites and their capacitive properties.

This thesis is broadly divided in two parts. The first part concerns the capacitive behaviour of YSZ and the defect structure of the space-charge layer. In the second part the capacitive behaviour of metal/YSZ composites with varying microstructure is described.

A general model for describing the (differential) capacitance in YSZ was derived on a thermodynamic basis. This model is based on the assumption that a random distribution of all oxygen vacancies is present over the entire oxygen sub-lattice. The model gives a qualitative description of the double-layer capacitance as a function of yttria concentration, temperature and bias potential. Based on the differential capacitance measurements, a defect structure for the near-surface layer of YSZ was proposed. On the assumption that only a part of the oxygen sub-lattice is accessible for mobile oxygen vacancies, thus limiting the maximum attainable oxygen vacancy fraction in

the double-layer, an improved model for describing the differential capacity in YSZ was obtained. The near-surface dielectric constant of YSZ was used as a fit parameter and its value appeared to result in permittivity values lower than reported in literature for the bulk YSZ. According to the developed model, the double-layer capacitance is proportional to $\varepsilon_r^{½}$, while for conventional dielectric materials that operate on the basis of ionic and electronic polarisation the capacitance is proportional to $\varepsilon_r$. Elevated temperatures (>400°C) are required for the formation of the double-layer capacitance, since at room temperature the mobility of the oxygen ions is insufficient. At high temperatures the capacitance is determined by the oxygen vacancy concentration in the double layer, while at room temperature the capacitance is determined by the crystal structure.

For composites with a randomly dispersed metal phase the employed preparation techniques did not result in significant differences in the room temperature dielectric properties. However, the homogeneity of the positional distribution of the metal phase decreased with increasing metal concentration. The capacitance of the composites increased with concentration of the metal phase. The component of the electrode surface area perpendicular to the electric field strength contributed to the enhancement of the capacity. However, the increase in capacity was merely attributed to an effective decrease in the distance between the electrodes. The normalised percolation theory was applied for fitting the data. For composites with a randomly distributed metal phase a percolation threshold close to the value of 31.2 vol% for random dual-phase composites with overlapping particles of equal size and shape was obtained. Comparable values for the enhancement in capacitance could not be verified experimentally. Most likely this is due to a very inhomogeneously distributed metal phase near the theoretical percolation threshold, resulting in conducting paths in the compacts.
At elevated temperatures, the entire YSZ/electrode interface contributes in the formation of the double-layer capacity. By creating large metallic networks that are connected with the electrodes, large capacitances up to 4.3 kF/m$^2$ were obtained. To decrease the required noble metal concentration, platinum was electrolytically deposited at the electrodes in a porous YSZ compact. A large electrode surface area was created in this manner.

However, at this temperature no pure double-layer capacitance was obtained and other diffusion and/or surface exchange processes occurred at or in the vicinity of the electrodes, which was attributed to the presence of pores. The largest electrode surface area was obtained in dense compacts consisting of a YSZ layer sandwiched between two layers of Pt/YSZ composites. At a Pt concentration above the percolation threshold, large three-dimensional structures were formed which resulted in large double-layer capacitances at high temperatures.

# Samenvatting

Conventionele condensatoren maken gebruik van een dielektrisch medium dat gepolariseerd wordt bij hoge frequenties. Ze worden vaak gebruikt voor ac en dc toepassingen. In tegenstelling tot conventionele condensatoren maken supercondensatoren gebruik van een elektrolyt waarin ruimteladingspolarisatie plaatsvindt bij frequenties onder 1 Hz. Het elektrische gedrag van supercondensatoren ligt tussen dat van conventionele condensatoren en batterijen in. In de ruimteladingslaag kan een enorme hoeveelheid lading opgeslagen worden. Omdat de ruimteladingslaag over het gehele grensvlak tussen elektrolyt en elektrode gevormd wordt, kan de capaciteit vergroot worden door gebruik te maken van een groot elektrode-oppervlak. Het werk beschreven in dit proefschrift handelt over de preparatie van supercondensatoren van metaal/yttria gestabiliseerd zirconia (YSZ) composieten en over de capacitieve eigenschappen ervan.

Dit proefschrift is globaal in twee delen verdeeld. Het eerste gedeelte handelt over het capacitieve gedrag van YSZ en de defectstructuur van de ruimteladingslaag. In het tweede deel is het capacitieve gedrag van metaal/YSZ composieten met een variërende microstructuur beschreven.

Uitgaand van de thermodynamica is een algemeen model afgeleid om de differentiële capaciteit in YSZ te beschrijven. Het model is gebaseerd op de aanname dat alle zuurstofvacatures aselect verdeeld zijn over het volledige zuurstofsubrooster. Dit model geeft een kwalitatieve beschrijving van de dubbellaagcapaciteit in YSZ als functie van de yttria concentratie, de temperatuur en de overpotentiaal. Op basis van differentiële capaciteitsmetingen is een defectstructuur voor de ruimteladingslaag in YSZ voorgesteld. Aange-

nomen dat slechts een deel van het zuurstofsubrooster toegankelijk is voor mobiele zuurstofvacatures, en op die manier de maximaal bereikbare fractie van zuurstofvacatures gelimiteerd wordt, is er een verbeterd model voor het beschrijven van de differentiële capaciteit in YSZ verkregen. De dielektrische constante van YSZ nabij het grensvlak met de elektrode is gebruikt als fitparameter en de verkregen waarde voor de permittiviteit ervan bleek lager te zijn dan de waarden die in de literatuur voor bulk YSZ beschreven zijn. Volgens het ontwikkelde model is de dubbellaagcapaciteit evenredig met $\varepsilon_r^{½}$, terwijl voor conventionele condensatoren die gebaseerd zijn op elektronische en ionische polarisatie de capaciteit evenredig is met $\varepsilon_r$. Voor het verkrijgen van een dubbellaagcapaciteit in YSZ, is het noodzakelijk de temperatuur te verhogen (>400ºC), omdat bij kamertemperatuur de mobiliteit van zuurstofionen te laag is. Bij hoge temperaturen wordt de capaciteit bepaald door zuurstofvacatureconcentratie in de dubbellaag, terwijl bij kamertemperatuur de capaciteit wordt bepaald door de kristalstructuur.

Voor composieten met een aselect verdeelde metaalfase heeft de gebruikte preparatietechniek geen significante invloed op de dielektrische eigenschappen bij kamertemperatuur. Echter, de positionele homogeniteit van de metaalfase verslechtert met een toename in de metaalconcentratie. De capaciteit van de composieten neemt toe met toenemende metaalconcentratie. De component van het elektrode-oppervlak die loodrecht op de elektrische veldsterkte staat, neemt deel aan de vergroting van de capaciteit. Echter, de vergroting wordt hoofdzakelijk gewijd aan de verkleining van de effectieve afstand tussen de elektroden. De genormaliseerde percolatietheorie is aangewend om de data te fitten. Voor composieten met een aselect verdeelde metaalfase ligt de verkregen waarde voor de percolatiegrens dicht bij de waarde van 31.2 vol% voor aselecte composieten met overlappende deeltjes van gelijke grootte en vorm. Vergelijkbare waarden voor de vergroting van de capaciteit zijn experimenteel niet geverifieerd. Hoogstwaarschijnlijk is dit veroorzaakt door een zeer inhomogeen verdeelde metaalfase indien de concentratie ervan net onder de percolatiegrens ligt, zodat elektrisch geleidende paden worden gevormd in de compacten.
Bij verhoogde temperaturen, neemt het gehele grensvlak tussen YSZ en de elektrode deel aan de vorming van de dubbellaagcapaciteit. Door grote me-

taalnetwerken die verbonden zijn met de elektrode te creëren, worden hoge capaciteiten tot ongeveer 4.3 $F/m^2$ verkregen. Om de vereiste hoeveelheid edelmetalen te reduceren, is in poreus YSZ platina elektrolytisch afgezet aan de elektroden. Op deze manier is er een groot elektrode-oppervlak gecreëerd. Echter, bij deze temperatuur is er geen zuivere dubbellaagcapaciteit verkregen en traden andere diffusie- en/of oppervlakte-uitwisselings-processen op, die toegewijd worden aan de aanwezigheid van poriën. Het grootste elektrode-oppervlak is bereikt in dichte compacten die bestaan uit een laag YSZ gesandwiched tussen twee lagen Pt/YSZ composieten. Bij een Pt concentratie boven de percolatiegrens worden grote drie dimensionale structuren gevormd, die resulteerden in hoge dubbellaagcapaciteiten.

# Dankwoord

Voordat ik ga vertellen hoe ik de afgelopen 4 jaar als AIO heb doorgebracht, wil ik eerst even vertellen hoe ik er ben toegekomen om als AIO onderzoek te doen.
Tijdens mijn afstuderen bij Membraantechnologie werd door verscheidene AIO's mij de positieve kanten van het AIO-schap verteld. Samen met de werkzaamheden tijdens mijn afstudeerperiode was dit overtuigend genoeg om zelf ook promotieonderzoek te doen.

Op de conferentie Euromembrane werd ik door Arian en Renate uitgenodigd om een kijkje te nemen bij AMK. Hier kreeg ik van HV de mogelijkheid om binnen de vakgroep promotieonderzoek uit te voeren.
Naast een professor heb ik ook nog 3 directe begeleiders versleten. Als eerste Manon die er voor gezorgd heeft dat ik ook daadwerkelijk het lab op aan de slag ging. Daarna was Bas mijn interim begeleider. Zijn voornaamste taak was het verzorgen van de koffie. En uiteindelijk was het André die er mede voor gezorgd heeft dat er diepgang in mijn proefschrift kwam.
Uiteraard zijn er ook nog anderen binnen de vakgroep geweest die een bijdrage aan het werk geleverd hebben. In niet preferentiële volgorde: Werner voor corrigeren van mijn manuscripten, Henny voor de theoretische ondersteuning (en natuurlijk ook de discussies in Australië), Bernard voor het simuleren en uitwerken van impedantie data, Marjan voor de image analyse dat geresulteerd heeft in een flinke bijdrage aan twee hoofdstukken en Herman voor het SEM werk.
Verder zijn er mensen van buiten de groep die analyses voor mij hebben uitgevoerd: Mark Smithers van het CMO voor SEM-EDX analyses, Louise

Vrielink van de vakgroep Chemische Analyse voor XRF bepalingen en Jan van den Enk van Akzo Nobel Central Research voor SEM-foto's verkregen met een in-lens detector. Natuurlijk wil ik de mensen van de werkplaats en in bijzonder Joop bedanken voor het bewerken van mijn samples.
Twee studenten heb ik mogen begeleiden in mijn tweede jaar: Rob Siebes als HBO stagiair en Ronald Greven als afstudeerder. Van beide staat werk beschreven in enkele hoofdstukken.

De afgelopen vier jaar heb ik met verschillende kamergenoten doorgebracht. Tomas verhuisde naar een andere kamer, zodat hij in rust kon schrijven. Hij was echter zelf de oorzaak van het lawaai. Elise hield het beter bij mij uit. Drieëneenhalf jaar lang hebben wij o.a. iedere ochtend de krant doorgenomen. Na Tomas hebben we even Ben als kamergenoot gehad. Ben, I really regret that you left and went back to America. Uiteindelijk is na het vertrek van Elise, Sankhanilay mijn nieuwe kamergenoot geworden gedurende het laatste half jaar van mijn promotietijd. Sankho, I think it is incredible that you could withstand all my music.

Ook wil ik Natascha en Marco bedanken, omdat zij als paranimfen naast mij op het podium plaatsnemen tijdens de verdediging van mijn proefschrift.

Tenslotte wil ik graag iedereen bedanken die de afgelopen vier jaar buiten het wetenschappelijke om, voor een prettige tijd hebben gezorgd binnen de vakgroep. Als eerste wil ik beginnen om iedereen die mee op studiereis, cursussen, excursies en congresbezoeken zijn geweest, bedanken voor het sociale gebeuren er omheen. Daarnaast zijn er ook een aantal vakgroepuitjes en sportieve evenementen georganiseerd. En natuurlijk mag ook de wekelijkse borrel niet vergeten worden. Tevens wil ik graag iedereen van MT die ik geregeld op donderdagavond in de kroeg tegenkwam, bedanken voor de gezelligheid, maar in het bijzonder Jon, omdat hij heeft geprobeerd de stijlfouten uit de lay-out van dit proefschrift te halen.

Ik hoop dat ik niemand vergeten ben. Ik eindig met het bedanken van Kim. Als eerste heb je een ontzettend mooie kaft voor mijn proefschrift ontworpen. Maar belangrijker, je bent mijn steun geweest en stond altijd voor me klaar in de afgelopen periode.

# Levensloop

Mark Gerard Hendrik Maria Hendriks werd op 4 maart 1973 geboren in Haps. In 1991 behaalde hij zijn VWO diploma aan het Merletcollege te Cuijk en aansluitend begon hij met zijn studie Chemische Technologie aan de Universiteit Twente. Hij liep stage bij ATO-DLO te Wageningen. Bij de vakgroep Membraantechnologie van prof. dr. dipl.-ing. H. Strathmann studeerde hij in 1997 af met als onderwerp de fysische eigenschappen van etheenionomeren. Hetzelfde jaar trad hij in dienst van de vakgroep Anorganische Materiaalkunde aan de Universiteit Twente, waar hij onder begeleiding van prof. dr. ir. H. Verweij onderzoek verrichtte aan ongestructuureerde tweefasen composieten voor supercondensatoren. De resultaten van dit onderzoek staan beschreven in dit proefschrift.